UCLA
UCLA Electronic Theses and Dissertations

Title

Functions and Regulation of Nuclear Lamins in Health and Disease

Permalink

Author

Jung, Hea Jin

Publication Date

2014

Peer reviewed|Thesis/dissertation

UNIVERSITY OF CALIFORNIA

Los Angeles

Functions and Regulation of Nuclear Lamins in Health and Disease

A dissertation submitted in partial satisfaction of the

requirements for the degree Doctor of Philosophy

in Molecular Biology

by

Hea Jin Jung

2014

ABSTRACT OF THE DISSERTATION

Functions and Regulation of Nuclear Lamins in Health and Disease

by

Hea Jin Jung

Doctor of Philosophy in Molecular Biology

University of California, Los Angeles, 2014

Professor Stephen G. Young, Chair

Nuclear lamins are intermediate filament proteins that form the nuclear lamina, a structural scaffolding for the nucleus. They interact with other nuclear proteins and the chromatin and are thought to participate in many fundamental cellular pathways. Most vertebrates have two-types of lamins: A-type (lamins A and C) and B-type (lamins B1 and B2). Nuclear lamins, particularly A-type lamins, have attracted considerable attention due to their association with many human genetic diseases. However, despite considerable interest in nuclear lamins, physiologic rationale for the different lamins is unclear. Also, the functional importance of the lamins in the brain has not been thoroughly investigated as the phenotypes of the associated genetic diseases are largely confined to mesenchymal tissues.

In this dissertation, we aimed to better understand distinctive functions and regulation of nuclear lamins in health and diseases, with an emphasis on the brain. In Chapter 2, we showed that prelamin A, but not lamin C, is down-regulated in the brain by a brain-specific microRNA,

miR-9 using a series of *in vitro* studies in cultured cells. In Chapter 3, we generated two new lines of *Lmna* knock-in mice to investigate whether the regulation of prelamin A by miR-9 is relevant *in vivo*. These studies, taken together, provided a ready explanation why children with Hutchinson-Gilford progeria syndrome (a progeroid syndrome caused by a mutant form of prelamin A) are spared from neurodegenerative disease: miR-9 selectively eliminates the expression of the culprit molecule—the toxic prelamin A molecule that leads to disease. In Chapter 4, we addressed the physiologic importance of the farnesyl lipid anchor in B-type lamins using knock-in mice expressing nonfarnesylated versions of lamin B1 and lamin B2. In this study, we showed that the farnesyl lipid anchor on lamin B1 is crucial for retaining the nuclear chromatin within the bounds of nuclear lamina during neuronal migration. In Chapter 5, we investigated whether nuclear lamins are essential for proliferation and differentiation of non-neuronal cells *in vivo* using keratinocyte-specific *Lmna/Lmnb1/Lmnb2* triple-knockout mice.

The dissertation of Hea Jin Jung is approved.

Karen Reue

Amy C. Rowat

Stephen G. Young, Committee Chair

University of California, Los Angeles

2014

dedicated to my family and my colleagues

TABLE OF CONTENTS

LIST OF TABLES AND FIGURES

Chapter 4.

ACKNOWLEDGEMENTS

First of all, I would like to thank my advisor Dr. Stephen G. Young for his tremendous support and great advices throughout my graduate studies. I also thank Dr. Loren G. Fong for his incredible guidance and continuous encouragement. They have been a strong guide force behind all my achievements as a graduate student. Without their supports, I would not have been able to overcome the challenges that I have encountered during my graduate studies.

I also deeply appreciate the great inputs and supports from my committee members, Drs. Steven G. Clarke, Karen Reue, Ellen M. Carpenter, and Amy C. Rowat. Their insightful feedback, while challenging, helped me to think one step further.

I would also like to thank all the current and previous Young lab members, especially lamin folks, for helping me along the way: Dr. Catherine Coffinier for excellent guidance during my first year in the laboratory and for teaching me many useful techniques to study brain development; Dr. Yiping Tu and Chika Nobumori for providing extra hands all the time and for being wonderful lab mates; Drs. Brandon S. J. Davies and Shao H. Yang for constructive discussions and advices; Angelica Tatar, Daniel Wu, and Richard H. Barnes II for their hard work to manage numerous mouse colonies; Dr. John M. Lee for sharing his experience to facilitate troubleshooting of my experiments. I also thank Drs. Anne P. Beigneux, Chris N. Goulbourne, and Adeyo Oludotun for their help in several occasions during my study.

Outside of my research group, I am also grateful to all the collaborators: Drs. Samuel J. Pleasure and Youngshik Choe for their technical help and inputs to data analysis for my first project; Dr. Tao Sun and Janet Hong for providing valuable samples and fruitful discussion; Drs. Pieter J. de Jong and Yuko Yoshinaga for generating constructs for new knock-in alleles.

xiv

I also want to acknowledge the Philip Whitcome Training program at UCLA for the continued financial support during the last three years of my studies.

Finally, I want to thank my friends and families for their constant support and encouragements. I am most grateful to my beloved husband Chan Youn for his unconditional support and full appreciation of my academic and personal endeavors. I couldn't have asked for a better partner!

Chapter 1 was reproduced from "Nuclear lamins in the brain - new insights into function and regulation" published in *Mol. Neurobiol.* 2013, 47:290–301 [DOI: 10.1007/s12035-012-8350-1] with minor modification. Chapter 2 contains a reprint of "Regulation of prelamin A but not lamin C by miR-9, a brain-specific microRNA" from *Proc. Natl. Acad. Sci. U. S. A.* 2012, 109:E423–431 [DOI: 10.1073/pnas.1111780109]. Chapter 3 contains a reprint of "New *Lmna* knock-in mice provide a molecular mechanism for the "segmental aging" in Hutchinson-Gilford progeria syndrome" from *Human Mol. Genet.* (Oxford University Press) 2013, 23:1506–1515 [DOI: 10.1093/hmg/ddt537]. Chapter 4 contains a reprint of "Farnesylation of lamin B1 is important for retention of nuclear chromatin during neuronal migration" from *Proc. Natl. Acad. Sci. U. S. A.* 2013, 110:E1923–1932 [DOI: 10.1073/pnas.1303916110]. All the reproduction and reprints used in this dissertation do not require permission from publishers with proper acknowledgement of the original sources of publication as an author of the articles.

VITA

2001–2005	B.S. in Biological Sciences, cum laude
	Seoul National University, South Korea
2005–2007	M.S. in Biological Sciences
	Seoul National University, South Korea; Microbial Physiology
2007–2009	Staff Research Associate I
	University of California, Los Angeles, CA; T cell immunology

SELECTED PUBLICATIONS

1. Srikanth S, **Jung HJ**, Ribalet B, Gwack Y. (2010) The intracellular loop of Orai1 plays a central role in fast inactivation of Ca2+ release-activated Ca2+ channels. *J. Biol. Chem.* 285:5066–5075.

2. Srikanth S, **Jung HJ**, Kim KD, Souda P, Whitelegge J, Gwack Y. (2010) A novel EF-hand protein, CRACR2A, is a cytosolic Ca2+ sensor that stabilizes CRAC channels in T cells. *Nat. Cell Biol.* 12:436–446.

3. Coffinier C, **Jung HJ**, Li Z, Nobumori C, Yun UJ, Farber EA, Davies BS, Weinstein MM, Yang SH, Lammerding J, Farahani JN, Bentolila LA, Fong LG, Young SG. (2010) Direct synthesis of lamin A, bypassing prelamin A processing, causes misshapen nuclei in fibroblasts but no detectable pathology in mice. *J. Biol. Chem.* 285:20818–20826.

4. Coffinier C, **Jung HJ**, Nobumori C, Chang S, Tu Y, Barnes RH, Yoshinaga Y, de Jong PJ, Vergnes L, Reue K, Fong LG, Young SG. (2011) Deficiencies in lamin B1 and lamin B2 cause neurodevelopmental defects and distinct nuclear shape abnormalities in neurons. *Mol. Biol. Cell* 22:4683–4693.

5. Yang SH, **Jung HJ**, Coffinier C, Fong LG, Young SG. (2011) Are B-type lamins essential in all mammalian cells? *Nucleus* 2:562–569.

6. **Jung HJ**, Coffinier C, Choe Y, Beigneux AP, Davies BSJ, S. Y, Barnes RH, Hong J, Sun T, Pleasure SJ, Young SG, and Fong LG (2012) Regulation of prelamin A but not lamin C by miR-9, a brain-specific microRNA. *Proc. Natl. Acad. Sci. U. S. A.* 109:E423–431.

7. Young SG, **Jung HJ**, Coffinier C, Fong LG. (2012) Understanding the roles of nuclear A- and B-type lamins in brain development. *J. Biol. Chem.* 287:16103–16110.

8. **Jung HJ**, Lee JM, Yang SH, Young SG, Fong LG. (2013) Nuclear lamins in the brain - new insights into function and regulation. *Mol. Neurobiol.* 47:290–301.

9. **Jung HJ**, Nobumori C, Goulbourne CN, Tu Y, Lee JM, Tatar A, Wu D, Yoshinaga Y, de Jong PJ, Coffinier C, Fong LG, Young SG. (2013) Farnesylation of lamin B1 is important for retention of nuclear chromatin during neuronal migration. *Proc. Natl. Acad. Sci. U. S. A.* 110:E1923–1932.

10. **Jung HJ**, Tu Y, Yang SH, Tatar A, Nobumori C, Wu D, Young SG, Fong LG. (2013) New *Lmna* knock-in mice provide a molecular mechanism for the "segmental aging" in Hutchinson-Gilford progeria syndrome *Human Mol. Genet.* 23:1506–1515.

Chapter 1:

Introduction

The Nuclear Lamins

The nuclear lamina is an intermediate filament meshwork located adjacent to the inner nuclear membrane. In vertebrates, it is composed largely of four proteins called nuclear lamins—lamins A, C, B1, and B2 (1). The lamins have been classified as A- and B-type based on their biochemical properties (2-4). The expression of the A-type lamins (lamins A and C) starts during the later stages of embryonic development and peaks postnatally; B-type lamins (lamins B1 and B2) are expressed in all cell types from the earliest stages of development (5, 6).

Lamins A and C are alternatively spliced products of the same gene, *LMNA* (Figure 1.1) (7). They are identical through the first 566 amino acids but diverge in their carboxyl-terminal domains. Lamin C terminates with exon 10 sequences and has 6 unique amino acids (not found in lamin A) at its carboxyl terminus. Prelamin A, the precursor to mature lamin A, includes sequences from two additional exons (exons 11 and 12), resulting in 98 unique amino acids at its carboxyl terminus. The 3′ UTRs of lamin C and prelamin A transcripts are also distinct. Lamin C's 3′ UTR, formed by intron 10 sequences, is short (~100 bp); prelamin A's 3′ UTR is ~1 kb in length and includes many sequences that have been conserved through mammalian evolution.

Lamins B1 and B2, are encoded by distinct genes, *LMNB1* (8) and *LMNB2* (9), respectively. These genes have a similar intron–exon structure, suggesting that they arose from a gene-duplication event (1, 10). Lamin B1 and lamin B2 proteins are ~60% identical at the amino acid level (11).

Like other intermediate filament proteins, all nuclear lamins have a highly conserved α-helical central rod domain (Figure 1.1) (12, 13). The rod domain is critical for lamin dimerization and for the formation of higher-order polymers (14). Lamins also have globular head and tail domains, with the tail domain containing a nuclear localization signals (NLS) (Figure 1.1) (12,

2

13).

Physiologic Importance of A-type Lamins

To assess the importance of the A-type lamins, Sullivan and coworkers (15) generated *Lmna* knockout mice (*Lmna*$^{-/-}$). *Lmna*$^{-/-}$ mice do not manifest developmental abnormalities and are indistinguishable from wild-type littermates at birth (15). Soon thereafter, however, *Lmna*$^{-/-}$ mice develop a cardiac and skeletal myopathy, and they die by 6–8 weeks of age. The absence of A-type lamins compromises the structural integrity of the nuclear envelope, resulting in misshapen nuclei, which likely plays a part in the pathogenesis of the muscle disease (16). The absence of lamins A and C also results in mislocalization of emerin, an inner nuclear membrane protein, to the endoplasmic reticulum. Emerin mutations cause muscular dystrophy in humans (2, 17-19).

Thus far, *unique* roles for lamin A and lamin C remain obscure. Fong *et al.* (20) created "lamin C–only mice" (*Lmna*$^{LCO/LCO}$) that do not produce prelamin A transcripts and make approximately twice-normal amounts of lamin C transcripts. Surprisingly, the absence of prelamin A and lamin A in *Lmna*$^{LCO/LCO}$ mice does not appear to have adverse consequences; these mice are normal in size and vitality and have no obvious disease phenotypes. Subtle abnormalities in nuclear shape can be detected in cultured *Lmna*$^{LCO/LCO}$ fibroblasts (16, 20), but it is unclear whether any such abnormalities actually occur in parenchymal cells of *Lmna*$^{LCO/LCO}$ mice. Later, Coffinier *et al.* (21) generated "mature lamin A–only mice" (*Lmna*$^{LAO/LAO}$) and Davies *et al.* (22) created "prelamin A–only mice" (*Lmna*$^{PLAO/PLAO}$). Both mouse models are incapable of producing lamin C transcripts, and all of the output of the *Lmna* gene is channeled into prelamin A transcripts (encoding mature lamin A in the case of *Lmna*$^{LAO/LAO}$ mice or full-

length prelamin A in *Lmna*[PLAO/PLAO] mice). The *Lmna*[LAO/LAO] and *Lmna*[PLAO/PLAO] mice are healthy and free of pathology. Misshapen nuclei can be observed in cultured *Lmna*[LAO/LAO] fibroblasts but were never observed in the tissues of *Lmna*[LAO/LAO] mice (21).

Prelamin A contains a "*CaaX*" motif at its carboxyl terminus (Figure 1.1), which triggers three sequential posttranslational *CaaX* processing steps: farnesylation of a carboxyl-terminal cysteine (the "*C*" of the *CaaX* motif), cleavage of the last three amino acids of the protein (*i.e.*, the "*–aaX*"), and carboxyl methylation of the newly exposed farnesylcysteine (23, 24). Prelamin A undergoes one additional processing step: cleavage of the last 15 amino acids of the protein, including the carboxyl-terminal farnesylcysteine methyl ester. This final step, carried out by the metalloprotease ZMPSTE24, releases mature lamin A. Lamin C does not have a *CaaX* motif and does not undergo any of these posttranslational processing steps.

Protein farnesylation and methylation have been assumed to be important for the association of the nuclear lamins with the inner nuclear membrane. This notion has been supported by *in vitro* evidence (25) but the *in vivo* relevance of these modifications remained uncertain until the development of *Lmna*[LAO/LAO] mice (21). *Lmna*[LAO/LAO] mice, which produce mature lamin A *directly*—completely bypassing prelamin A synthesis and processing—are phenotypically normal. The levels of mature lamin A in cells and tissues are normal, and there is no significant defect in the ability of lamin A to reach the nuclear rim. Thus, the posttranslational processing of prelamin A is quite dispensable, at least in laboratory mice.

While the posttranslational processing of prelamin A appears to be dispensable, it is important to emphasize that *defects in prelamin A processing can elicit severe disease*. For example, ZMPSTE24 deficiency abolishes the final endoproteolytic cleavage event in lamin A biogenesis, leading to an accumulation of farnesyl–prelamin A in cells and progeria-like disease

phenotypes—both in humans and in mice (26-29). These disease phenotypes can be eliminated by reducing prelamin A synthesis with a single *Lmna* knockout allele (30) or a single *Lmna*[LCO] allele (20), clearly demonstrating that farnesyl–prelamin A was responsible for disease. Also, the classic progeroid syndrome of children, Hutchinson-Gilford progeria syndrome, is caused by a *LMNA* mutation that prevents the conversion of farnesyl–prelamin A to mature lamin A (31, 32). Finally, abolishing *all* prelamin A processing steps leads to cardiomyopathy, as illustrated by a gene-targeted mouse model by Davies *et al.* (22). They created a "nonfarnesylated prelamin A–only" mouse (*Lmna*[nPLAO/nPLAO]) by replacing the cysteine in prelamin A's *CaaX* motif with a serine. In *Lmna*[nPLAO/nPLAO] mice, prelamin A does not undergo farnesylation, nor does it undergo any of the subsequent posttranslational processing steps. The nonfarnesylated prelamin A in *Lmna*[nPLAO/nPLAO] mice is targeted quite normally to the nuclear rim, indistinguishable from mature lamin A in wild-type mice, but the *Lmna*[nPLAO/nPLAO] mice develop a dilated cardiomyopathy and die by 6–8 months of age (22).

Physiologic Importance of B-type Lamins in Mammalian Cells

The B-type lamins have been assumed, based on *in vitro* studies (33-37), to be essential in eukaryotic cells, with unique and vital roles in DNA replication, the formation of the mitotic spindle, gene transcription, and a variety of other processes in the cell nucleus. However, until recently, the importance of B-type lamins had never been tested *in vivo* with appropriate mouse models. Yang *et al.* (38, 39) generated *Lmnb1* and *Lmnb2* conditional knockout alleles, making it possible to eliminate B-type lamins in specific cell types. Remarkably, the loss of both lamin B1 and B2 in skin keratinocytes has no perceptible effect on keratinocyte growth or on the complex developmental programs involved in the generation of the skin and adnexal structures.

5

Misshapen nuclei can be observed in *Lmnb1/Lmnb2*–deficient keratinocytes in culture, but misshapen nuclei were never found within the skin of the keratinocyte-specific *Lmnb1/Lmnb2*– deficient mice (38). Similarly, the loss of B-type lamins has no adverse effects on liver hepatocytes (39). These studies suggest that B-type lamins are dispensable, at least in some cell types, and raise doubts about whether the B-type lamins truly have *unique* roles in mitosis, DNA replication, *etc*. Of note, skin keratinocytes and hepatocytes express A-type lamins; thus, it is possible that the nuclear lamin proteins have redundant roles in the cell nucleus and the A-type lamins are able to compensate for the loss of both B-type lamins.

Both lamin B1 and lamin B2 terminate with a *CaaX* motif (Figure 1.1) and undergo farnesylation, endoproteolytic cleavage of the last three amino acids, and methylation of the farnesylcysteine. Unlike prelamin A, however, there is no additional endoproteolytic cleavage step; thus, the B-type lamins retain their carboxyl-terminal farnesylcysteine methyl ester. For both lamin B1 and lamin B2, the physiological relevance of the carboxyl-terminal posttranslational processing events is uncertain and needs to be investigated by creating knock-in mice that express nonfarnesylated versions of these proteins.

A Role for B-type Lamins in Brain Development

The essential role of B-type lamins in the developing brain was first uncovered by Coffinier *et al.* (40) during the characterization of lamin B2–deficient mice (*Lmnb2$^{-/-}$*). *Lmnb2$^{-/-}$* mice die at birth; however, newborn *Lmnb2$^{-/-}$* mice are normal in size and there are no histopathological abnormalities in any organs, except for the brain. The brain in *Lmnb2$^{-/-}$* mice is slightly smaller than normal, and there is a striking defect in the layering of neurons within the cerebral cortex. Subsequent studies of *Lmnb2$^{-/-}$* embryos revealed a defect in the migration of neurons from the

ventricular zone to the cortical plate. The neuronal migration defect was documented both by BrdU birthdating experiments and immunohistochemical studies with cortical layer–specific markers (40). The development of the cerebellum is also profoundly abnormal in *Lmnb2*$^{-/-}$ embryos, with a complete absence of foliation and an absence of a discrete Purkinje cell layer. The layering of neurons in the hippocampus is also perturbed in *Lmnb2*$^{-/-}$ embryos (40).

Occasional neurons in the cortical plate of *Lmnb2*$^{-/-}$ embryos have "comet-shaped" nuclei with detached centrosomes (located >20 μm from the cell nuclei) (41). These "stretched out" nuclei were never observed in wild-type brains. Lamin B1 remains uniformly distributed at the nuclear rim in *Lmnb2*$^{-/-}$ neurons.

We proposed that the "stretched out" nuclei in *Lmnb2*$^{-/-}$ neurons are likely a consequence of the deformational stresses associated with nucleokinesis during neuronal migration (42, 43). A crucial step in neuronal migration is pulling the cell nucleus forward (by cytoplasmic motors) toward the centrosome in the direction of the leading edge of the cell (42, 43). We suspect that the structural integrity of the nuclear envelope is compromised by the absence of lamin B2 (particularly since there is little or no *Lmna* expression in neurons during development) (41). We have suggested that the same forces that are meant to pull the nucleus forward are responsible for "stretching out" the nucleus (creating the distinctive comet-shaped nucleus) in *Lmnb2*$^{-/-}$ neurons (41-43).

Lmnb2$^{-/-}$ embryonic fibroblasts exhibit few abnormalities; *Lmnb2*$^{-/-}$ fibroblasts grow normally and do not exhibit aneuploidy (40). Staining of *Lmnb2*$^{-/-}$ embryonic fibroblasts with antibodies against several nuclear envelope proteins did not uncover abnormalities in nuclear shape (40).

After uncovering a role for lamin B2 in the developing brain, Coffinier and coworkers

7

were interested in ascertaining the importance of lamin B1 in brain development (41).   In approaching this problem, they built on earlier studies by Vergnes *et al.* (44), who had generated lamin B1–deficient mice (*Lmnb1*$^{\Delta/\Delta}$) with a gene-trap ES cell clone. *Lmnb1*$^{\Delta/\Delta}$ mice synthesize a lamin B1–βgeo fusion protein that lacks a large fraction of the lamin B1 coding sequences, including two known phosphorylation sites, the nuclear localization signal, and the carboxyl-terminal *CaaX* motif (44). *Lmnb1*$^{\Delta/\Delta}$ mice were abnormally small during development and died shortly after birth, with abnormalities in lung and bones (44). In the work by Vergnes and coworkers, the possibility of neuropathology was not specifically investigated, but the authors did note that the calvarium in *Lmnb1*$^{\Delta/\Delta}$ mice was abnormally flattened and that these mice had abnormalities in the cranial sutures (44).   Interestingly, *Lmnb1*$^{\Delta/\Delta}$ embryonic fibroblasts in culture had misshapen nuclei and exhibited a reduced replication rate, polyploidy, and premature senescence (44).

When Coffinier *et al.* (41) examined the brains of *Lmnb1*$^{\Delta/\Delta}$ embryos, they found that the characteristic layering of neurons in the cerebral cortex is markedly abnormal. Using a combination of BrdU birthdating and immunohistochemistry studies, they showed that the neuronal layering defect is due to defective neuronal migration. They also found that the cortical plate of *Lmnb1*$^{\Delta/\Delta}$ embryos is abnormally thin, with fewer neuronal progenitor cells and more apoptotic cells, implying a defect in neuronal survival. The cerebellum of *Lmnb1*$^{\Delta/\Delta}$ embryos is small and devoid of foliation.

In *Lmnb1*$^{\Delta/\Delta}$ embryos, many of the neurons in the cortical plate contain a solitary nuclear bleb. Also, lamin B2 is asymmetrically distributed at the nuclear rim, with a large fraction of the lamin B2 being located at the rim of the nuclear bleb (41). The authors suggested that the solitary bleb might be the consequence of the deformational forces that occur with nucleokinesis during

neuronal migration (41). We have observed the same "solitary nuclear blebs" in cells of peripheral tissues of *Lmnb1*$^{\Delta/\Delta}$ embryos (unpublished observations), raising the possibility that deformational forces on cell nuclei could exist in peripheral tissues as well.

To investigate the role of the B-type lamins in the postnatal brain, Coffinier *et al.* (41) took advantage of a forebrain-specific *Cre* transgene (*Emx1-Cre*) (45) and conditional knockout alleles for *Lmnb1* and *Lmnb2* (38) to create forebrain-specific *Lmnb1* and *Lmnb2* knockout mice (*Emx1-Cre Lmnb1*$^{fl/fl}$ and *Emx1-Cre Lmnb2*$^{fl/fl}$, respectively). Immunohistochemical studies showed that the knockout mutations worked as planned; ~90% of the cells in the cortical plate of *Emx1-Cre Lmnb1*$^{fl/fl}$ and *Emx1-Cre Lmnb2*$^{fl/fl}$ embryos have no lamin B1 or lamin B2, respectively. Both forebrain-specific knockout mouse strains are viable, and by four months of age, *Emx1-Cre Lmnb1*$^{fl/fl}$ and *Emx1-Cre Lmnb2*$^{fl/fl}$ mice exhibit a markedly smaller forebrain, suggesting that the postnatal survival of neurons is impaired. Mice lacking both lamin B1 and lamin B2 in the forebrain (*Emx1-Cre Lmnb1*$^{fl/fl}$*Lmnb2*$^{fl/fl}$) were also generated. In *Emx1-Cre Lmnb1*$^{fl/fl}$*Lmnb2*$^{fl/fl}$ embryos, it is possible to identify neurons lacking both lamin B1 and lamin B2. However, in adult *Emx1-Cre Lmnb1*$^{fl/fl}$*Lmnb2*$^{fl/fl}$ mice, the forebrain is completely atrophic; the thin layer of tissue representing the forebrain does not contain neurons, nor does it contain any cells lacking lamins B1 and B2. Thus, it would appear that neurons in the adult brain do not survive in the absence of both B-type lamins.

Misshapen cell nuclei are common in forebrain neurons of *Emx1-Cre Lmnb1*$^{fl/fl}$ and *Emx1-Cre Lmnb2*$^{fl/fl}$ embryos. Many neurons in *Emx1-Cre Lmnb1*$^{fl/fl}$ embryos contain a solitary nuclear bleb, and comet-shaped nuclei are observed in neurons of *Emx1-Cre Lmnb2*$^{fl/fl}$ embryos. Interestingly, however, few of the neurons in the forebrain of *adult Emx1-Cre Lmnb1*$^{fl/fl}$ and

Emx1-Cre Lmnb2^{fl/fl} mice are misshapen, perhaps because neurons of the adult brain (unlike the neurons of embryos) express lamin C (41, 46).

At this point, we know that both lamin B1 and lamin B2 are crucial for brain development and postnatal neuron survival (40, 41). We also know that the neuropathology in the lamin B2–deficient mice is distinct from that in lamin B1–deficient mice (40, 41). Recently, Lee *et al.* (47) showed that increased expression of one B-type lamin only *partially* ameliorate the abnormalities associated with the loss of the other by generating "reciprocal knock-in mice", supporting an idea that B-type lamins might have unique roles in brain development. However, all these observations do not provide clear-cut insights into how lamin B1 and lamin B2 function differently in brain development; further studies will be required to address this issue.
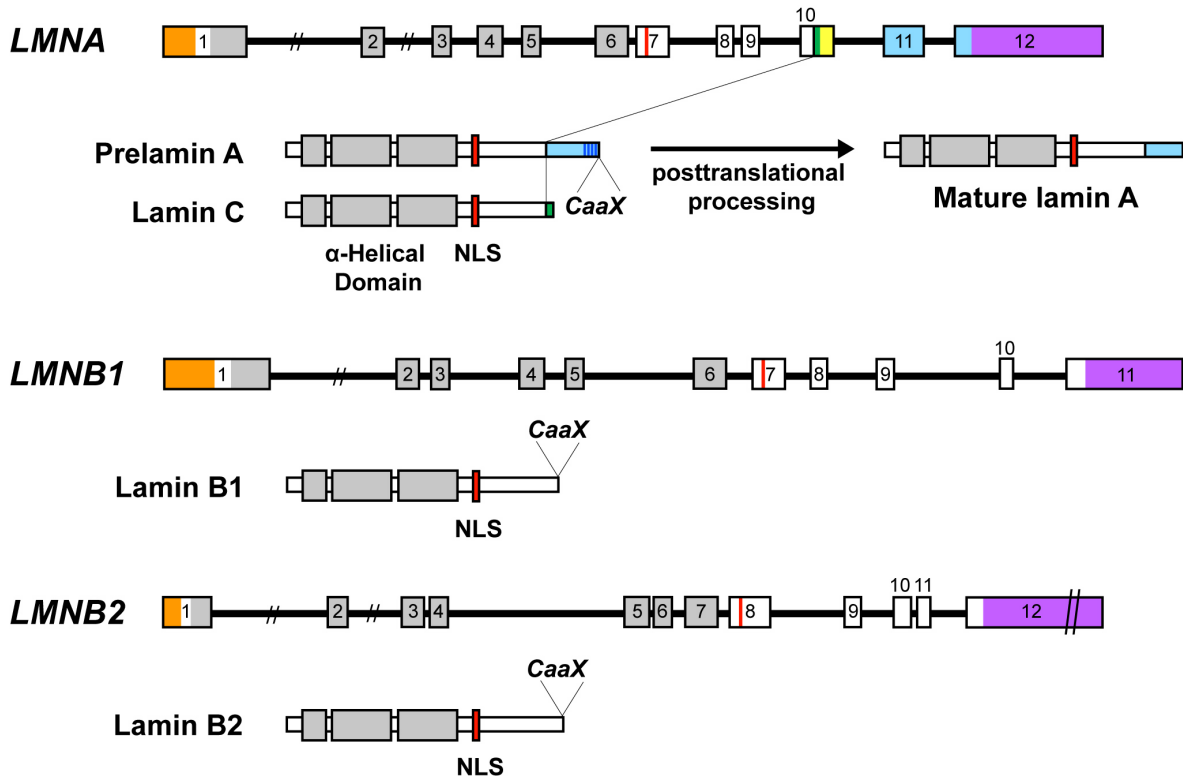
Figure 1.1 Schematic diagram of nuclear lamin genes and nuclear lamin structure. All nuclear lamins have α-helical central rod domains (in grey) flanked by globular head and tail domains. The tail domains contain a nuclear localization signal (NLS, in red). Prelamin A (664 amino acids) and lamin C (572 amino acids) are alternatively spliced products of a single gene, *LMNA*. Lamin C terminates with exon 10 sequences and contains 6 unique amino acids at its carboxyl terminus (in green); prelamin A contains sequences from exons 11 and 12 and contains 98 unique amino acids at its carboxyl terminus (in sky blue). The 3′ UTR for lamin C is yellow; the 3′ UTRs for the other nuclear lamins are purple. The 5′ UTRs are colored orange. Lamin A (646 amino acids) is formed from prelamin A by a series of four posttranslational processing events and involves the removal of the final 18 amino acids of prelamin A. Lamin B1 (586 amino acids) and lamin B2 (600 amino acids) are produced from independent genes, *LMNB1* and *LMNB2,* respectively. All of the lamins,

except lamin C, contain a carboxyl-terminal *CaaX* motif, which triggers protein farnesylation. The farnesylated segment of prelamin A (in sky blue with blue stripes) is removed during the biogenesis of mature lamin A.

REFERENCES

1. Melcer S, Gruenbaum Y, and Krohne G (2007) Invertebrate lamins. *Exp Cell Res* 313:2157-2166.

2. Broers JL, Ramaekers FC, Bonne G, Yaou RB, and Hutchison CJ (2006) Nuclear lamins: laminopathies and their role in premature ageing. *Physiol Rev* 86:967-1008.

3. Worman HJ (2012) Nuclear lamins and laminopathies. *J Pathol* 226:316-325.

4. Dittmer TA, and Misteli T (2011) The lamin protein family. *Genome Biol* 12:222.

5. Rober RA, Weber K, and Osborn M (1989) Differential timing of nuclear lamin A/C expression in the various organs of the mouse embryo and the young animal: a developmental study. *Development* 105:365-378.

6. Lebel S, Lampron C, Royal A, and Raymond Y (1987) Lamins A and C appear during retinoic acid-induced differentiation of mouse embryonal carcinoma cells. *J Cell Biol* 105:1099-1104.

7. Lin F, and Worman HJ (1993) Structural organization of the human gene encoding nuclear lamin A and nuclear lamin C. *J Biol Chem* 268:16321-16326.

8. Lin F, and Worman HJ (1995) Structural organization of the human gene (LMNB1) encoding nuclear lamin B1. *Genomics* 27:230-236.

9. Biamonti G, Giacca M, Perini G, Contreas G, Zentilin L, Weighardt F, Guerra M, Della Valle G, Saccone S, Riva S, and et al. (1992) The gene for a novel human lamin maps at a highly transcribed locus of chromosome 19 which replicates at the onset of S-phase. *Mol Cell Biol* 12:3499-3506.

10. Erber A, Riemer D, Hofemeister H, Bovenschulte M, Stick R, Panopoulou G, Lehrach H, and Weber K (1999) Characterization of the Hydra lamin and its gene: A molecular phylogeny of metazoan lamins. *J Mol Evol* 49:260-271.

11. Davies BS, Coffinier C, Yang SH, Jung HJ, Fong LG, and Young SG (2011) Posttranslational processing of nuclear lamins. The Enzymes, eds F. Tamanoi, C. A. Hrycyna, and M. O. Bergo (Elsevier, Amsterdam), Vol 29, pp 21-41.

12. Fisher DZ, Chaudhary N, and Blobel G (1986) cDNA sequencing of nuclear lamins A and C reveals primary and secondary structural homology to intermediate filament proteins. *Proc Natl Acad Sci U S A* 83:6450-6454.

13. McKeon FD, Kirschner MW, and Caput D (1986) Homologies in both primary and secondary structure between nuclear envelope and intermediate filament proteins. *Nature* 319:463-468.

14. Heitlinger E, Peter M, Lustig A, Villiger W, Nigg EA, and Aebi U (1992) The role of the head and tail domain in lamin structure and assembly: analysis of bacterially expressed chicken lamin A and truncated B2 lamins. *J Struct Biol* 108:74-89.

15. Sullivan T, Escalante-Alcalde D, Bhatt H, Anver M, Bhat N, Nagashima K, Stewart CL, and Burke B (1999) Loss of A-type lamin expression compromises nuclear envelope integrity leading to muscular dystrophy. *J Cell Biol* 147:913-920.

16. Lammerding J, Schulze PC, Takahashi T, Kozlov S, Sullivan T, Kamm RD, Stewart CL, and Lee RT (2004) Lamin A/C deficiency causes defective nuclear mechanics and mechanotransduction. *J Clin Invest* 113:370-378.

17. Bione S, Maestrini E, Rivella S, Mancini M, Regis S, Romeo G, and Toniolo D (1994) Identification of a novel X-linked gene responsible for Emery-Dreifuss muscular dystrophy. *Nat Genet* 8:323-327.

18. Ellis JA, Craxton M, Yates JR, and Kendrick-Jones J (1998) Aberrant intracellular targeting and cell cycle-dependent phosphorylation of emerin contribute to the Emery-Dreifuss muscular dystrophy phenotype. *J Cell Sci* 111 (Pt 6):781-792.

19. Worman HJ, Fong LG, Muchir A, and Young SG (2009) Laminopathies and the long strange trip from basic cell biology to therapy. *J Clin Invest* 119:1825-1836.

20. Fong LG, Ng JK, Lammerding J, Vickers TA, Meta M, Cote N, Gavino B, Qiao X, Chang SY, Young SR, Yang SH, Stewart CL, Lee RT, Bennett CF, Bergo MO, and Young SG (2006) Prelamin A and lamin A appear to be dispensable in the nuclear lamina. *J Clin Invest* 116:743-752.

21. Coffinier C, Jung HJ, Li Z, Nobumori C, Yun UJ, Farber EA, Davies BS, Weinstein MM, Yang SH, Lammerding J, Farahani JN, Bentolila LA, Fong LG, and Young SG (2010) Direct synthesis of lamin A, bypassing prelamin a processing, causes misshapen nuclei in fibroblasts but no detectable pathology in mice. *J Biol Chem* 285:20818-20826.

22. Davies BS, Barnes RH, 2nd, Tu Y, Ren S, Andres DA, Spielmann HP, Lammerding J, Wang Y, Young SG, and Fong LG (2010) An accumulation of non-farnesylated prelamin A causes cardiomyopathy but not progeria. *Hum Mol Genet* 19:2682-2694.

23. Davies BS, Coffinier C, Yang SH, Barnes RH, 2nd, Jung HJ, Young SG, and Fong LG (2011) Investigating the purpose of prelamin A processing. *Nucleus* 2:4-9.

24. Davies BS, Fong LG, Yang SH, Coffinier C, and Young SG (2009) The posttranslational processing of prelamin A and disease. *Annu Rev Genomics Hum Genet* 10:153-174.

25. Hennekes H, and Nigg EA (1994) The role of isoprenylation in membrane attachment of nuclear lamins. A single point mutation prevents proteolytic cleavage of the lamin A precursor and confers membrane binding properties. *J Cell Sci* 107 (Pt 4):1019-1029.

26. Bergo MO, Gavino B, Ross J, Schmidt WK, Hong C, Kendall LV, Mohr A, Meta M, Genant H, Jiang Y, Wisner ER, Van Bruggen N, Carano RA, Michaelis S, Griffey SM, and Young SG (2002) Zmpste24 deficiency in mice causes spontaneous bone fractures, muscle weakness, and a prelamin A processing defect. *Proc Natl Acad Sci U S A* 99:13049-13054.

27. Pendas AM, Zhou Z, Cadinanos J, Freije JM, Wang J, Hultenby K, Astudillo A, Wernerson A, Rodriguez F, Tryggvason K, and Lopez-Otin C (2002) Defective prelamin A processing and muscular and adipocyte alterations in Zmpste24 metalloproteinase-deficient mice. *Nat Genet* 31:94-99.

28. Moulson CL, Go G, Gardner JM, van der Wal AC, Smitt JH, van Hagen JM, and Miner JH (2005) Homozygous and compound heterozygous mutations in ZMPSTE24 cause the laminopathy restrictive dermopathy. *J Invest Dermatol* 125:913-919.

29. Navarro CL, Cadinanos J, De Sandre-Giovannoli A, Bernard R, Courrier S, Boccaccio I, Boyer A, Kleijer WJ, Wagner A, Giuliano F, Beemer FA, Freije JM, Cau P, Hennekam RC, Lopez-Otin C, Badens C, and Levy N (2005) Loss of ZMPSTE24 (FACE-1) causes autosomal recessive restrictive dermopathy and accumulation of Lamin A precursors. *Hum Mol Genet* 14:1503-1513.

30. Fong LG, Ng JK, Meta M, Cote N, Yang SH, Stewart CL, Sullivan T, Burghardt A, Majumdar S, Reue K, Bergo MO, and Young SG (2004) Heterozygosity for Lmna deficiency eliminates the progeria-like phenotypes in Zmpste24-deficient mice. *Proc Natl Acad Sci U S A* 101:18111-18116.

31. De Sandre-Giovannoli A, Bernard R, Cau P, Navarro C, Amiel J, Boccaccio I, Lyonnet S, Stewart CL, Munnich A, Le Merrer M, and Levy N (2003) Lamin a truncation in Hutchinson-Gilford progeria. *Science* 300:2055.

32. Eriksson M, Brown WT, Gordon LB, Glynn MW, Singer J, Scott L, Erdos MR, Robbins CM, Moses TY, Berglund P, Dutra A, Pak E, Durkin S, Csoka AB, Boehnke M, Glover TW, and Collins FS (2003) Recurrent de novo point mutations in lamin A cause Hutchinson-Gilford progeria syndrome. *Nature* 423:293-298.

33. Harborth J, Elbashir SM, Bechert K, Tuschl T, and Weber K (2001) Identification of essential genes in cultured mammalian cells using small interfering RNAs. *J Cell Sci* 114:4557-4565.

34. Belmont AS, Zhai Y, and Thilenius A (1993) Lamin B distribution and association with peripheral chromatin revealed by optical sectioning and electron microscopy tomography. *J Cell Biol* 123:1671-1685.

35. Tsai MY, Wang S, Heidinger JM, Shumaker DK, Adam SA, Goldman RD, and Zheng Y (2006) A mitotic lamin B matrix induced by RanGTP required for spindle assembly. *Science* 311:1887-1893.

36. Moir RD, Montag-Lowy M, and Goldman RD (1994) Dynamic properties of nuclear lamins: lamin B is associated with sites of DNA replication. *J Cell Biol* 125:1201-1212.

37. Tang CW, Maya-Mendoza A, Martin C, Zeng K, Chen S, Feret D, Wilson SA, and Jackson DA (2008) The integrity of a lamin-B1-dependent nucleoskeleton is a fundamental determinant of RNA synthesis in human cells. *J Cell Sci* 121:1014-1024.

38. Yang SH, Chang SY, Yin L, Tu Y, Hu Y, Yoshinaga Y, de Jong PJ, Fong LG, and Young SG (2011) An absence of both lamin B1 and lamin B2 in keratinocytes has no effect on cell proliferation or the development of skin and hair. *Hum Mol Genet* 20:3537-3544.

39. Yang SH, Jung HJ, Coffinier C, Fong LG, and Young SG (2011) Are B-type lamins essential in all mammalian cells? *Nucleus* 2:562-569.

40. Coffinier C, Chang SY, Nobumori C, Tu Y, Farber EA, Toth JI, Fong LG, and Young SG (2010) Abnormal development of the cerebral cortex and cerebellum in the setting of lamin B2 deficiency. *Proc Natl Acad Sci U S A* 107:5076-5081.

41. Coffinier C, Jung HJ, Nobumori C, Chang S, Tu Y, Barnes RH, 2nd, Yoshinaga Y, de Jong PJ, Vergnes L, Reue K, Fong LG, and Young SG (2011) Deficiencies in lamin B1 and lamin B2 cause neurodevelopmental defects and distinct nuclear shape abnormalities in neurons. *Mol Biol Cell* 22:4683-4693.

42. Solecki DJ, Govek EE, Tomoda T, and Hatten ME (2006) Neuronal polarity in CNS development. *Genes Dev* 20:2639-2647.

43. Salina D, Bodoor K, Eckley DM, Schroer TA, Rattner JB, and Burke B (2002) Cytoplasmic dynein as a facilitator of nuclear envelope breakdown. *Cell* 108:97-107.

44. Vergnes L, Peterfy M, Bergo MO, Young SG, and Reue K (2004) Lamin B1 is required for mouse development and nuclear integrity. *Proc Natl Acad Sci U S A* 101:10428-10433.

45. Gorski JA, Talley T, Qiu M, Puelles L, Rubenstein JL, and Jones KR (2002) Cortical excitatory neurons and glia, but not GABAergic neurons, are produced in the Emx1-expressing lineage. *J Neurosci* 22:6309-6314.

46. Jung HJ, Coffinier C, Choe Y, Beigneux AP, Davies BS, Yang SH, Barnes RH, 2nd, Hong J, Sun T, Pleasure SJ, Young SG, and Fong LG (2012) Regulation of prelamin A but not lamin C by miR-9, a brain-specific microRNA. *Proc Natl Acad Sci U S A* 109:E423-431.

47. Lee JM, Tu Y, Tatar A, Wu D, Nobumori C, Jung HJ, Yoshinaga Y, Coffinier C, de Jong PJ, Fong LG, and Young SG (2014) Reciprocal knock-in mice to investigate the functional redundancy of lamin B1 and lamin B2. *Mol Biol Cell*.

Chapter 2:

Regulation of Prelamin A but Not Lamin C by MiR-9, a Brain-specific MicroRNA

Regulation of prelamin A but not lamin C by miR-9, a brain-specific microRNA

Hea-Jin Jung[a], Catherine Coffinier[b], Youngshik Choe[c], Anne P. Beigneux[b], Brandon S. J. Davies[b], Shao H. Yang[b], Richard H. Barnes II[b], Janet Hong[d], Tao Sun[d], Samuel J. Pleasure[c], Stephen G. Young[a,b,e,1], and Loren G. Fong[b,1]

[a]Molecular Biology Institute and Departments of [b]Medicine and [e]Human Genetics, University of California, Los Angeles, CA 90095; [c]Department of Neurology, University of California, San Francisco, CA 94158; and [d]Department of Cell and Developmental Biology, Weill Medical College of Cornell University, New York, NY 10065

Lamins A and C, alternatively spliced products of the *LMNA* gene, are key components of the nuclear lamina. The two isoforms are found in similar amounts in most tissues, but we observed an unexpected pattern of expression in the brain. Western blot and immunohisto-chemistry studies showed that lamin C is abundant in the mouse brain, whereas lamin A and its precursor prelamin A are restricted to endothelial cells and meningeal cells and are absent in neurons and glia. Prelamin A transcript levels were low in the brain, but this finding could not be explained by alternative splicing. In lamin A-only knockin mice, where alternative splicing is absent and all the output of the gene is channeled into prelamin A transcripts, large amounts of lamin A were found in peripheral tissues, but there was very little lamin A in the brain. Also, in knockin mice expressing exclusively progerin (a toxic form of prelamin A found in Hutchin-son–Gilford progeria syndrome), the levels of progerin in the brain were extremely low. Further studies showed that prelamin A expression, but not lamin C expression, is down-regulated by a brain-specific microRNA, miR-9. Expression of miR-9 in cultured cells reduced lamin A expression, and this effect was abolished when the miR-9–binding site in the prelamin A 3′ UTR was mutated. The down-regulation of prelamin A expression in the brain could explain why mouse models of Hutchinson–Gilford progeria syndrome are free of central nervous system pathology.

genetic diseases | A-type lamins | nucleus | differential gene expression | silencing

The nuclear lamina, an intermediate filament meshwork located adjacent to the inner nuclear membrane, provides scaffolding for the cell nucleus and plays a role in many vital processes in the cell, including the regulation of gene expression and chromatin structure (1, 2). The nuclear lamina is composed primarily of four lamin proteins: lamins A, B1, B2, and C (3). Lamins B1 and B2, generally referred to as the "B-type lamins," are products of independent genes (*LMNB1* and *LMNB2*, respectively). Lamins A and C, called the "A-type lamins," are alternatively spliced products of the same gene, *LMNA*, and are found in roughly similar amounts in most tissues (4). The lamin C transcript contains exon 1–10 sequences, whereas the transcript for prelamin A (the precursor to lamin A) contains exon 1–12 sequences; the 3′ UTRs of the two transcripts are distinct.

Prelamin A, but not lamin C, terminates with a *CaaX* motif and undergoes farnesylation of the carboxyl-terminal cysteine (the "*C*" of the *CaaX* motif). Following protein farnesylation, prelamin A undergoes three additional processing steps: endo-proteolytic release of the last three amino acids of the protein (i.e., the *–aaX*), methylation of the newly exposed farnesylcys-teine, and a second endoproteolytic cleavage event, mediated by ZMPSTE24, that releases 15 additional amino acids from the carboxyl terminus, including the farnesylcysteine methyl ester (5, 6). The last cleavage step releases mature lamin A.

Lamins A and C have attracted considerable interest with the discovery that mutations in *LMNA* cause multiple human diseases (5). Missense mutations involving residues common to lamins A and C have been shown to cause muscular dystrophy,

cardiomyopathy, and lipodystrophy (5). However, a few mutations, for example those causing Hutchinson–Gilford progeria syndrome (HGPS), alter the structure of prelamin A without affecting lamin C (7, 8). In HGPS, single-nucleotide mutations lead to aberrant mRNA splicing, resulting in the synthesis of a mutant prelamin A, generally called "progerin," that has an in-frame deletion of 50 amino acids. That deletion does not affect the farnesylation or methylation of the carboxyl terminus but abolishes the final step in lamin A biogenesis; hence, progerin retains a farnesylcysteine methyl ester at its carboxyl terminus. Progerin is toxic to cells and elicits pathology in multiple tissues, resulting in phenotypes resembling physiologic aging (e.g., atherosclerosis, alopecia, and osteoporosis) (9). However, some phenotypes commonly associated with aging, for example senile dementia, are absent. Several years ago, Yang et al. (10) generated a knockin mouse model that produces high levels of progerin (*Lmna*[HG/+] mice); these mice develop many progeria-like disease phenotypes; however, the central nervous system is free of disease.

We sought to understand why knockin mice that synthesize a toxic protein, namely progerin, might be spared from central nervous system pathology. One potential explanation would be that the brain, in contrast to other tissues, synthesizes mainly lamin C and little prelamin A. In the current study, we tested that possibility and in the process uncovered a mechanism for the regulation of prelamin A expression.

Results

We began by using Western blots to examine lamin A and lamin C expression in different tissues of wild-type mice (*Lmna*^{+/+}) (Fig. 1*A*). Consistent with earlier studies (4, 11, 12), large amounts of both lamin A and lamin C were found in the liver, heart, and kidney, with the lamin A band being slightly more intense than the lamin C band (Fig. 1*A*). In contrast, the cerebellum and cerebral cortex expressed mainly lamin C and far less lamin A (Fig. 1*A*). Neither lamin A nor lamin C was expressed in tissues of *Lmna*^{−/−} mice (13).

The preferential expression of lamin C in the brain was supported further by Western blots of tissue extracts from *Zmpste24*^{−/−} mice (Fig. 1*B*). ZMPSTE24 deficiency abolishes the production of mature lamin A and leads to the accumulation of a farnesylated form of prelamin A in cells (14, 15). We observed

Fig. 1. Distinct expression patterns of lamins A and C in the mouse brain. (*A*) Western blot of tissue extracts from *Lmna*$^{+/+}$ (wild-type) and *Lmna*$^{-/-}$ mice with antibodies against lamin A/C, lamin B2, and actin. (*B*) Western blot of tissue extracts from *Zmpste24*$^{+/+}$ and *Zmpste24*$^{-/-}$ mice (14) with antibodies against lamin A/C, prelamin A, and actin. (*C*) Immunofluorescence microscopy images of tissues from wild-type (*Zmpste24*$^{+/+}$) and *Zmpste24*$^{-/-}$ mice. Frozen sections of liver, cerebellum, and cerebral cortex were stained with antibodies against prelamin A (green) and lamin A/C (red); DNA was stained with DAPI. Prelamin A was undetectable in *Zmpste24*$^{+/+}$ mice. Prelamin A was present in the brain of *Zmpste24*$^{-/-}$ mice but only in scattered cells within the parenchyma of the brain and meningeal cells. (Scale bar, 100 μm.)

substantial amounts of prelamin A in the peripheral tissues of *Zmpste24*$^{-/-}$ mice, but far less prelamin A was detected in the cerebellum and cerebral cortex (Fig. 1*B*).

The low levels of prelamin A expression in the brain of *Zmpste24*$^{-/-}$ mice were obvious by immunohistochemistry (Fig. 1*C*). In the tissues of wild-type mice (*Zmpste24*$^{+/+}$), staining for prelamin A was virtually undetectable, reflecting the fact that prelamin A is converted efficiently to mature lamin A (Fig. 1*C*) (16). In the liver of *Zmpste24*$^{-/-}$ mice, prelamin A accumulates; hence cell nuclei were stained with both a prelamin A-specific

antibody and a lamin A/C antibody. In the brain, however, the staining patterns for the two antibodies were different; the lamin A/C antibody bound to the nuclei of all cells, but staining with the prelamin A antibody was restricted to scattered cells in the parenchyma of the brain and meningeal cells on the surface of the brain.

Similar immunohistochemical findings were observed in tissues of wild-type mice stained with antibodies against lamin A, lamin C, and lamin B2 (Fig. S1). In the liver of wild-type mice, cell nuclei were stained with both lamin A- and lamin C-specific antibodies. In the brain, nearly all cells were stained by the lamin C antibody, but only cells along the surface of the brain and scattered cells within the brain were stained positively with the lamin A antibody (Fig. S1). As expected, neither lamin A nor lamin C was detected in *Lmna*$^{-/-}$ mouse tissues, and lamin B2 was expressed by all cells in both wild-type and *Lmna*$^{-/-}$ mice (Fig. S1).

We suspected that most prelamin A- and lamin A-positive cells within the brain parenchyma (Fig. 1*C* and Fig. S1) were vascular endothelial cells. To examine this notion, a fluorescently labeled tomato lectin (17) was injected i.v. into wild-type mice to stain endothelial cells, and the tissues then were examined by immunohistochemistry (Fig. 2*A* and Fig. S2). Again, we found ubiquitous expression of lamin C in the brain, whereas lamin A expression was restricted to meningeal cells along the surface of the brain and cells associated with lectin-stained blood vessels. Staining of the brain with an antibody against CD31 (a marker of endothelial cells) confirmed that most lamin A-expressing cells in the brain are vascular cells (Fig. 2*B*).

To characterize lamin A-expressing cells in the brain further, we stained brain sections from wild-type mice with an antibody against lamin A in combination with an antibody against lamin C, GFAP, Olig2, Zic2, or NeuN (Fig. S3). The antibodies against GFAP and a transcription factor, Olig2, identified astrocytes and oligodendrocytes, respectively; an antibody against NeuN was used as a neuronal marker, and an antibody against Zic2 served as a marker for Purkinje cells. We observed lamin C expression throughout the brain, including Purkinje cells and granular cells of the cerebellum (Fig. S3 *A and C*, *Top*). In contrast, lamin A was not found in Zic2$^+$ Purkinje cells in the cerebellum or Olig2$^+$ oligodendrocytes in the cerebellum and hippocampus (Fig. S3 *A and B*). Most regions of the brain that were stained positively for GFAP were devoid of lamin A (Fig. S3 *A and B*). NeuN$^+$ cells in the granular layer of the cerebellum were stained positively for lamin C but not lamin A (Fig. S3*C*). These observations, combined with the lectin/CD31 immunohisto-chemistry studies (Fig. 2 and Fig. S2), suggest that most cells in the brain express lamin C but that lamin A is restricted mainly to vascular and meningeal cells.

Cultured neurons also preferentially express lamin C. We isolated neural progenitor cells (NPCs) from the cortex of E13.5 wild-type mouse embryos and allowed them to differentiate in culture. By Western blot, a prominent lamin C band was detected after 12 d of culture, but the lamin A band was faint (Fig. S4*A*). Immunocytochemistry with antibodies against lamin A, lamin C, and β3 tubulin (a neuron-specific tubulin) supported the idea that neurons express primarily lamin C. Cell nuclei that were surrounded by β3 tubulin (TU-20)-positive cytoplasm were positive for lamin C but not lamin A (Fig. S4 *B–D*), whereas lamin A-expressing cells were negative for β3 tubulin (Fig. S4 *B–D*).

The preferential expression of lamin C protein in the brain prompted us to examine the expression of prelamin A and lamin C transcripts. We began with Northern blots using a probe common to prelamin A and lamin C transcripts (Fig. 3*A*). In the kidney of wild-type mice, the intensities of the prelamin A and lamin C bands were similar. The intensities of the lamin C bands in the brain were similar to those in the kidney, but the prelamin A bands were faint. We also examined transcripts in two *Lmna* knockin mice—
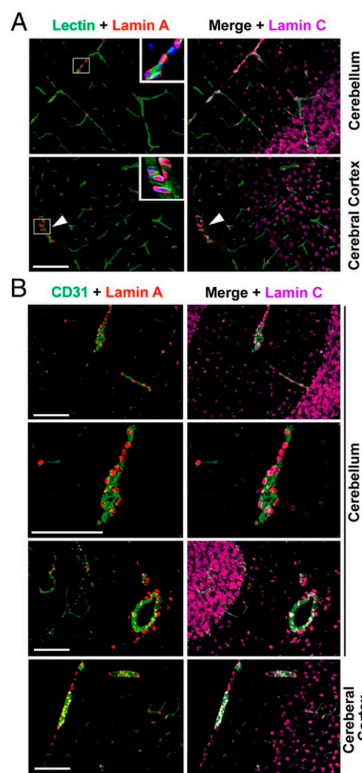
Fig. 2. Cells expressing lamin A in the mouse brain are located predominantly in blood vessels and meninges. (*A*) FITC-labeled tomato lectin (17) (green) was injected i.v. into wild-type mice to stain blood vessels. Frozen sections of the brain were stained for lamin A (red) and lamin C (magenta). Lamin C was found in most cells in the brain, but lamin A was found mainly in association with capillaries or meningeal cells lining the surface of the brain (arrowhead). (Scale bar, 100 μm.) *Insets* show high-magnification views of lamin A expression in lectin-positive blood vessels. Nuclei were stained with DAPI (blue). (*B*) Frozen sections of the brain from wild-type mice were stained with antibodies against lamin A (red), lamin C (magenta), and CD31 (green). Most lamin A–positive cells were found in association with CD31, a marker of endothelial cells. (Scale bars, 100 μm.)

Lmna$^{\text{LAO/LAO}}$ mice that express exclusively mutant prelamin A transcripts encoding mature lamin A (18) and *Lmna*$^{\text{nHG/nHG}}$ mice that express mutant prelamin A transcripts encoding non-farnesylated progerin (*Materials and Methods*) (12). Lamin C transcripts were absent, as expected, in both knockin models, but, similar to wild-type mice, the levels of prelamin A transcripts were much lower in the brain than in the kidney (Fig. 3*A*).

We performed quantitative RT-PCR (qRT-PCR) on RNA from tissues of wild-type mice to quantify (*i*) prelamin A transcripts, using primers unique to prelamin A; (*ii*) lamin C transcripts, using primers unique to lamin C; (*iii*) lamin B1 transcripts; and (*iv*) total *Lmna* transcripts, using primers that bind to sequences common to prelamin A and lamin C (Fig. 3*B*). Expression levels were normalized to those in the liver (set as 1.0). Consistent with the Northern blots, the levels of lamin C transcripts in the cerebellum and cerebral cortex were nearly (∼85%) as high as those in the peripheral tissues (Fig. 3*B*). In contrast, the levels of prelamin A transcripts in the cerebellum
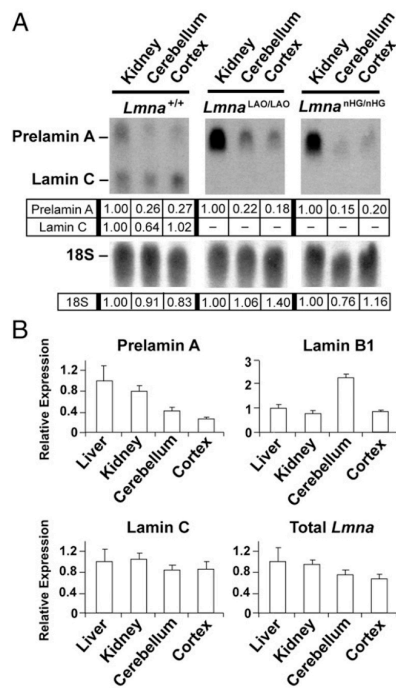
Fig. 3. Preferential expression of lamin C transcripts in the mouse brain. (*A*) Northern blot of total RNA from *Lmna*$^{+/+}$, *Lmna*$^{\text{LAO/LAO}}$, and *Lmna*$^{\text{nHG/nHG}}$ mice with a ^{32}P-labeled probe made from cDNA sequences shared by prelamin A and lamin C transcripts. An 18S rRNA probe was used as a loading control. Signals were quantified with ImageJ software, and values were normalized to those in the kidney (set at a value of 1.0). (*B*) qRT-PCR analysis of prelamin A, lamin B1, lamin C, and total *Lmna* transcripts in wild-type mouse tissues. Data were normalized to cyclophilin A, and gene expression was compared with that in the liver (which was set at 1.0). Values represent mean ± SD from four different wild-type mice.

and cortex were only 25–40% of those in the liver. Consistent with those results, total *Lmna* transcripts were ∼65–75% as high as those in the liver.

The preferential expression of lamin C in the brain was confirmed by in situ hybridization. In the brain of a wild-type mouse, *Lmna* expression was detected easily with a riboprobe common to prelamin A and lamin C, but not with a prelamin A-specific probe (Fig. S5). As expected, no hybridization signal was detected in the brain of an *Lmna*$^{-/-}$ mouse (Fig. S5).

We initially suspected that alternative mRNA splicing would explain the preferential expression of lamin C in the brain. To test this idea, we examined lamin A expression in *Lmna*$^{\text{LAO/LAO}}$ mice in which all the output of the *Lmna* gene is channeled into the production of mutant prelamin A transcripts encoding mature lamin A (18). Because lamin C splicing is absent in these mice, we expected to find increased levels of lamin A in the brain (i.e., levels comparable to lamin C levels in the brain of wild-type mice). To our surprise, Western blots revealed very low levels of lamin A in the cerebellum and cortex (Fig. 4*A*), consistent with our Northern blot findings (Fig. 3*A*). Furthermore, by immuno-histochemistry, lamin A was nearly absent in the brain of *Lmna*$^{\text{LAO/LAO}}$ mice, except in vascular structures and meningeal cells (Fig. 4*B*). Thus, even though all the output of the *Lmna*$^{\text{LAO}}$ allele was channeled into production of prelamin A transcripts,

23
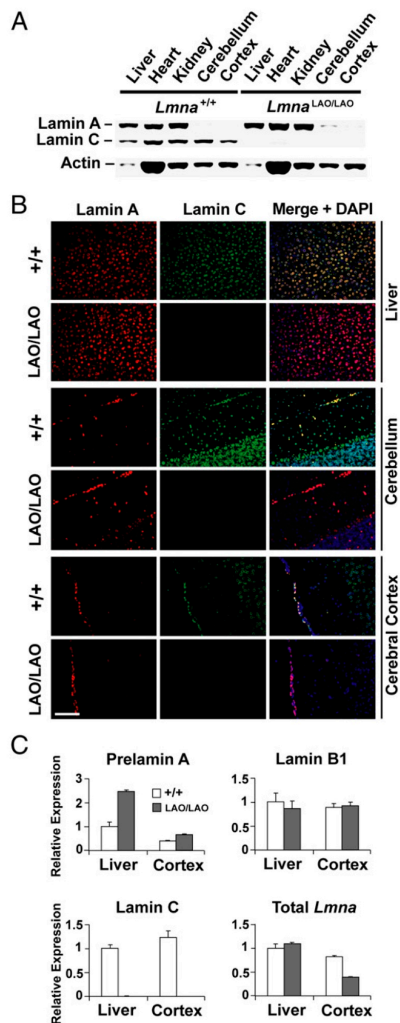
Fig. 4. Low expression levels of lamin A in the brain of *Lmna*[LAO/LAO] mice, in which all the output of the *Lmna* gene is channeled into the production of prelamin A transcripts (18). (*A*) Western blot of tissue extracts from *Lmna*^{+/+} and *Lmna*[LAO/LAO] mice with antibodies against lamin A/C and actin. (*B*) Immunofluorescence microscopy of the liver, cerebellum, and cerebral cortex from *Lmna*^{+/+} and *Lmna*[LAO/LAO] mice. Sections were stained with antibodies against lamin A (red) and lamin C (green), and nuclei were visualized with DAPI. The lamin A expression pattern in the brain of *Lmna*[LAO/LAO] mice was virtually identical to that in wild-type mice (Figs. 1 and 2), with scattered lamin A-positive vascular cells. (Scale bar, 100 μm.) (*C*) qRT-PCR analysis of prelamin A, lamin B1, lamin C, and total *Lmna* transcripts in the liver and cortex of *Lmna*^{+/+} and *Lmna*[LAO/LAO] mice. Data were normalized to cyclophilin A, and gene expression was compared with that of the wild-type liver (which was set at 1.0). Values represent mean ± SD from three pairs of mice.

the levels of lamin A in the brain of *Lmna*[LAO/LAO] mice were low, similar to the situation in wild-type mice (Fig. 4 *A* and *B*).

The low levels of lamin A in the brain of *Lmna*[LAO/LAO] mice, as judged by both Western blots and immunohistochemistry, prompted us to investigate further the *Lmna* transcript levels in

those mice (Fig. 4*C*). In the liver of *Lmna*[LAO/LAO] mice, the total *Lmna* transcript levels were virtually identical to those in wild-type mice (i.e., the absence of lamin C expression was offset by twice-normal expression of prelamin A). In the cerebral cortex, however, total *Lmna* transcript levels were much lower than those in wild-type mice (Fig. 4*C*).

We also examined the expression of progerin in the brain of mice harboring an *Lmna*[nHG] allele (which yields prelamin A transcripts encoding nonfarnesylated progerin but no lamin C transcripts) (12). Again, lamin A and progerin levels were quite low in the cerebellum and cerebral cortex of *Lmna*[nHG/+] and *Lmna*[nHG/nHG] mice (Fig. 5), in keeping with findings in wild-type (Fig. 1*A*), *Zmpste24*^{−/−} (Fig. 1*B*), and *Lmna*[LAO/LAO] mice (Fig. 4*A*).

We considered the possibility that the low levels of prelamin A transcripts in the brain might be caused by low transcription rates. To address this possibility, we measured heterogeneous nuclear RNA (hnRNA) levels (i.e., pre-mRNA levels) for prelamin A in the brain and liver of wild-type and *Lmna*[LAO/LAO] mice. Interestingly, prelamin A hnRNA levels were higher in the brain than in the liver (Fig. S6 *A* and *B*), weighing against the possibility of reduced prelamin A transcription in the brain. Also, we considered the possibility that the low levels of prelamin A transcripts in the brain somehow might relate to the use of a different *Lmna* promoter in the brain. However, 5′-RACE experiments did not support this idea; the 5′ UTR of *Lmna* transcripts in the brain was identical to that in other tissues (Fig. S6*C*).

The low levels of lamin A in the brain of *Lmna*[LAO/LAO] mice and the low levels of progerin in the brain of *Lmna*[nHG/nHG] mice led us to suspect that the brain must have a mechanism other than alternative splicing for reducing prelamin A expression, and we hypothesized that this mechanism might involve the prelamin A 3′ UTR. The prelamin A 3′ UTR contains sequences that are predicted by miRanda (http://www.microrna.org/microrna/home. do) to be binding sites for two brain-specific microRNAs—one for miR-9 (site 2 in Fig. 6*A*) and one for miR-129. In addition, by scanning the 3′ UTR sequences, we identified another potential miR-9–binding site in the prelamin A 3′ UTR (site 1 in Fig. 6*A*). We also identified a potential miR-9–binding site in the lamin C 3′ UTR (C-site 1 in Fig. 6*A*).

To assess the relevance of miR-9 and miR-129 in regulating lamin A/C expression, miR-9 or miR-129 expression vectors were transfected into HeLa cells (which do not express either microRNA), and cells were subjected to selection with puromycin. HeLa cells transfected with miR-9 expressed high levels of miR-9, but these levels were lower than those in the cerebral cortex of 1-mo-old mice (Fig. S7). Transfection of the miR-129 vector yielded miR-129 levels that were higher than those in the cerebral cortex of 1-mo-old mice (Fig. S7). As judged by Western blots, lamin A levels in miR-9–expressing cells fell by ∼50% relative to lamin C, but there were no significant changes in lamin A levels in miR-129–transfected cells (Fig. 6 *B* and *C*).
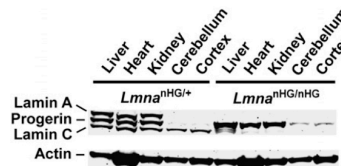
Fig. 5. Western blot analysis of lamin A, lamin C, and progerin expression in tissues of *Lmna*[nHG/+] and *Lmna*[nHG/nHG] mice with antibodies against lamin A/C and actin.

24
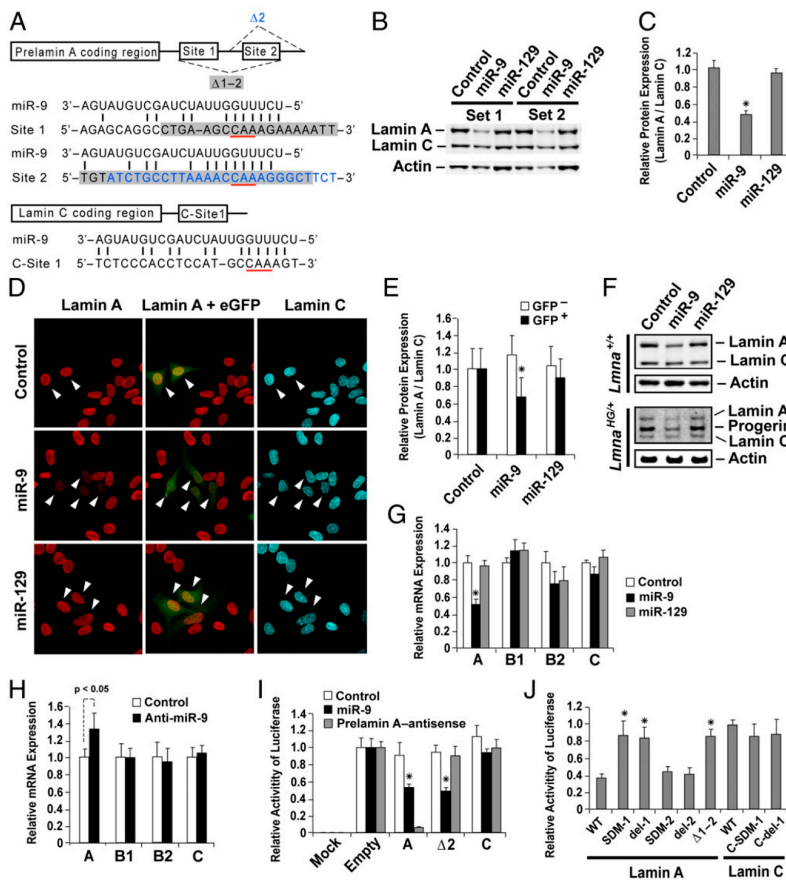
Fig. 6. Down-regulation of lamin A expression by miR-9. (*A*) Predicted miR-9–binding sites in the 3′ UTR of prelamin A and lamin C. The regions that were truncated in luciferase reporter vectors (Δ2 and Δ1–2; see *I* and *J*) are shown, and the exact sequences are indicated by blue font (Δ2) or highlighted in gray (Δ1–2). The three nucleotides that were mutated or deleted in other mutant constructs (SDM-1, del-1, SDM-2, del-2, C-SDM-1, and C-del-1; *J*) are underlined in red. (*B*) Western blot analysis of lamin A and C expression in HeLa cells 3.5 d after transfection with an empty vector, an miR-9 expression vector, or an miR-129 expression vector. All cells had been subjected to puromycin selection. Shown are representative data from two independent experiments (set 1 and set 2). (*C*) Quantification of the lamin A signals in the Western blots (normalized to lamin C levels). Results show mean ± SD from four independent experiments. (*D*) Immunofluorescence microscopy to assess lamin A and C expression in HeLa cells that had been transiently transfected with miR-9 or miR-129 expression vectors (or an empty vector). Transfected cells were identified by EGFP expression (arrowheads). (*E*) Quantification of the immunofluorescence signals from the immunofluorescence microscopy experiments. The lamin A signals were normalized to lamin C. Values represent mean ± SD (from examining ≥146 cells per condition). (*F*) Western blot studies of immortalized *Lmna*^{+/+} and *Lmna*[HG/+] fibroblasts transduced with lentiviruses encoding miR-9 or miR-129 (or an empty vector). All cells had been subjected to puromycin selection. (*G*) qRT-PCR analysis of prelamin A, lamin B1, lamin B2, and lamin C transcript levels in HeLa cells transfected with miR-9 or miR-129 expression vectors (or an empty vector). All cells had been subjected to puromycin selection. Data were normalized to cyclophilin A, and gene expression was compared with that of empty vector–transfected cells (set at 1.0). Values represent mean ± SD from four independent experiments. (*H*) qRT-PCR analysis of prelamin A, lamin B1, lamin B2, and lamin C expression levels in differentiated NPCs transfected with an miR-9 antisense oligonucleotide or a control antisense oligonucleotide. Data were normalized to cyclophilin A, and gene expression in the miR-9 antisense–transfected cells was compared with that of cells transfected with the control oligonucleotides (set at 1.0). Values represent mean ± SD from three independent experiments. (*I*) Luciferase assays in HeLa cells that had been cotransfected with an empty vector or an miR-9 expression vector along with luciferase plasmids harboring the prelamin A 3′ UTR, a truncated version of the prelamin A 3′ UTR (Δ2; see schematic in *A*), or the lamin C 3′ UTR. After 30 h, firefly luciferase activities were measured, normalized to levels of Renilla luciferase activities, and compared with those of empty luciferase vector (pmirGLO)–transfected cells (set at 1.0). An antisense oligonucleotide against prelamin A was used as a control. Values represent mean ± SD from three independent experiments. (*J*) Luciferase assays with luciferase reporter vectors in which the miR-9 seed-binding sequence (CCAAAG) in the 3′ UTR of prelamin A and lamin C was mutated. From left to right: WT, wild-type 3′ UTR of prelamin A; SDM-1, substitution of the three nucleotides in site 1 of the prelamin A 3′ UTR (CAA) with ACC; del-1, deletion of the CAA in site 1 of the prelamin A 3′ UTR; SDM-2, replacement of the CAA in site 2 of the prelamin A 3′ UTR by ACC; del-2, deletion of the CAA in site 2 of the prelamin A 3′ UTR; Δ1–2, an internal truncation encompassing both sites 1 and 2 of the prelamin A 3′ UTR; WT, wild-type 3′ UTR of lamin C; C-SDM-1, replacement of CAA by ACC in site 1 of the lamin C 3′ UTR; C-del-1, deletion of the CAA in site 1 of the lamin C 3′ UTR. After 24 h, firefly luciferase activities were measured, normalized to levels of Renilla luciferase activities, and compared with those from the cells transfected with the luciferase vector containing the wild-type 3′ UTR of lamin C (set at 1.0). Values represent mean ± SD from three independent experiments. *$P < 0.0001$.

Jung et al. PNAS | **February 14, 2012** | vol. 109 | no. 7 | E427

25

We also used immunocytochemistry to assess the effects of miR-9 on the expression of lamin A, lamin C, and lamin B1 in transiently transfected cells (transfected cells could be identified because the microRNA expression vectors also produced EGFP) (Fig. 6 *D* and *E* and Fig. S8). Fluorescence microscopy revealed that miR-9, but not miR-129, reduced lamin A expression in transfected HeLa cells (Fig. 6*D* and Fig. S8). Neither miR-9 nor miR-129 affected lamin C expression (Fig. 6*D*). Quantification of the fluorescent signals with Volocity software (Perkin-Elmer) indicated that lamin A expression was reduced by ~40% in miR-9–transfected cells, relative to lamin C (Fig. 6*E*) or lamin B1 (Fig. S8).

The effects of miR-9 on lamin A expression also were examined in immortalized mouse embryonic fibroblasts (MEFs) (Fig. 6*F*). Wild-type MEFs and MEFs heterozygous for a progerin-only knockin allele ($Lmna^{HG/+}$) were transduced with lentiviruses encoding miR-9 or miR-129 and subjected to puromycin selection. The expression of miR-9, but not miR-129, lowered lamin A levels (relative to lamin C) in $Lmna^{+/+}$ cells, as judged by Western blots (Fig. 6*F*). In $Lmna^{HG/+}$ cells, miR-9 reduced levels of lamin A and progerin, but not lamin C (Fig. 6*F*).

We used qRT-PCR to quantify the effects of miR-9 expression on transcript levels of different nuclear lamins in HeLa cells (Fig. 6*G*). These studies showed that miR-9 expression reduced the levels of prelamin A transcripts but not those of the other lamins (Fig. 6*G*). We also tested whether suppressing endogenous miR-9 expression in differentiated neural progenitor cells would affect prelamin A transcript levels. Neural progenitor cells isolated from embryonic day 13.5 (E13.5) cortical explants were cultured in differentiation medium for 13 d and then transfected with an antisense oligonucleotide against miR-9 or a control oligonucleotide (with no homology to miR-9). When the cells were transfected with the miR-9 antisense oligonucleotide, miR-9 levels fell to almost undetectable levels, and prelamin A transcript levels increased by ~25% (Fig. 6*H*).

We suspected that the effects of miR-9 on prelamin A transcript levels were mediated by direct binding of miR-9 to the prelamin A 3′ UTR. To test this possibility, HeLa cells were transfected with an miR-9 expression vector (or an empty vector) along with luciferase reporter vectors containing a wild-type version of the prelamin A 3′ UTR or a truncated version of the prelamin A 3′ UTR (Δ2, containing site 1 but not site 2; see schematic in Fig. 6*A*) or the lamin C 3′ UTR. As a control, we transfected cells with an antisense oligonucleotide against the prelamin A 3′ UTR (19). MiR-9 overexpression lowered luciferase expression from the luciferase reporter vector containing the entire prelamin A 3′ UTR but not from the vector containing the lamin C 3′ UTR (Fig. 6*I*). Interestingly, miR-9 also reduced luciferase expression with the vector lacking site 2 in the prelamin A 3′ UTR (Δ2, Fig. 6*I*), suggesting that the effects of miR-9 were mediated by site 1 in the prelamin A 3′ UTR. As expected, the effects of the antisense oligonucleotide on luciferase expression were not observed with the Δ2 mutant (Fig. 6*I*), which lacks the sequence complementary to the antisense oligonucleotide (downstream of site 2 in the prelamin A 3′ UTR).

To determine if site 1 in the prelamin A 3′ UTR mediates the effects of miR-9 on prelamin A transcript levels, we generated luciferase reporter vectors in which the miR-9 seed-binding sequence (CCAAAG) in site 1 or site 2 was mutated. The mutations included (*i*) replacing the three nucleotides of site 1 (CAA) with ACC (SDM-1); (*ii*) deleting the CAA in site 1 (del-1); (*iii*) replacing the CAA in site 2 with ACC (SDM-2); (*iv*) deleting the CAA in site 2 (del-2); and (*v*) a truncation encompassing both sites 1 and 2 (Δ1–2) (see schematic in Fig. 6*A*). The putative miR-9 seed-binding sequence in the lamin C 3′ UTR also was examined with two mutations: (*i*) substitution of the CAA with ACC (C-SDM-1) and (*ii*) deletion of the CAA (C-del-1) (see schematic in Fig. 6*A*). Luciferase reporter studies with the new

vectors supported the notion that site 1 is crucial (Fig. 6*J*). MiR-9 expression reduced luciferase expression from the vector containing the wild-type prelamin A 3′ UTR, but when the CAA in site 1 was mutated or deleted (SDM-1, del-1, Δ1–2), the effect of miR-9 on luciferase expression was abolished (Fig. 6*J*). In contrast, when the CAA in the prelamin A site 2 was mutated or deleted (SDM-2, del-2), miR-9 expression remained effective in lowering luciferase expression, similar to results with the wild-type version of the prelamin A 3′ UTR. Mutation or deletion of the CAA in the lamin C 3′ UTR (C-SDM-1, C-del-1) had no effect on luciferase expression levels (Fig. 6*J*).

To confirm the specificity of the regulation of prelamin A by miR-9, we generated a mutant version of miR-9 expression vector by replacing TTG in the miR-9 seed sequence (CTTTGG) with GGT. When the mutant miR-9 expression vector was tested in luciferase-prelamin A 3′ UTR experiments (identical to those shown in Fig. 6*I*), we found no effect of the mutant miR-9 vector on the expression of luciferase-prelamin A 3′ UTR constructs (Fig. S9*A*). In contrast, the wild-type miR-9 expression vector lowered luciferase expression (Fig. S9*A*), as it did in the experiments in Fig. 6*I*.

We also examined the impact of the mutant miR-9 expression vector on prelamin A transcripts in HeLa cells, and we found that it had no effect (Fig. S9*B*). In addition to prelamin A, we examined the effects of the wild-type and mutant miR-9 expression vectors on two predicted miR-9 target genes, *RBMS3* and *RBM9*, which are thought to encode RNA-binding proteins (20, 21). The wild-type miR-9 expression vector significantly reduced *RBMS3* transcripts; no such effect was detected in cells transfected with the mutant miR-9 vector (Fig. S9*B*). The effects of miR-9 on *RBM9* expression were more modest (Fig. S9*B*). Given that RBMS3 and RBM9 are thought to be RNA-binding proteins, one conceivably could hypothesize that miR-9–mediated changes in RBMS3 or RBM9 might influence changes in prelamin A expression. However, when we knocked down expression of those genes with siRNAs, no effects on prelamin A expression were detected (Fig. S9*C*).

The miR-9 overexpression studies, along with the antisense knockdown experiments, suggested that miR-9 plays a role in regulating lamin A expression in the brain. To explore this issue further, we assessed lamin A expression in the forebrain and cerebellum of both forebrain-specific *Dicer*-knockout mice ($Emx1$-$Cre\ Dicer^{fl/fl}$) and control mice ($Emx1$-$Cre\ Dicer^{fl/+}$) (22, 23). The forebrain-specific *Dicer*-knockout mice lack the capacity to produce microRNAs in the forebrain; hence, we suspected that these mice might have higher levels of lamin A in the forebrain (but not in the cerebellum, where *Dicer* expression is preserved). Indeed, as judged by Western blots, lamin A expression was significantly higher in the forebrain of forebrain-specific *Dicer*-knockout mice, but expression in the cerebellum remained low (Fig. S10*A*). Similar results were observed in immunohistochemistry experiments (Fig. S10*B*).

Discussion

The two splice isoforms of the *LMNA* gene, lamins A and C, are major components of the nuclear lamina and are found in roughly similar amounts in cultured fibroblasts and a variety of tissues, including heart, liver, and kidney (4, 11, 12). In the current study, we show that the situation is quite different in the mouse brain. The levels of lamin A in the cerebral cortex and cerebellum are far lower than those in other tissues, as judged by both Western blots and immunohistochemistry. The only cells in the brain that express significant amounts of lamin A are vascular cells and the cells lining the surface of the brain. We observed similar findings in $Zmpste24^{-/-}$ mice (14), which lack the zinc metalloprotease that converts farnesyl-prelamin A to mature lamin A. In those mice, prelamin A is found in the brain, but it is confined to vascular and meningeal cells. Also, only trace

26

amounts of progerin are found in the cerebral cortex and cerebellum of progerin-only knockin mice (a mouse model of HGPS) (12). Farnesylated prelamin A (in $Zmpste24^{-/-}$ mice) and progerin (in the case of HGPS knockin mice) are toxic proteins that elicit multisystem disease phenotypes, but the central nervous system is spared. A plausible explanation for the absence of brain pathology is that the synthesis of the toxic prelamin A proteins is very low in the brain.

RNA studies supported the Western blot and immunohistochemistry findings; Northern blots revealed a low ratio of prelamin A to lamin C transcripts in the cerebral cortex and cerebellum, and those results were confirmed by qRT-PCR studies. We went on to show that the low levels of prelamin A in the brain are caused, at least in part, by removal of prelamin A transcripts by miR-9, a brain-specific microRNA. Multiple lines of evidence support this conclusion. First, transfection of HeLa cells with an miR-9 expression vector lowered lamin A expression levels, as judged by Western blots and immunocytochemistry. Also, when wild-type and $Lmna^{HG/+}$ mouse fibroblasts were transduced with lentiviruses encoding miR-9, the levels of lamin A and progerin proteins in the cells fell significantly. Third, expression of miR-9 in HeLa cells reduced prelamin A transcript levels but had no significant effects on transcript levels of lamin C, lamin B1, or lamin B2. A mutant miR-9 expression vector containing a mutation in the seed-binding site had no effect on the expression of prelamin A. Fourth, an antisense oligonucleotide against miR-9 increased prelamin A transcript levels in differentiated neural progenitor cells. In subsequent studies, we identified site 1 (Fig. 6A) as the relevant miR-9–binding site in the prelamin A 3′ UTR. Mutation of that site eliminated the capacity of miR-9 to down-regulate the expression of luciferase reporters containing the prelamin A 3′ UTR. As expected, the mutant miR-9 expression vector did not affect the expression of the luciferase-prelamin A 3′ UTR constructs. The microRNA databases have identified a potential miR-129–binding site in the prelamin A 3′ UTR, but we never observed a consistent effect of miR-129 on prelamin A transcript levels or lamin A protein levels in cells.

In overexpression studies, miR-9 reduced prelamin A transcript levels and lamin A protein levels by ∼50%. It is noteworthy, however, that the levels of miR-9 expression that we achieved in transfected cells were only ∼10% of the levels in the cortex of mouse brains. Had we achieved more physiological levels of miR-9 expression, it is conceivable that we would have observed an even greater reduction of prelamin A/lamin A expression in the transfected cells. In contrast, the levels of miR-129 expression in transfected cells were far greater than those in mouse cortex.

The low levels of prelamin A transcripts and lamin A protein in the brain of $Lmna^{LAO/LAO}$ mice were pivotal in leading us to consider the potential role of microRNAs in regulating prelamin A expression. In $Lmna^{LAO/LAO}$ mice, all the output of the $Lmna$ gene is channeled into prelamin A transcripts. Had mRNA splicing been responsible for the low levels of lamin A expression in wild-type brains, we would have observed increased levels of lamin A in the brain of $Lmna^{LAO/LAO}$ mice, comparable to levels in other tissues. However, prelamin A transcript levels in $Lmna^{LAO/LAO}$ brains were quite low, as were levels of lamin A protein, providing a strong argument against a role for alternative splicing in limiting prelamin A/lamin A expression in the brain. Also, low progerin levels in the brain of progerin-only mice (in which all the output of the gene is channeled into mutant prelamin A transcripts) further supported this conclusion.

The miR-9 overexpression studies, along with the luciferase reporter studies, supported the idea that miR-9 binds to the prelamin A 3′ UTR and down-regulates prelamin A expression in the brain. However, we cannot exclude the possibility that other mechanisms act in an accessory fashion to reduce lamin A expression in the brain. We considered low transcription rates as a contributing factor in the low levels of prelamin A expression in the brain. Arguing against this possibility, however, was the fact that prelamin A hnRNA levels were higher in the brain than in the liver. We also considered the possibility that a distinct promoter for $Lmna$ in the brain somehow might underlie the low levels of prelamin A expression in the brain, but the 5′-RACE studies uncovered no evidence that this was the case.

Although our cell-culture experiments strongly supported the idea that miR-9 plays an important role in regulating lamin A expression in the mouse brain, in vivo studies ultimately will be important for better defining the relationship between miR-9 and prelamin A expression in the brain. As a first step, we assessed lamin A expression in forebrain-specific $Dicer$-knockout mice (which lack the ability to produce microRNAs in the forebrain) (22, 23). Interestingly, lamin A levels were higher in the forebrain of these mice, but the levels of lamin A in the cerebellum remained low.

These studies with $Dicer$-knockout mice obviously are consistent with the notion that miR-9 regulates lamin A expression in the brain, but we would emphasize that interpretation of these studies is not straightforward, given that $Dicer$ eliminates all microRNAs, and not just miR-9; thus indirect effects on gene expression could occur. In the future, it would be interesting to create and examine miR-9–knockout and overexpression models to assess the effect of miR-9 on lamin A expression, but, again, there likely will be caveats in the interpretation of those experiments, given that miR-9 has other targets as well as prelamin A.

The only cells in the brain of wild-type mice that expressed large amounts of lamin A were vascular and meningeal cells; very little lamin A was observed in neurons or glia. The latter findings are consistent with the fact that both neurons and glia express high levels of miR-9 (24–26). However, many subtleties in the regulation of prelamin A expression by miR-9 still need to be defined. For example, whether there is a simple inverse relationship between miR-9 levels and prelamin A expression in different cell types within the brain—or in different regions of the brain—is not known. Also, the temporal pattern of miR-9 expression in different cell types of the brain is not clear. Thus far, nearly all our studies have been performed on mice that were <5 mo of age, and it is unclear whether miR-9 expression—and the preferential expression of lamin C in the brain—persists in older mice. Even less is known about prelamin A regulation in other species. The patterns of lamin A and lamin C expression in the human brain, for instance, have not been explored at different developmental stages. Furthermore, even though the miR-9–binding site in the prelamin A 3′ UTR is conserved in humans, we do not know if its functional significance is conserved also. In any case, we were intrigued by recent studies of lamin A/C expression in induced pluripotent stem cells generated from human HGPS fibroblasts (27). Upon differentiation into mesenchymal stem cells, lamin A and progerin were expressed highly, but when the same cells were differentiated into neural progenitors, lamin C was the predominant isoform, and the levels of lamin A and progerin were low (27).

The fact that lamin C is expressed highly in the brain implies that it may play an important role in that tissue, but the mouse clearly has evolved a strategy to limit the production of lamin A. Why such a strategy exists is unknown, but one possibility is that the precursor to lamin A, farnesyl-prelamin A, interferes with lamin B1 and lamin B2, both of which are farnesylated proteins with critical functions in the brain. In recent studies, Coffinier et al. (28, 29) have shown that the B-type lamins are crucial for neuronal migration and neuronal viability in the brain. It is conceivable that farnesyl-prelamin A—if produced at high levels in the brain—might compete with the B-type lamins for binding sites along the inner nuclear membrane, whereas lamin C would not. In the future, this concept, along with the physiologic importance of limiting lamin A synthesis in the brain, could be

27

tested by creating genetically modified mice that produce exclusively prelamin A, rather than lamin C, in the brain.

Aside from providing a window into nuclear lamin biology, the current studies might point to possible strategies for disease therapeutics. The brain makes little prelamin A/lamin A and is spared from the toxicity of mutant forms of prelamin A (e.g., progerin). What the brain achieves with a microRNA could be useful for other tissues. Several years ago, Fong et al. (19) suggested that it might be possible to treat prelamin A-related progeroid syndromes with antisense oligonucleotides against the prelamin A 3′ UTR. Given the current findings, this strategy deserves renewed scrutiny.

Materials and Methods

Mutant Mice. *Zmpste24*^{−/−} mice have been described previously (14). *Lmna*[LAO/LAO] mice produce exclusively mutant prelamin A transcripts that yield mature lamin A (bypassing prelamin A synthesis and processing) (18). The production of mature lamin A from the *Lmna*[LAO] transcript, rather than from prelamin A, results from a deletion of the sequences encoding the last 18 amino acids of prelamin A (18). No lamin C is produced by the *Lmna*[LAO] allele because of the deletion of intron 10 (18). The 3′ UTR in the *Lmna*[LAO] allele is identical to that of the wild-type allele. We also used *Lmna*[nHG/nHG] mice, which yield exclusively nonfarnesylated progerin from mutant prelamin A transcripts. The *Lmna*[nHG] allele has a deletion of introns 10 and 11 along with the last 150 bp of exon 11; it also contains a cysteine-to-serine substitution in the prelamin A *CaaX* motif (12). The 3′ UTR in the *Lmna*[nHG] allele also retains the wild-type prelamin A 3′ UTR. We used *Lmna*[nHG/nHG] mice rather than otherwise identical knockin mice expressing farnesylated progerin (10) because *Lmna*[nHG/nHG] mice survive to adulthood. Finally, we examined forebrain-specific *Dicer*-knockout mice (*Emx1-Cre Dicer*^{fl/fl}) and control mice (*Emx1-Cre Dicer*^{fl/+}) (22, 23).

Western Blots. Snap-frozen mouse tissues were ground with a mortar and pestle, resuspended in PBS containing 1 mM PMSF, 1 mM NaF, and protease inhibitors (Roche), and then homogenized with a tissue grinder. Protein extracts from HeLa cells and immortalized MEFs were prepared by lysing cells in urea buffer (30, 31). Protein extracts were size-fractionated on 4–12% gradient polyacrylamide Bis-Tris gels (Invitrogen) and then transferred to nitrocellulose membrane. Primary antibodies were a goat polyclonal antibody against lamin A/C (1:400) (sc6215; Santa Cruz); a rat monoclonal antibody against prelamin A (32) (final concentration, 2.5 μg/mL); a mouse monoclonal antibody against lamin B2 (1:400) (33-21000; Invitrogen); a goat polyclonal antibody against actin (1:1,000) (sc1616; Santa Cruz); and a mouse monoclonal antibody against β3 tubulin (TUJ-1) (1:1,000) (sc-58888; Santa Cruz). Antibody binding was detected with IR-Dye–conjugated secondary antibodies (Rockland) and an Odyssey infrared scanner (LI-COR).

Immunofluorescence Microscopy. Mouse tissues were embedded in Optimum Cutting Temperature compound, cryosectioned (10 μm), fixed in methanol, rinsed with acetone, permeabilized with 0.1% (vol/vol) Triton X-100 in Tris-buffered saline, and preincubated with PBS containing 1 mM CaCl₂, 1 mM MgCl₂, 10% (vol/vol) FBS, and 0.2% (wt/vol) BSA. For cultured cells (HeLa cells and neural progenitor cells), the cells were grown on coverslips, washed with PBS containing 1 mM CaCl₂ and 1 mM MgCl₂, fixed in methanol, rinsed in acetone, and permeabilized with 0.1% (vol/vol) Triton X-100 in PBS containing 1 mM CaCl₂ and 1 mM MgCl₂. The following primary antibodies were used: a rat monoclonal antibody against prelamin A (final concentration, 6 μg/mL) (32); a rabbit polyclonal antibody against lamin C (1:200) (LS-B2972; Lifespan Biosciences); a rabbit monoclonal antibody against lamin A/C (1:100) (2921-1; Epitomics); a mouse monoclonal antibody against mature lamin A (1:400) (MAB3540; Millipore); a goat polyclonal antibody against lamin B1 (1:250) (sc6217; Santa Cruz); a hamster monoclonal antibody against CD31 (1:200) (MAB1398Z; Millipore); a rabbit polyclonal antibody against GFAP (1:100) (18-0063; Zymed); a rabbit polyclonal antibody against Olig2 (1:500) (AB9610; Millipore); a rabbit polyclonal antibody against Zic2 (1:200) (AB15392; Millipore); a mouse monoclonal antibody against NeuN (1:500) (MAB377; Millipore); and a mouse monoclonal antibody against β3 tubulin (TU-20) (1:4,000) (ab7751; Abcam). Binding of secondary antibodies was detected with Alexa Fluor 488/568/647-labeled donkey/goat antibodies against rabbit, rat, mouse, or hamster IgG (Invitrogen). After washing and postfixation, DNA was stained with DAPI to visualize nuclei. In some experiments, sections were incubated with an Alexa Fluor 488/555-conjugated anti-lamin A antibody (1:400) (MAB3540; Millipore); an Alexa Fluor 647-conjugated anti-lamin B1 antibody (1:250) (sc6217; Santa Cruz); and an

Alexa Fluor 555-conjugated anti-lamin B2 antibody (1:250) (33-2100; Invitrogen). To stain blood vessels, FITC-labeled tomato lectin (Vector Laboratories) was injected i.v. into mice as described (17). Epifluorescence microscopy images were obtained with an Axiovert 200MOT microscope equipped with an ApoTome, and processed with Axiovert 4.6 software (all from Zeiss). Confocal fluorescence microscopy was performed with a Zeiss LSM700 laser-scanning microscope. Images along the z axis were captured sequentially, and merged images were generated using Zen 2010 software (Zeiss). To quantify the fluorescence signals, Volocity 3D rendering software (version 5.4; PerkinElmer Improvision) was used to identify nuclei in each image and to measure fluorescence signals from each nucleus.

RNA Studies. Snap-frozen mouse tissues were homogenized in TRI reagent (Molecular Research Center), and total RNA was extracted according to the manufacturer's protocol. RNA (15 μg) was size-fractionated on a 1% (wt/vol) agarose/formaldehyde gel and transferred to a Nytran SuPerCharge nylon membrane (Schleicher and Schuell). The membrane was hybridized with a [³²P]dCTP-labeled *Lmna* cDNA probe containing exon 1–4 sequences (shared by prelamin A and lamin C transcripts). A ³²P-labeled 18S cDNA probe was used as a loading control. Signals were detected by autoradiography (CL-XPosure Film; Pierce) and quantified by ImageJ software.

Levels of total *Lmna* transcripts, along with levels of prelamin A, lamin C, lamin B1, and lamin B2 transcripts, were assessed by qRT-PCR. For cultured cells (HeLa cells and neural progenitor cells), total RNA was isolated with an RNeasy kit (Qiagen). After DNase I (Ambion) treatment, RNA was reverse transcribed with random primers, oligo(dT) and SuperScript III (Invitrogen). qPCR reactions were prepared with SYBR Green PCR Master Mix (Bioline) and performed on a 7900 Fast Real-Time PCR system (Applied Biosystems). Transcript levels were determined by the comparative cycle threshold method and normalized to levels of cyclophilin A. All primers used are listed in Table S1.

Overexpression of MicroRNAs. HeLa cells were transfected with lentiviral microRNA expression vectors (GeneCopoeia) with FugeneHD (Roche). One day later, transfected cells were subjected to selection with puromycin (final concentration, 5–10 mg/mL) for 2–3 d. For immunocytochemistry studies, no puromycin was added to the cells so that the slides would contain non-transfected control cells. Immortalized MEFs were transduced with lentiviruses encoding miR-9 or miR-129 [generated by the University of California, Los Angeles Vector Core facility from lentiviral microRNA expression vectors (GeneCopoeia)]. Transduced MEFs were subjected to selection with puromycin (final concentration, 5 mg/mL).

MicroRNA levels were assessed by qRT-PCR. Total RNA was isolated with an RNeasy kit (Qiagen), treated with DNase I (Ambion), and reverse transcribed with the miRCURY LNA Universal cDNA synthesis kit (Exiqon). qPCR reactions were prepared with SYBR Green PCR Master Mix and LNA PCR primers (all from Exiqon), and performed on a 7900 Fast Real-Time PCR system (Applied Biosystems). Transcript levels were determined by the comparative cycle threshold method and normalized to levels of U6 snRNA.

Knockdown of miR-9 in Differentiated NPCs. NPCs were isolated from the cerebral cortex of mouse embryos at eE13.5 (33). Cells were plated on poly-L-lysine–coated six-well plates (∼8 × 10⁵ cells per well) and cultured in differentiation medium (1:1 mixture of DMEM/F12 and Neurobasal medium supplemented with N2, B27, and penicillin/streptomycin) (33). After 13 d, NPCs were transfected, using FugeneHD (Roche), with an miR-9 antisense oligonucleotide (miRCURY LNA microRNA Power inhibitor against miR-9) or a control antisense oligonucleotide (both from Exiqon). After 7 d, RNA was isolated with an RNeasy kit (Qiagen) and analyzed by qRT-PCR as described earlier.

Luciferase Reporter Assay. The full-length prelamin A 3′ UTR, mutant versions of the prelamin A 3′ UTR, or the lamin C 3′ UTR were cloned downstream of a firefly luciferase gene in pmirGLO (Promega), which contains a Renilla luciferase gene for normalization of the firefly luciferase signal. HeLa cells were transfected with the luciferase reporter vectors along with an empty vector or an miR-9 expression vector (34). In some experiments, we tested the effect of a mutant version of the miR-9 expression vector in which the TTG in the miR-9 seed sequence (CTTTGG) was replaced by GGT. After 24–30 h, cell lysates were analyzed for firefly- and Renilla-luciferase activities with a GloMax luminometer (Promega).

28

1. Dauer WT, Worman HJ (2009) The nuclear envelope as a signaling node in development and disease. *Dev Cell* 17:626–638.
2. Schirmer EC, Foisner R (2007) Proteins that associate with lamins: Many faces, many functions. *Exp Cell Res* 313:2167–2179.
3. Dechat T, et al. (2008) Nuclear lamins: Major factors in the structural organization and function of the nucleus and chromatin. *Genes Dev* 22:832–853.
4. Lin F, Worman HJ (1993) Structural organization of the human gene encoding nuclear lamin A and nuclear lamin C. *J Biol Chem* 268:16321–16326.
5. Worman HJ, Fong LG, Muchir A, Young SG (2009) Laminopathies and the long strange trip from basic cell biology to therapy. *J Clin Invest* 119:1825–1836.
6. Davies BS, Fong LG, Yang SH, Coffinier C, Young SG (2009) The posttranslational processing of prelamin A and disease. *Annu Rev Genomics Hum Genet* 10:153–174.
7. Eriksson M, et al. (2003) Recurrent de novo point mutations in lamin A cause Hutchinson-Gilford progeria syndrome. *Nature* 423:293–298.
8. De Sandre-Giovannoli A, et al. (2003) Lamin a truncation in Hutchinson-Gilford progeria. *Science* 300:2055.
9. Hennekam RC (2006) Hutchinson-Gilford progeria syndrome: Review of the phenotype. *Am J Med Genet A* 140:2603–2624.
10. Yang SH, et al. (2005) Blocking protein farnesyltransferase improves nuclear blebbing in mouse fibroblasts with a targeted Hutchinson-Gilford progeria syndrome mutation. *Proc Natl Acad Sci USA* 102:10291–10296.
11. Worman HJ, Lazaridis I, Georgatos SD (1988) Nuclear lamina heterogeneity in mammalian cells. Differential expression of the major lamins and variations in lamin B phosphorylation. *J Biol Chem* 263:12135–12141.
12. Yang SH, Andres DA, Spielmann HP, Young SG, Fong LG (2008) Progerin elicits disease phenotypes of progeria in mice whether or not it is farnesylated. *J Clin Invest* 118:3291–3300.
13. Sullivan T, et al. (1999) Loss of A-type lamin expression compromises nuclear envelope integrity leading to muscular dystrophy. *J Cell Biol* 147:913–920.
14. Leung GK, et al. (2001) Biochemical studies of *Zmpste24*-deficient mice. *J Biol Chem* 276:29051–29058.
15. Bergo MO, et al. (2002) *Zmpste24* deficiency in mice causes spontaneous bone fractures, muscle weakness, and a prelamin A processing defect. *Proc Natl Acad Sci USA* 99:13049–13054.
16. Young SG, Meta M, Yang SH, Fong LG (2006) Prelamin A farnesylation and progeroid syndromes. *J Biol Chem* 281:39741–39745.
17. Davies BSJ, et al. (2010) GPIHBP1 is responsible for the entry of lipoprotein lipase into capillaries. *Cell Metab* 12:42–52.
18. Coffinier C, et al. (2010) Direct synthesis of lamin A, bypassing prelamin a processing, causes misshapen nuclei in fibroblasts but no detectable pathology in mice. *J Biol Chem* 285:20818–20826.
19. Fong LG, et al. (2006) Prelamin A and lamin A appear to be dispensable in the nuclear lamina. *J Clin Invest* 116:743–752.
20. Fritz D, Stefanovic B (2007) RNA-binding protein RBMS3 is expressed in activated hepatic stellate cells and liver fibrosis and increases expression of transcription factor Prx1. *J Mol Biol* 371:585–595.
21. Yeo GW, et al. (2009) An RNA code for the FOX2 splicing regulator revealed by mapping RNA-protein interactions in stem cells. *Nat Struct Mol Biol* 16:130–137.
22. Murchison EP, Partridge JF, Tam OH, Cheloufi S, Hannon GJ (2005) Characterization of Dicer-deficient murine embryonic stem cells. *Proc Natl Acad Sci USA* 102:12135–12140.
23. Kawase-Koga Y, Otaegi G, Sun T (2009) Different timings of Dicer deletion affect neurogenesis and gliogenesis in the developing mouse central nervous system. *Dev Dyn* 238:2800–2812.
24. Deo M, Yu JY, Chung KH, Tippens M, Turner DL (2006) Detection of mammalian microRNA expression by in situ hybridization with RNA oligonucleotides. *Dev Dyn* 235:2538–2548.
25. Smirnova L, et al. (2005) Regulation of miRNA expression during neural cell specification. *Eur J Neurosci* 21:1469–1477.
26. Lau P, et al. (2008) Identification of dynamically regulated microRNA and mRNA networks in developing oligodendrocytes. *J Neurosci* 28:11720–11730.
27. Zhang J, et al. (2011) A human iPSC model of Hutchinson Gilford Progeria reveals vascular smooth muscle and mesenchymal stem cell defects. *Cell Stem Cell* 8:31–45.
28. Coffinier C, et al. (2010) Abnormal development of the cerebral cortex and cerebellum in the setting of lamin B2 deficiency. *Proc Natl Acad Sci USA* 107:5076–5081.
29. Coffinier C, et al. (2011) Deficiencies in lamin B1 and lamin B2 cause neurodevelopmental defects and distinct nuclear shape abnormalities in neurons. *Mol Biol Cell* 22:4683–4693.
30. Fong LG, et al. (2004) Heterozygosity for Lmna deficiency eliminates the progeria-like phenotypes in Zmpste24-deficient mice. *Proc Natl Acad Sci USA* 101:18111–18116.
31. Steinert P, Zackroff R, Aynardi-Whitman M, Goldman RD (1982) Isolation and characterization of intermediate filaments. *Methods Cell Biol* 24:399–419.
32. Lee R, et al. (2010) Genetic studies on the functional relevance of the protein prenyltransferases in skin keratinocytes. *Hum Mol Genet* 19:1603–1617.
33. Ader M, Meng J, Schachner M, Bartsch U (2000) Formation of myelin after transplantation of neural precursor cells into the retina of young postnatal mice. *Glia* 30:301–310.
34. Delaloy C, et al. (2010) MicroRNA-9 coordinates proliferation and migration of human embryonic stem cell-derived neural progenitors. *Cell Stem Cell* 6:323–335.

PNAS PLUS

MEDICAL SCIENCES

29

Supporting Information

Jung et al. 10.1073/pnas.1111780109

SI Materials and Methods

In Situ Hybridization. Tissues from 30-d-old mice were collected after perfusion with 4% (wt/vol) paraformaldehyde (PFA). Fixed tissues were cryoprotected in 20% (vol/vol) sucrose before embedding in Optimum Cutting Temperature (OCT) compound (Sakura Finetek). Sections (20-μm) were cut on a cryostat and mounted onto Colorfrost slides (Fisher Scientific). In situ hybridization was performed as described (1). Slides were warmed to room temperature, treated with proteinase K (50 mg/mL) for 20 min, and fixed with 4% (wt/vol) PFA for 10 min. Acetylation was performed using 0.25% (wt/vol) acetic anhydride in 0.1 M triethanolamine, pH 8.0, for 10 min, followed by three washes with PBS. Slides were incubated with hybridization buffer [50% (vol/vol) formamide, 5× SSC, 0.3 mg/mL yeast tRNA, 100 mg/mL heparin, 1× Denhardt's solution, 0.1% (vol/vol) Tween-20, 0.1% (wt/vol) 3-[(3-cholamidopropyl)dimethylammonio]-1-propane-sulfonate, 5 mM EDTA] for 10 min at 65 °C, followed by overnight incubation with a digoxigenin-labeled probe (300 ng/mL). Five high-stringency washes were performed with 0.2× SSC at 65 °C. Slides then were incubated with horseradish alkaline phosphatase-conjugated anti-digoxigenin and nitroblue tetrazolium/5-bromo-4-chloro-indolyl phosphate (Roche) for signal detection. The riboprobe common to prelamin A and lamin C transcripts and the riboprobe specific for prelamin A corresponded to lamin A cDNA nucleotides 388–1213 and 2288–3027, respectively (GenBank accession number: NM.001002011.1).

5′-RACE. RNA was extracted from tissues with TRI reagent (Molecular Research Center). After DNase I (Ambion) treatment, RNA was reverse transcribed with *Lmna*-specific antisense primer-1 (5′-TCCTTGGAGTTGAGAAGAGCCT-3′) and reverse transcriptase using the Roche HTS 5′-RACE kit. The first-strand cDNA was purified with High Pure 96 UF Cleanup Plate (Roche), poly-(A) tailed with dATP and terminal transferase (HTS 5′-RACE kit; Roche), and used in two sequential PCR reactions: (*i*) Oligo(dT) Anchor Primer (HTS 5′-RACE kit; Roche) and *Lmna* specific antisense primer-2 (5′-TGAACTCCTCACGCACTTT-GCT-3′) and (2) PCR Anchor Primer (HTS 5′-RACE kit; Roche) and *Lmna*-specific antisense primer-3 (5′-TTGGCCACAGAATC-AAGGGTCT-3′). The PCR products were size-fractionated on an agarose gel and sequenced with *Lmna* -specific antisense primer 4 (5′-ACCTCTTCAGACTCAGTGATGCGA-3′). DNA sequencing results were analyzed with Sequencher 5.0.

Knockdown of RMBS3 and RBM9. HeLa cells were transfected with ON-TARGET plus Nontargeting Pool or ON-TARGET plus SMARTpool siRNA (Dharmacon) against RBMS3 or RBM9 (at a final concentration of 33 nM) using Lipofectamine 2000 (Invitrogen). After 24 h, total RNA was isolated with an RNeasy kit (Qiagen) and analyzed by quantitative RT-PCR (qRT-PCR) as described earlier.

1. Li G, et al. (2008) Regional distribution of cortical interneurons and development of inhibitory tone are regulated by Cxcl12/Cxcr4 signaling. *J Neurosci* 28:1085–1098.

30
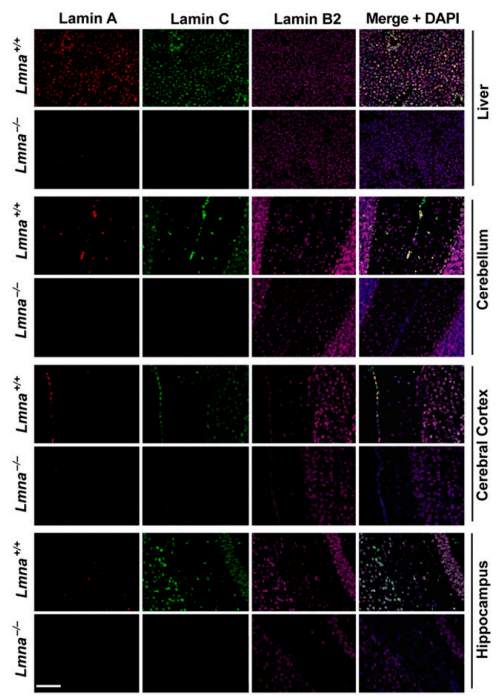
Fig. S1. Immunofluorescence microscopy of tissues from *Lmna*^{+/+} and *Lmna*^{−/−} mice (1). Sections were stained for lamin A (red), lamin C (green), and lamin B2 (magenta). DNA was stained with DAPI (blue). In the brain of *Lmna*^{+/+} mice, lamin C expression was widespread, whereas lamin A expression was restricted to scattered vascular cells. Neither lamin A nor lamin C was detected in *Lmna*^{−/−} mice. (Scale bar, 100 μm.)

1. Sullivan T, et al. (1999) Loss of A-type lamin expression compromises nuclear envelope integrity leading to muscular dystrophy. *J Cell Biol* 147:913–920.

31
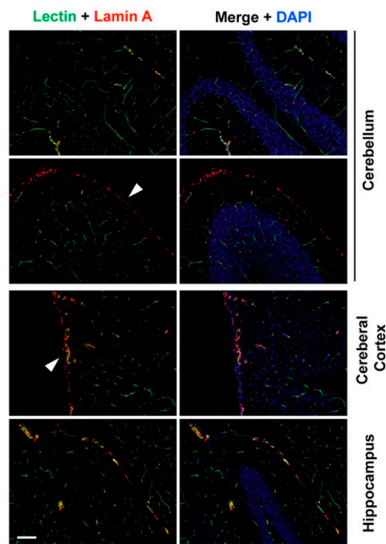
Fig. S2. Immunofluorescence microscopy on brain sections from a wild-type mouse that was injected i.v. with a fluorescently labeled tomato lectin (green), revealing that lamin A (red) was located largely or exclusively in lectin-positive blood vessels and in meningeal cells lining the surface of the cerebral cortex (arrowheads). (Scale bar, 100 μm.)

32
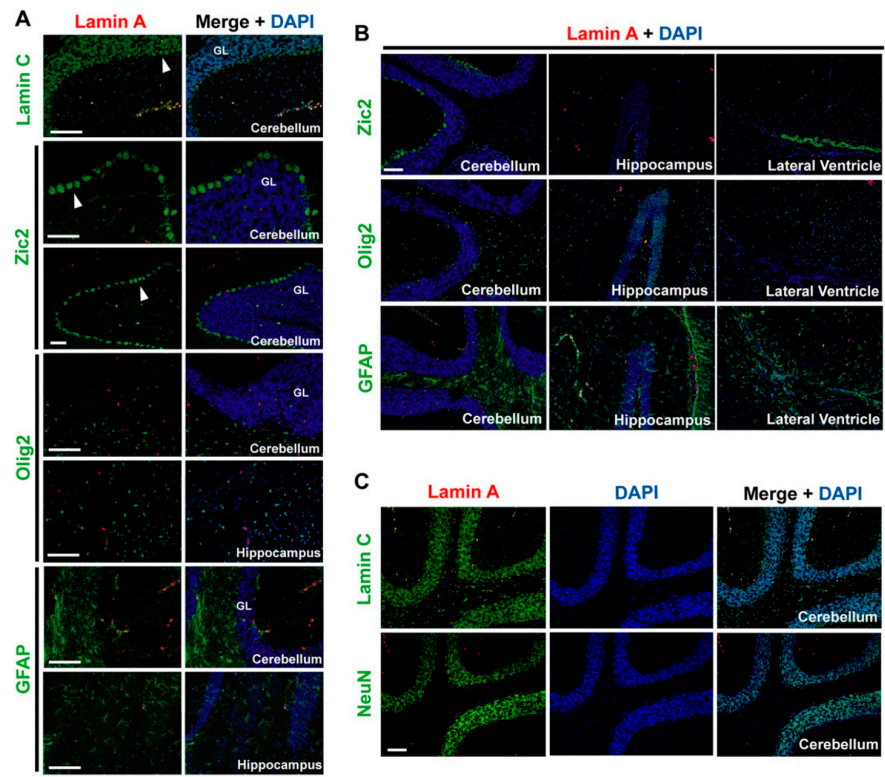
Fig. S3. Characterization of lamin A-expressing cells in the wild-type mouse brain with different markers. (*A* and *B*) Brain sections were stained for lamin C, Zic2, Olig2, or GFAP (green) along with an antibody against lamin A (red). We observed no colocalization of lamin A with Zic2 or Olig2. Lamin C-positive neurons (including Purkinje cells; arrowheads) in the cerebellum did not express lamin A. Many cells that stained positively for GFAP did not express lamin A. GL, granular layer. (*B*) Low-magnification images. (*C*) Sections of cerebellum stained for lamin C or NeuN (green) along with lamin A (red). (Scale bar, 100 μm.)

33
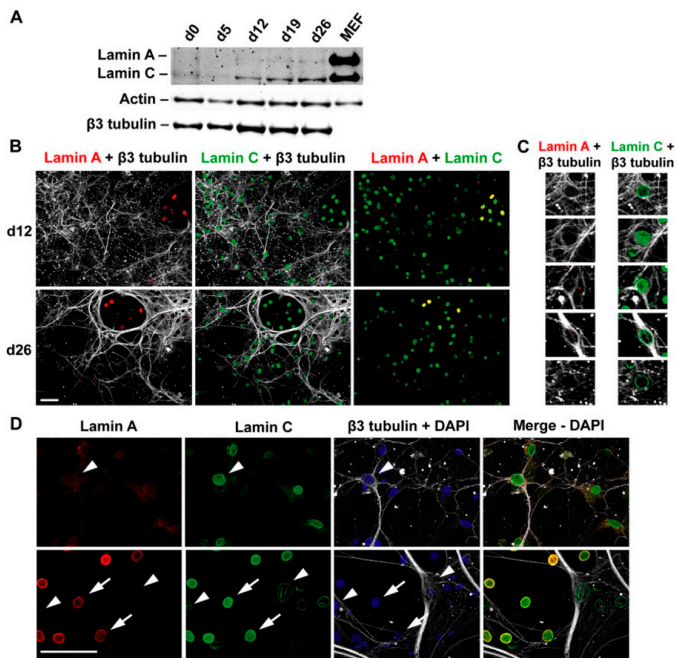
Fig. S4. Preferential expression of lamin C in differentiated neural progenitor cells (NPCs). (*A*) Western blot of protein extracts from differentiated NPCs. NPCs were isolated from the cortex of embryonic day 13.5 mouse embryos (1) and cultured on poly-ʟ-lysine–coated six-well plates in differentiation medium for up to 26 d. At different time points, cell extracts were prepared and blotted with antibodies specific for lamin A/C, actin, or β3 tubulin (TUJ-1). Mouse embryonic fibroblasts (MEFs) were used as a control. (*B–D*) Immunofluorescence microscopy of NPCs differentiated in culture for 12 (d12) or 26 d (d26) with antibodies against lamin A (red), lamin C (green), and β3 tubulin (TU-20) (white). Most β3 tubulin-positive cells expressed only lamin C, whereas β3 tubulin-negative cells expressed both lamin A and lamin C. (*C* and *D*) High-magnification images revealing lamin C but no lamin A in β3 tubulin-positive cells. (Scale bar, 50 μm.)

1. Ader M, Meng J, Schachner M, Bartsch U (2000) Formation of myelin after transplantation of neural precursor cells into the retina of young postnatal mice. *Glia* 30:301–310.
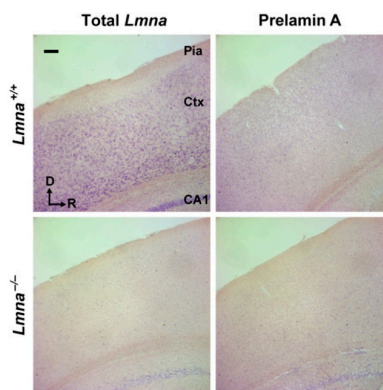
Fig. S5. In situ hybridization on brain sections from a wild-type mouse and a *Lmna*-knockout mouse (*Lmna*⁻/⁻) with a probe common to prelamin A and lamin C or a probe specific for prelamin A. Little or no hybridization was observed in the *Lmna*⁻/⁻ sections. Ctx, cortex; D, dorsal; Pia, pia mater; R, rostral. (Scale bar, 100 μm.)

34
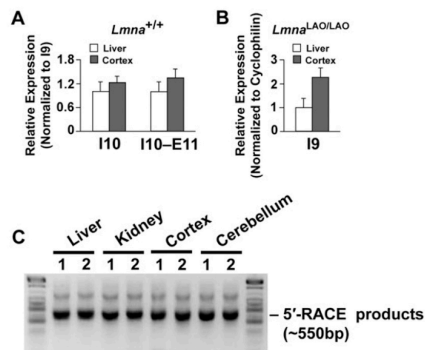
Fig. S6. Analysis of prelamin A and lamin C heterogeneous nuclear RNA (hnRNA) levels and analysis of prelamin A promoter use. (*A* and *B*) qRT-PCR analysis of total *Lmna* and prelamin A hnRNA levels in the liver and cerebral cortex of *Lmna*^{+/+} (wild-type) and *Lmna*[LAO/LAO] mice. Intron 9-specific primers (I9) were used to measure total *Lmna* hnRNA levels in tissues from both mice. Intron 10-specific primers (I10) and primers specific for the intron 10–exon 11 junction (I10–E11) were used to measure prelamin A hnRNA levels in wild-type mice; the prelamin A hnRNA levels (I10 and I10–E11) were normalized to the total *Lmna* hnRNA levels (I9). For *Lmna*[LAO/LAO] mice, hnRNA levels were assessed with the intron 9 primer set (introns 10 and 11 are absent in these mice) and normalized to cyclophilin A. Gene expression levels in cortex were compared with those in the liver (which was set at 1.0). Values represent mean ± SD from four pairs of mice (including three pairs used in Fig. 4*C*). (*C*) 5′-RACE to define the 5′ UTRs of prelamin A transcripts in different tissues of wild-type mice. 5′-RACE was performed with RNA from liver, kidney, cortex, and cerebellum of two wild-type mice. Shown is an ethidium bromide-stained agarose gel of the 5′-RACE products. DNA sequencing revealed that the prelamin A 5′ UTR was identical in all tissues, corresponding to sequences in the database (National Center for Biotechnology Information reference sequence: NM_001002011.2).
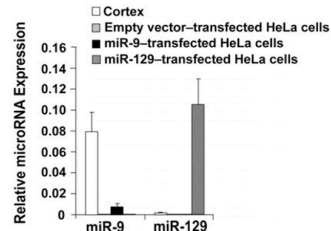
Fig. S7. qRT-PCR analysis of the levels of miR-9 or miR-129 in HeLa cells transfected with miR-9 or miR-129 expression vectors. Cells were subjected to puromycin selection for 2 d before RNA was extracted. RNA samples from the cerebral cortex of 1-mo-old wild-type mice were used as a control. Data were normalized to U6 snRNA. Values represent mean ± SD from four independent experiments.

35
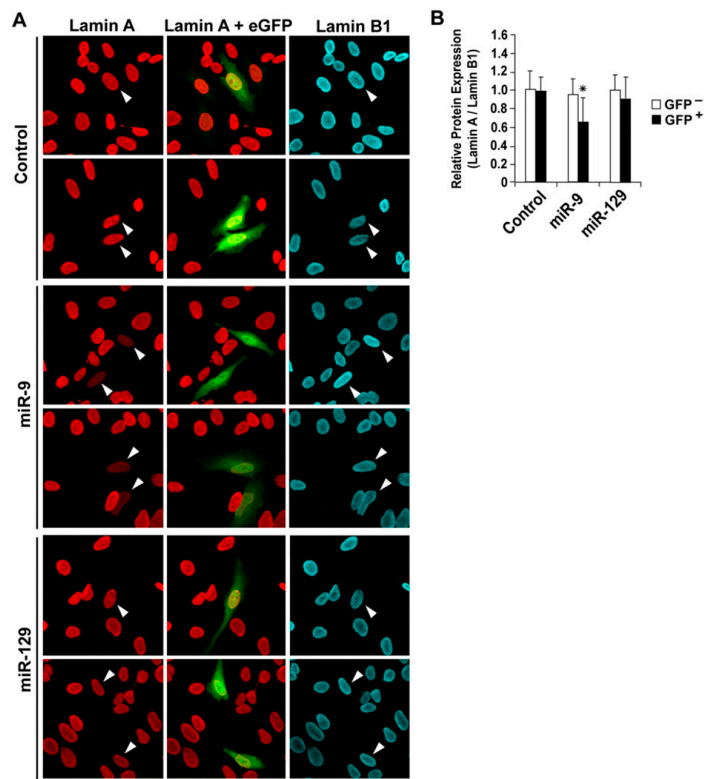
Fig. S8. Assessing lamin A and lamin B1 expression in HeLa cells expressing miR-9 or miR-129. (*A*) Immunofluorescence microscopy using antibodies against lamin A (red) and lamin B1 (cyan) in HeLa cells that had been transfected with miR-9 or miR-129 expression vectors. Empty vector-transfected cells were used as a control. Transfected cells were identified by EGFP expression (arrowheads). (*B*) Quantification of immunofluorescence signals from the immunofluorescence microscopy experiments (see *A*). The levels of lamin A expression in GFP⁻ and GFP⁺ cells were normalized to those of lamin B1. Values represent mean $\pm$ SD (from examination of $\geq$27 cells per condition). *$P < 0.0001$.

36
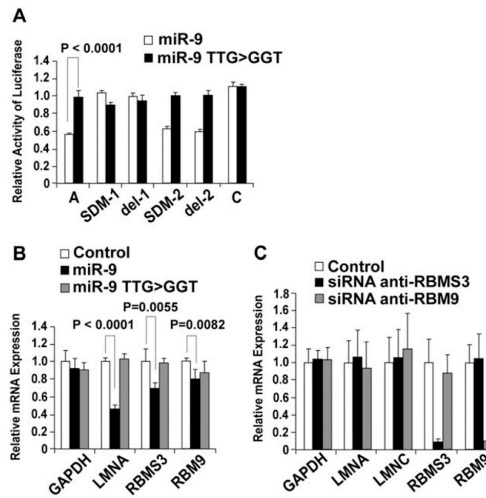
Fig. S9. Assessing the impact of a mutant miR-9 expression vector on prelamin A expression and testing the impact of miR-9 expression on other putative miR-9 target genes. (*A*) Luciferase assays in HeLa cells that had been cotransfected with wild-type miR-9 or a mutant mir-9 in which the TTG sequence in the seed-binding sequence was changed to GGT (TTG>GGT). We used the same luciferase constructs that were used in Fig. 6*J*. Values represent mean ± SD from three independent experiments. (*B*) qRT-PCR analysis of prelamin A, RBMS3, and RBM9 transcript levels in cells that had been transfected with the wild-type miR-9 expression vector or the mutant (TTG>GGT) miR-9 vector. Data were normalized to cyclophilin A, and gene expression was compared with that of empty vector-transfected cells (set at 1.0). The expression of GAPDH, another housekeeping gene, was measured also. Values represent mean ± SD from four independent experiments. (*C*) qRT-PCR analysis of prelamin A and lamin C expression in HeLa cells in which RBMS3 or RBM9 expression had been knocked down with specific siRNAs. Data were normalized to cyclophilin A, and gene expression levels were compared with those in cells that had been transfected with control, nontargeting siRNAs (set at 1.0). Values represent mean ± SD from four independent experiments.
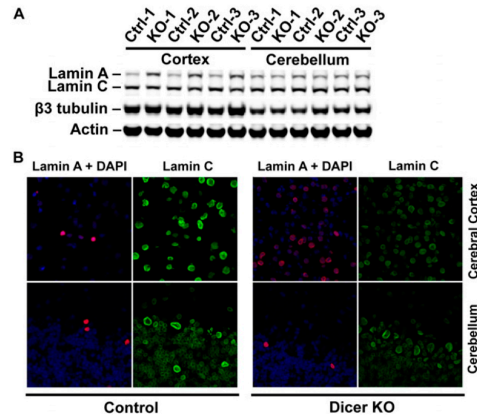
Fig. S10. Increased expression of lamin A in the cortex of *Emx1-Cre Dicer*–knockout mice (1, 2). (*A*) Western blot of tissue extracts from *Emx1-Cre Dicer*–knockout mice with antibodies against lamin A/C. Loading controls included β3 tubulin (TUJ-1, a neuron-specific tubulin), and actin. (*B*) Immunofluorescence microscopy images of cerebral cortex and cerebellum from *Emx1-Cre Dicer*–knockout mice. Frozen sections were stained with antibodies against lamin A (red) and lamin C (green); DNA was stained with DAPI.

1. Murchison EP, Partridge JF, Tam OH, Cheloufi S, Hannon GJ (2005) Characterization of Dicer-deficient murine embryonic stem cells. *Proc Natl Acad Sci USA* 102:12135–12140.
2. Kawase-Koga Y, Otaegi G, Sun T (2009) Different timings of Dicer deletion affect neurogenesis and gliogenesis in the developing mouse central nervous system. *Dev Dyn* 238: 2800–2812.

37

Table S1. Primer sequences for qRT-PCR studies

Gene	Species	Sequences (5′–3′)
Lamin A	Mouse	ggttgaggacaatgaggatga
		tgagcgcaggttgtactcag
Lamin B1	Mouse	caactgacctcatctggaagaac
		tgaagactgtgcttctctgagc
Lamin B2	Mouse	cagaggtggcagagcttcga
		gtctccttctccaactgcttctt
Lamin C	Mouse	gacaatgaggatgacgacgag
		ttaatgaaaagactttggcatgg
Lamin A/C	Mouse	cctatcgaaagctgctggag
		cctgagactgggatgagtg
Cyclophilin A	Mouse	tgagcactggagagaaagga
		ccattatggcgtgtaaagtca
Lamin A	Human	ctcctacctcctgggcaact
		aggtcccagattacatgatgct
Lamin B1	Human	gctgctcctcaactatgctaag
		gaattcagtgctgcttcatattctc
Lamin B2	Human	agttggacgaggtcaacaagag
		ggactccaggtccttcacac
Lamin C	Human	ctcagtgactgtggttgagga
		agtgcaggctcggcctc
Cyclophilin A	Human	acttcatcctaaagcatacgggt
		gccttctttcactttgccaaac
Lamin A (intron 9)	Mouse	accgagctctcagttgtgtccttt
		acaaccttgtccaacctctgatgc
Lamin A (intron 10)	Mouse	gtggacagggttctggatttgtgt
		aagtgtgcatgcaatgggagtgag
Lamin A (intron 10–exon 11)	Mouse	aagtcagtcccaaactcgctgt
		Tgagcgcaggttgtactcag

38

Chapter 3:

New *Lmna* Knock-in Mice Provide a Molecular Mechanism for the "Segmental Aging" in

Hutchinson-Gilford Progeria Syndrome

New *Lmna* knock-in mice provide a molecular mechanism for the 'segmental aging' in Hutchinson−Gilford progeria syndrome[†]

Hea-Jin Jung[1], Yiping Tu[2], Shao H. Yang[2], Angelica Tatar[2], Chika Nobumori[2], Daniel Wu[2], Stephen G. Young[1,2,3,∗] and Loren G. Fong[2,∗]

[1]Molecular Biology Institute, [2]Department of Medicine, and [3]Department of Human Genetics, University of California, Los Angeles, CA 90095, USA

Lamins A and C (products of the *LMNA* gene) are found in roughly equal amounts in peripheral tissues, but the brain produces mainly lamin C and little lamin A. In HeLa cells and fibroblasts, the expression of prelamin A (the precursor to lamin A) can be reduced by miR-9, but the relevance of those cell culture studies to lamin A regulation in the brain was unclear. To address this issue, we created two new *Lmna* knock-in alleles, one (*Lmna*^PLAO-5NT) with a 5-bp mutation in a predicted miR-9 binding site in prelamin A's 3′ UTR, and a second (*Lmna*^PLAO-UTR) in which prelamin A's 3′ UTR was replaced with lamin C's 3′ UTR. Neither allele had significant effects on lamin A levels in peripheral tissues; however, both substantially increased prelamin A transcript levels and lamin A protein levels in the cerebral cortex and the cerebellum. The increase in lamin A expression in the brain was more pronounced with the *Lmna*^PLAO-UTR allele than with the *Lmna*^PLAO-5NT allele. With both alleles, the increased expression of prelamin A transcripts and lamin A protein was greater in the cerebral cortex than in the cerebellum. Our studies demonstrate the *in vivo* importance of prelamin A's 3′ UTR and its miR-9 binding site in regulating lamin A expression in the brain. The reduced expression of prelamin A in the brain likely explains why children with Hutchinson−Gilford progeria syndrome (a progeroid syndrome caused by a mutant form of prelamin A) are spared from neurodegenerative disease.

INTRODUCTION

Lamins A and C (the A-type lamins) are alternatively spliced products of the *LMNA* gene (1). *LMNA* mutations have been linked to many diseases, including muscular dystrophy, cardiomyopathy, partial lipodystrophy, neuropathy and progeroid syndromes (2). Most of these mutations are located in sequences shared by prelamin A (the precursor to lamin A) and lamin C, but some, including the one for Hutchinson−Gilford progeria syndrome (HGPS; OMIM 176670), are located in sequences unique to prelamin A. The HGPS mutation has no effect on lamin C but leads to the synthesis of a mutant prelamin A that is toxic to cells and tissues (3,4).

Lamins A and C are expressed in roughly similar amounts in most tissues, but we recently encountered an exception: the brain

produces mainly lamin C and little lamin A (5). The preferential synthesis of lamin C in the brain is intriguing because it suggested a new insight into the spectrum of disease phenotypes in HGPS. Children with HGPS have multiple disease phenotypes resembling premature aging, but they are spared from senile dementia. The absence of neurodegenerative disease could be due to the fact that the brain makes mainly lamin C and little of the toxic prelamin A.

We initially suspected that alternative splicing would explain the preferential synthesis of lamin C in the brain, but this was not the case. Lamin A expression in the brain was also low in 'lamin A-only' knock-in mice (6), where alternative splicing is absent and all of the output of the gene is channeled into prelamin A (5). Additional studies suggested that prelamin A expression

---

∗To whom correspondence should be addressed at: 695 Charles E. Young Dr South, Los Angeles, CA 90095, USA. Tel: +1 3108254997;
Fax: +1 3102672722; Email: lfong@mednet.ucla.edu (L.G.F.) or sgyoung@mednet.ucla.edu (S.G.Y.).
†The abstract has been published online on the ASCB website (2013) for the ASCB annual meeting. Abstract No. 1622. http://www.miracd.com/Verify/ASCB2013/submission/temp/rad838C6.pdf

might be regulated by miR-9, a microRNA that is expressed highly in the brain. When miR-9 was expressed in HeLa cells and mouse embryonic fibroblasts (MEFs), prelamin A transcripts were reduced but lamin C was unaffected (5).

The cell culture studies on miR-9 regulation of prelamin A left several questions unanswered. One was whether the experiments with cultured non-neuronal cells (i.e. HeLa cells and MEFs) were relevant to prelamin A regulation in the brain, particularly since microRNA-target interactions can be context-dependent (7–10). A second issue was whether other sequences in prelamin A's 3′ UTR, apart from the miR-9 binding site, might be important in regulating prelamin A expression. A third issue was whether the preferential expression of lamin C in the brain is crucial for brain homeostasis and whether lamin A expression in the brain would lead to adverse consequences. To address these issues, we created and characterized two new lines of *Lmna* knock-in mice with mutations in prelamin A's 3′ UTR— one with a 5-bp mutation in the predicted miR-9 binding site and a second in which prelamin A's 3′ UTR was replaced with lamin C's 3′ UTR.

RESULTS

We used sequence-replacement vectors to create two *Lmna* knock-in alleles, one ($Lmna^{plao-5nt}$) in which a predicted miR-9 seed-binding site in exon 12 (CCAAAG, within prelamin A's 3′ UTR) (5) was changed to ACCCTG, and a second ($Lmna^{plao-utr}$) in which prelamin A's 3′ UTR was replaced with lamin C's 3′ UTR (Fig. 1). Both vectors eliminated introns 10 and 11; consequently, the new alleles produced exclusively prelamin A and no lamin C (11). To be certain that the 'ACCCT' mutation in the $Lmna^{PLAO-5NT}$ allele would be effective in abolishing the effect of miR-9 on prelamin A transcripts, we performed reporter assays with a luciferase vector linked to prelamin A's 3′ UTR (Supplementary Material, Fig. S1). The ACCCT mutation in the 3′ UTR abolished the ability of miR-9 to reduce luciferase expression in HeLa cells and U-87 MG cells (a human glioblastoma cell line) (Supplementary Material, Fig. S1B and C).

We used western blots to assess relative amounts of lamins A and C in the cerebral cortex, cerebellum, heart, liver and kidney of wild-type, $Lmna^{plao-5nt/plao-5nt}$, $Lmna^{plao-utr/plao-utr}$ and $Lmna$-$^{plao/plao}$ mice. [$Lmna$plao/plao mice lack introns 10 and 11 and therefore produce exclusively prelamin A, but they have no mutations in prelamin A's 3′ UTR (11).] Large amounts of both lamins A and C were present in the peripheral tissues of wild-type mice; in the brain, lamin C was abundant, but lamin A expression was low (Fig. 2A). Lamin A levels were higher in $Lmna^{plao/plao}$ mice than in wild-type mice (including in the brain), reflecting the fact that all of the output of the $Lmna^{PLAO}$ allele is channeled into prelamin A (rather than into both lamin C and prelamin A). Like $Lmna^{plao/plao}$ mice, $Lmna^{plao-5nt/plao-5nt}$ and $Lmna^{plao-utr/plao-utr}$ mice expressed exclusively lamin A. In all three lines, the amount of lamin A in peripheral tissues, relative to actin, was similar, but there were obvious differences in the brain. In the cerebral cortex of $Lmna^{plao-5nt/plao-5nt}$ mice, the level of lamin A was 2.28 ± 0.33-fold higher, relative to actin, than in $Lmna^{plao/plao}$ mice ($P < 0.005$; Fig. 2B); in the cerebellum, the level of lamin A was 1.66 ± 0.27-fold higher ($P < 0.05$). The

differences were more striking in $Lmna^{plao-utr/plao-utr}$ mice. In those mice, the lamin A level in the cerebral cortex was 4.30 ± 0.84-fold higher than in $Lmna^{plao/plao}$ mice ($P < 0.0005$); in the cerebellum, the lamin A level was 1.99 ± 0.24-fold higher ($P < 0.005$).

Consistent changes were observed at the RNA level (Fig. 2E). Prelamin A transcripts in the cerebral cortex of $Lmna^{plao-5nt/plao-5nt}$ mice were 1.75 ± 0.21-fold higher than in $Lmna^{plao/plao}$ mice ($P < 0.005$). In $Lmna^{plao-utr/plao-utr}$ mice, prelamin A transcripts in the cerebral cortex were 3.24 ± 0.44-fold higher than in $Lmna^{plao/plao}$ mice ($P < 0.0005$). Prelamin A transcripts in the cerebellum were 1.60 ± 0.19-fold higher in $Lmna^{plao-5nt/plao-5nt}$ mice than in $Lmna^{plao/plao}$ mice ($P < 0.005$) and 1.92 ± 0.36-fold higher in $Lmna^{plao-utr/plao-utr}$ mice than in $Lmna^{plao/plao}$ mice ($P < 0.005$). There were no substantial differences in prelamin A transcript levels in the heart, liver, and kidney of $Lmna^{plao-5nt/plao-5nt}$, $Lmna^{plao-utr/plao-utr}$ and $Lmna^{plao/plao}$ mice.

The changes in lamin A expression in $Lmna^{plao-5nt/plao-5nt}$ and $Lmna^{plao-utr/plao-utr}$ mice were not accompanied by substantial changes in the expression of lamins B1 or B2. Quantitative analyses of western blots uncovered minor fluctuations in lamins B1 and B2 levels in the tissues of $Lmna^{plao-5nt/plao-5nt}$ and $Lmna^{plao-utr/plao-utr}$ mice (Fig. 2C and D; Supplementary Material, Fig. S2), but the significance of these changes is questionable because consistent changes were not observed at the RNA level (Fig. 2H and I).

To determine if the amounts of lamin A expression in the central nervous system of $Lmna^{plao-utr/plao-utr}$ and $Lmna^{plao-5nt/plao-5nt}$ mice were similar to the total amount of A-type lamins (i.e. lamins A and C) in the brain of wild-type mice, we quantified total *Lmna* transcripts with PCR primers common to lamins A and C (Fig. 2F). Total *Lmna* transcript levels in the cerebral cortex of $Lmna^{plao-5nt/plao-5nt}$ mice were $54.3 \pm 9.6\%$ of the levels in wild-type mice ($P < 0.0005$). In $Lmna^{plao-utr/plao-utr}$ mice, total *Lmna* transcript levels in the cerebral cortex were $88.8 \pm 11.3\%$ of the levels in wild-type mice ($P > 0.05$). In the cerebellum, total *Lmna* transcripts in $Lmna^{plao-5nt/plao-5nt}$ and $Lmna^{plao-utr/plao-utr}$ mice were somewhat lower than in wild-type mice (68.0 ± 4.7 and $80.7 \pm 10.0\%$, respectively; $P < 0.05$).

Mice that were heterozygous for the knock-in mutations exhibited consistent changes in lamin A expression (Supplementary Material, Fig. S3). Lamin A expression in the cerebral cortex and cerebellum was significantly higher in $Lmna^{plao-5nt/+}$ and $Lmna^{plao-utr/+}$ mice than in $Lmna^{plao/+}$ mice. In peripheral tissues, the amounts of lamin A, relative to actin, were similar in $Lmna^{plao-5nt/+}$, $Lmna^{plao-utr/+}$ mice and $Lmna^{plao/+}$ mice.

A recent study by Senyuk *et al.* (12) reported that miR-9 is expressed in myeloid cells and promotes myeloid differentiation. To assess the impact of the $Lmna^{PLAO-5NT}$ knock-in mutation on lamin A expression in myeloid cells, we used western blots to compare the relative amounts of lamins A and C in bone marrow myeloid cells and peritoneal macrophages (Supplementary Material, Fig. S4A). Lamin A expression was lower than lamin C in both bone marrow myeloid cells and peritoneal macrophages in wild-type mice. Lamin A expression was higher in $Lmna^{plao/+}$ mice than in wild-type mice, as expected. However, unlike the situation in the brain, the levels of lamin A expression were not further increased in $Lmna^{plao-5nt/+}$ mice (Supplementary Material, Fig. S4A), demonstrating that miR-9 does not play a significant role in regulating prelamin A

41
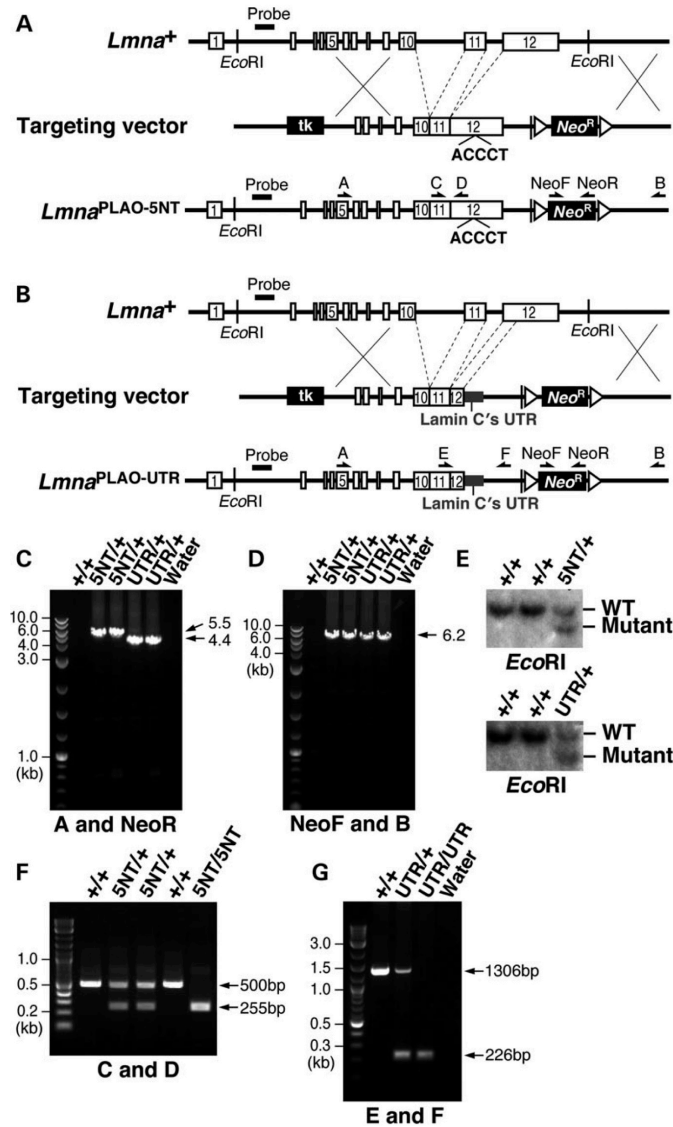
Figure 1. Knock-in mice expressing prelamin A transcripts with mutations in the 3′ UTR. (**A**) Strategy to create the *Lmna*[PLAO-5NT] allele, in which 5-nt of the seed-binding sequence in a predicted miR-9 binding site in prelamin A's 3′ UTR (CCAAAG) (5) were replaced with ACCCTG. Introns 10 and 11 were also deleted; consequently, the targeted allele yields exclusively prelamin A (and no lamin C) (11). Exons are depicted as white boxes; *lox*P sites are represented by arrowheads; the position of the 5′ flanking probe and *Eco*RI sites for Southern blotting are also identified. Primer locations for the 5′ (primers A and NeoR) and 3′ (primers NeoF and B) long-range PCRs and genotyping PCRs (primers C and D) are indicated with arrows. (**B**) Strategy to create the *Lmna*[plao-utr] allele, in which prelamin A's 3′ UTR was replaced with lamin C's 3′ UTR (grey). Introns 10 and 11 were deleted. Primer locations for the 5′ (primers A and NeoR) and 3′ (primers NeoF and B) long-range PCRs and genotyping PCRs (primers E and F) are indicated with arrows. (**C**) The 5′ long-range PCRs with the *Lmna*[PLAO-5NT] and *Lmna*[plao-utr] alleles yield 5.5 kb (lanes 3 and 4) and 4.4 kb (lanes 5 and 6) fragments, respectively. No PCR product was amplified from wild-type DNA (lane 2). (**D**) The 3′ long-range PCRs with the *Lmna*[PLAO-5NT] and *Lmna*[plao-utr] alleles yield a 6.2 kb fragment (lanes 3–6); no product was amplified from wild-type DNA (lane 2). (**E**) Southern blot analysis to identify targeted mouse ES cell clones for the *Lmna*[PLAO-5NT] and *Lmna*[plao-utr] alleles. Genomic DNA was digested with *Eco*RI, and the blot was hybridized with a 5′ flanking probe (A and B). (**F**) Genotyping PCR for the *Lmna*[PLAO-5NT] allele yields a 255 bp fragment, whereas wild-type DNA yields a 500 bp fragment. (**G**) Genotyping PCR with the *Lmna*[plao-utr] allele yields a 226 bp fragment, whereas wild-type DNA yields a 1.3 kb fragment.

42
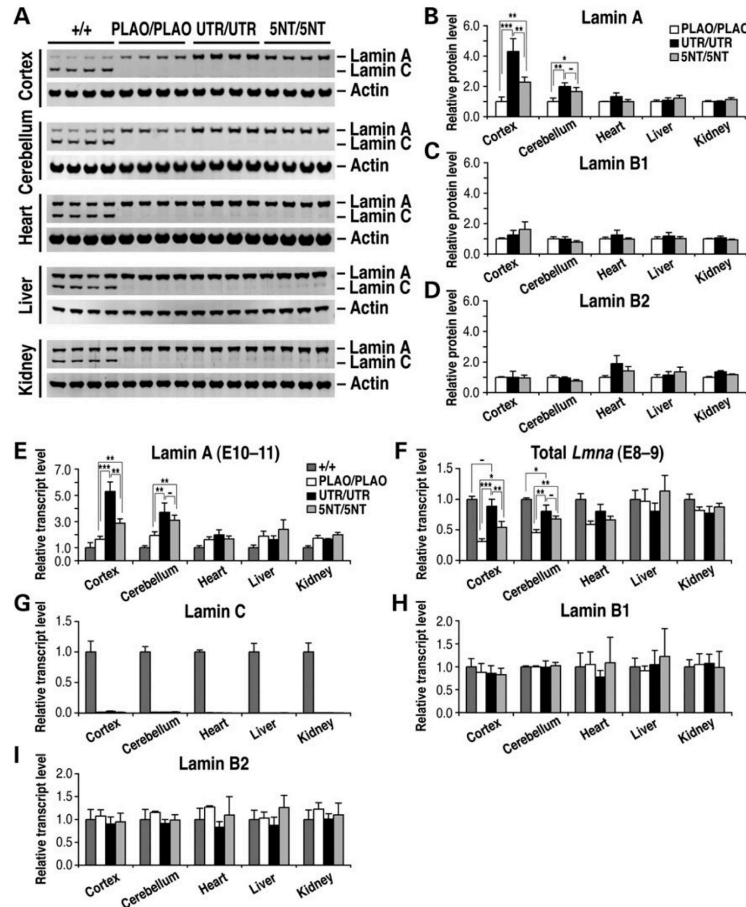
Figure 2. Higher lamin A expression in the brain of *Lmna*^plao-5nt/plao-5nt and *Lmna*^plao-utr/plao-utr mice. (**A**) Western blot analysis of lamins A and C expression in the cerebral cortex, cerebellum, heart, liver and kidney from *Lmna*^+/+ (+/+), *Lmna*^plao/plao (PLAO/PLAO) (11), *Lmna*^plao-utr/plao-utr (UTR/UTR) and *Lmna*^plao-5nt/plao-5nt (5NT/5NT) mice with antibodies against lamin A/C and actin. All samples are from 1-month-old mice. (**B–D**) Quantification of lamin protein levels relative to actin (A; Supplementary Material, Fig. S2). Values represents mean ± SD. *$P < 0.05$; **$P < 0.005$; ***$P < 0.0005$; (−) $P > 0.05$. (**E–I**) Lamin transcript levels, as judged by quantitative reverse transcription polymerase chain reaction in the same tissues analyzed in (A)–(D). Transcript levels were normalized to cyclophilin A and compared with levels in wild-type mice (set at 1.0). Values represent the mean ± SD.

expression in bone marrow myeloid cells or peritoneal macrophages. Of note, the levels of miR-9 expression in myeloid cells were far lower than those in the cerebral cortex and rather similar to the miR-9 levels in other peripheral tissues Supplementary Material, Fig. S4B.

The higher levels of lamin A in the cerebral cortex of *Lmna*^plao-5nt/plao-5nt and *Lmna*^plao-utr/plao-utr mice were easily detectable by immunohistochemistry (Fig. 3). Lamin A-positive cells were abundant throughout the cerebral cortex in both lines of mice, but were particularly striking in *Lmna*^plao-utr/plao-utr mice (Fig. 3). In wild-type and *Lmna*^plao/plao mice, lamin A staining in the cerebral cortex was minimal; only a few cells were positive

for lamin A, reflecting the fact that capillary endothelial cells express lamin A (5).

We used immunohistochemistry to test the possibility that the impact of the *Lmna*^PLAO-5NT and *Lmna*^plao-utr mutations might vary in different regions of the brain. In the cortex of *Lmna*^plao-utr/+ mice, most lamin C-positive cells expressed lamin A; the same was the case in *Lmna*^plao-5nt/+ mice, although the intensity of lamin A expression in those mice, relative to lamin C, was lower (Supplementary Material, Fig. S5A). In the corpus callosum and in the arbor vitae of the cerebellum, the expression of lamin A was similar in *Lmna*^plao-5nt/+ and *Lmna*^plao-utr/+ mice (Supplementary Material, Fig. S5A and

43
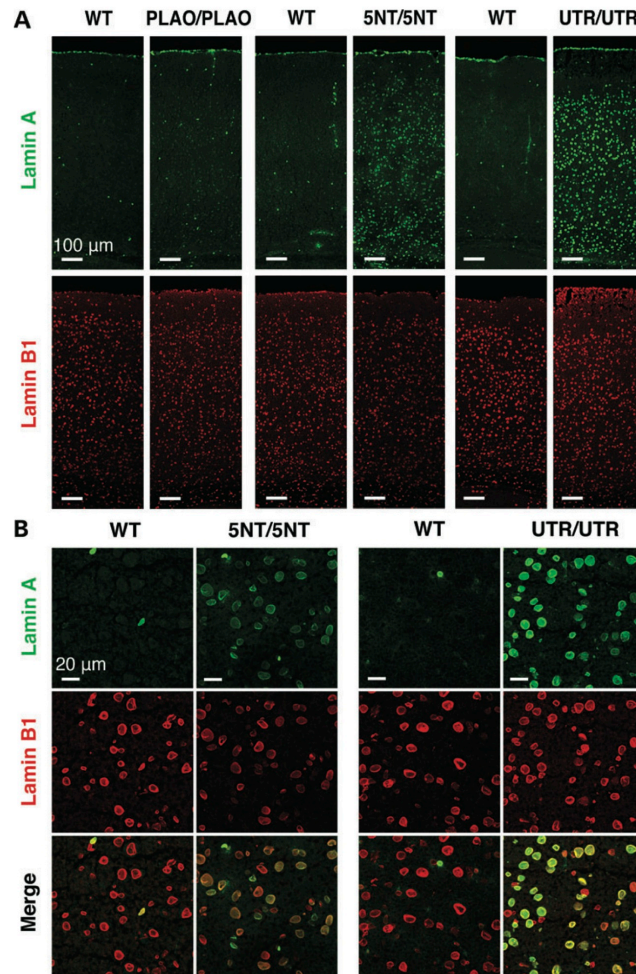
Figure 3. Immunofluorescence microscopy of the cerebral cortex from *Lmna*[plao/plao] (PLAO/PLAO), *Lmna*[plao-5nt/plao-5nt] (5NT/5NT), *Lmna*[plao-utr/plao-utr] (UTR/UTR) and wild-type (WT) littermate mice, revealing increased lamin A expression in the mice harboring mutations in prelamin A's 3′ UTR. (**A** and **B**) Low- and high-magnification images of the cerebral cortex stained with antibodies against lamin A (green) and lamin B1 (red). The scattered lamin A-positive cells in wild-type and *Lmna*[plao/plao] mice are endothelial cells (5). Scale bar in (A), 100 μm; (B), 20 μm.

B). In some regions of the brain, e.g. the striatum, lamin A expression was low in both *Lmna*[plao-5nt/+] and *Lmna*[PLAO-UTR/+] mice (Supplementary Material, Fig. S5 and Table S1). In the striatum, miR-9 expression was robust, as judged by *in situ* hybridization (Supplementary Material, Fig. S6A). Consistent with that finding, the magnitude of the increase in prelamin A transcripts (as measured by qRT-PCR) in the striatum of *Lmna*[plao-utr/plao-utr] mice was similar to that in the cortex (Supplementary Material, Fig. S6B and C). We suspect that our inability to observe a significant increase in lamin A expression in the striatum of *Lmna*[plao-utr/+] mice by immunohistochemistry probably relates to the low levels of *Lmna* expression in that site, given that lamin C expression was also low in the same tissue sections (Supplementary Material, Fig. S5).

To further define lamin A expression in the brain, we stained brain sections from *Lmna*[plao-5nt/+], *Lmna*[plao-5nt/plao-5nt], *Lmna*[plao-utr/+] and *Lmna*[plao-utr/plao-utr] mice with an antibody against lamin A—along with an antibody against NeuN (neuronal nuclei), Olig2 (oligodendrocyte lineage transcription factor 2) or GFAP (glial fibrillary acidic protein) (Fig. 4; Supplementary Material, Fig. S7). In the cerebral cortex and hippocampus of *Lmna*[plao-5nt/+] and *Lmna*[plao-utr/+] mice, all NeuN-positive

44
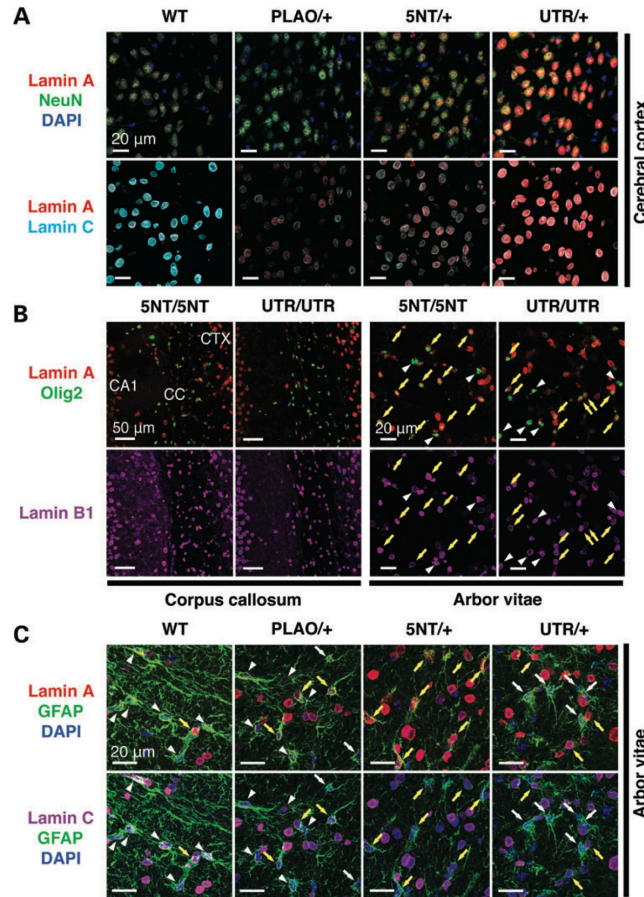
Figure 4. Lamin A expression in different cell types in the brain of *Lmna*^plao-5nt/+, *Lmna*^plao-5nt/plao-5nt, *Lmna*^plao-utr/+ and *Lmna*^plao-utr/plao-utr mice. (**A**) Immunofluorescence microscopy of the cerebral cortex from *Lmna*^plao-5nt/+ (5NT/+) and *Lmna*^plao-utr/+ (UTR/+) mice stained with antibodies against lamin A (red), lamin C (cyan) and NeuN (green). (**B**) Immunofluorescence microscopy of the corpus callosum or the arbor vitae from *Lmna*^plao-5nt/plao-5nt (5NT/5NT) and *Lmna*^plao-utr/plao-utr (UTR/UTR) mice stained with antibodies against lamin A (red), Olig2 (green) and lamin B1 (magenta). (**C**) Immunofluorescence microscopy of the arbor vitae from *Lmna*^plao-5nt/+ (5NT/+) and *Lmna*^plao-utr/+ (UTR/+) mice stained with antibodies against lamin A (red), lamin C (magenta) and GFAP (green). White arrowheads indicate cells in which lamin A expression was undetectable, even though these cells expressed lamin C (C) or lamin B1 (B); white arrows indicate cells in which neither lamin A nor lamin C was detectable; yellow arrows indicate lamin C-expressing cells in which lamin A expression was robust. Scale bars: as indicated in the figures. CTX, cerebral cortex; CC, corpus callosum.

neurons were stained positively for lamins A and C, but lamin A staining was more intense in *Lmna*^plao-utr/+ mice (Fig. 4A; Supplementary Material, Fig. S7A). In both *Lmna*^plao-5nt/+ and *Lmna*^plao-utr/+ mice, lamin A expression was observed in most Olig2-positive oligodendrocytes (Fig. 4B, yellow arrows). The expression of lamin A in GFAP/lamin C-positive astrocytes in *Lmna*^plao-5nt/+ and *Lmna*^plao-utr/+ mice was less evident, likely due to low expression of A-type lamins in astrocytes (Fig. 4C; Supplementary Material, Fig. S7B, yellow arrows).

The health and vitality of *Lmna*^plao-5nt/plao-5nt and *Lmna*^plao-utr/plao-utr mice were indistinguishable from wild-type littermates (Supplementary Material, Fig. S8A and B). At 1 month of age, the size and morphology of the brain in *Lmna*^plao-5nt/plao-5nt and *Lmna*^plao-utr/plao-utr, and wild-type mice were similar (Fig. 5A and B). We found no evidence for abnormal layering of neurons or lower numbers of neurons in brains of knock-in mice (Fig. 5C and D; Supplementary Material, Fig. S8C–E). In addition, we found no evidence that the expression of lamin A (rather than lamin C) in the brain resulted in misshapen cell nuclei or mislocalization of other nuclear membrane proteins (Fig. 3B; Supplementary Material, Fig. S9). Older *Lmna*^plao-5nt/plao-5nt (at 6.5 months of age) and

45
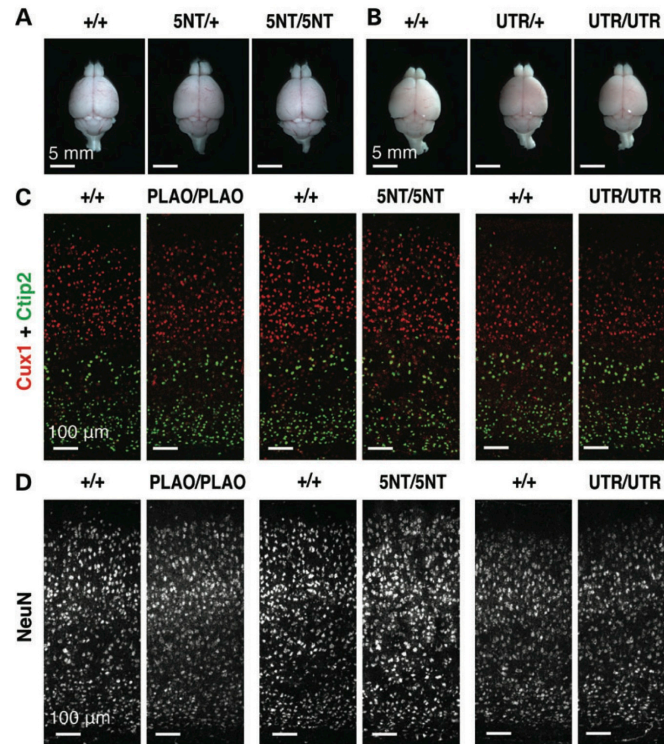
Figure 5. *Lmna*^plao-5nt/plao-5nt and *Lmna*^plao-utr/plao-utr mice have no detectable neuropathology. (**A** and **B**) Brains from 1-month-old *Lmna*^+/+ (+/+), *Lmna*^plao-5nt/+ (5NT/+), *Lmna*^plao-5nt/plao-5nt (5NT/5NT), *Lmna*^plao-utr/+ (UTR/+) and *Lmna*^plao-utr/plao-utr (UTR/UTR) mice, viewed from the top. Scale bar, 5 mm. (**C** and **D**) Immunofluorescence microscopy of the cerebral cortex from 1-month-old *Lmna*^plao/plao (PLAO/PLAO), *Lmna*^plao-5nt/plao-5nt (5NT/5NT), *Lmna*^plao-utr/plao-utr (UTR/UTR) and wild-type (+/+) littermate mice stained with antibodies against Cux1 (red) and Ctip2 (green) (C) or NeuN (white) (D). Scale bar, 100 μm.

Lmna^plao-utr/plao-utr mice (at 9.5 months of age) remained healthy (Supplementary Material, Fig. S10); neither loss of neurons nor increased cell death was observed (Supplementary Material, Fig. S10D and E). *Lmna*^plao-utr/plao-utr mice were also indistinguishable from wild-type mice by SHIRPA (SmithKline Beecham, Harwell, Imperial College and Royal London Hospital phenotype assessment) behavioral screens and by rotarod tests (13,14) (Supplementary Material, Fig. S11 and Table S2).

DISCUSSION

Earlier studies by Jung *et al.* (5) with transfected cells suggested that the low levels of lamin A expression in the brain might be due to regulation of prelamin A transcripts by miR-9. A subsequent study suggested the same possibility (15). While intriguing, these reports dealt solely with cultured cells, and whether the experiments were actually relevant to lamin A expression in the brain was unclear. In the current study, we addressed that issue by creating two new lines of *Lmna*

knock-in mice—one in which a 5-nucleotide (nt) mutation was introduced into the predicted miR-9 binding site in prelamin A's 3′ UTR (*Lmna*^plao-5nt/plao-5nt) and a second in which prelamin A's 3′ UTR was replaced with lamin C's 3′ UTR (*Lmna*^plao-utr/plao-utr). Both mouse models produced increased amounts of lamin A in the brain, providing strong support for the role of miR-9 in regulating prelamin A expression in the central nervous system. The discovery that miR-9 is crucial in determining prelamin A production is clinically important: the limited expression of prelamin A in the brain likely explains why children with HGPS are spared from neurodegenerative disease.

The *Lmna*^PLAO-5NT and *Lmna*^plao-utr alleles lacked introns 10 and 11, eliminating any possibility of the alternative splicing event that normally leads to lamin C synthesis. The fact that both knock-in mice were 'prelamin A-only' models was a boon for our studies, making it possible for us to quantify the impact of the 3′ UTR mutations on prelamin A/lamin A expression without having to worry about effects on prelamin A/lamin C splicing. As a control, we simultaneously evaluated prelamin

A/lamin A expression levels in prelamin A-only mice lacking any 3′ UTR mutations (*Lmna*$^{plao/plao}$ mice) (11). Lamin A expression in the brain of *Lmna*$^{plao/plao}$ mice was low.

The expression of prelamin A transcripts and lamin A protein in the cerebral cortex and cerebellum of *Lmna*$^{plao-5nt/plao-5nt}$ mice was significantly higher than in *Lmna*$^{plao/plao}$ mice. The sole difference between these models was the 5-nt mutation in prelamin A's 3′ UTR. We are confident that this mutation was effective in eliminating miR-9-mediated regulation because it abolished the ability of miR-9 to inhibit the expression of a luciferase reporter (linked to prelamin A's 3′ UTR). Also, this mutation resulted in significantly increased expression of prelamin A transcripts in the brain (where miR-9 expression is robust) but had no effect on prelamin A transcripts in peripheral tissues (where miR-9 is absent).

The increase in prelamin A/lamin A expression in the cerebral cortex was more substantial in *Lmna*$^{plao-utr/plao-utr}$ mice than in *Lmna*$^{plao-5nt/plao-5nt}$ mice. The mutation in the *Lmna*$^{plao-utr}$ allele was obviously more extensive, eliminating both the miR-9 binding site and ~1 kb of additional sequences in prelamin A's 3′ UTR. The higher levels of lamin A expression in the brain of *Lmna*$^{plao-utr/plao-utr}$ mice, compared with *Lmna*$^{plao-5nt/plao-5nt}$ mice, suggest that other sequences in prelamin A's 3′ UTR play a role in regulating prelamin A. The possibility is certainly plausible because large stretches of prelamin A's 3′ UTR (and not simply the region surrounding the miR-9 binding site) have been conserved in mammalian evolution. Interestingly, the effects of the *Lmna*$^{plao-utr}$ allele on prelamin A/lamin A expression varied in different regions of the brain. The increase in prelamin A expression in the cerebral cortex of *Lmna*$^{plao-utr/plao-utr}$ mice was greater than in *Lmna*$^{plao-5nt/plao-5nt}$ mice, but in the cerebellum, the increase in prelamin A expression was fairly similar in the two lines of mice. These findings suggest that the regulation of lamin A in the cerebellum could depend primarily on the miR-9 binding site, whereas lamin A regulation in the cortex could involve both the miR-9 site and other, as-yet-undefined, 3′ UTR sequences. It is also possible that the differences in lamin A regulation in different parts of the brain relate, at least in part, to distinct impacts of the two knock-in mutations on different cell types and to different populations of cells in different regions of the brain. By immunohistochemistry, lamin A expression in NeuN-positive cortical neurons was increased in both *Lmna* knock-in lines, and the effects were clearly greater in *Lmna*$^{plao-utr/plao-utr}$ mice. However, the increase in lamin A expression in Olig2-positive oligodendrocytes was less impressive in both knock-in lines, and the increase in lamin A in GFAP-positive astrocytes was nearly undetectable. As a result, we could not discern significant differences between the two knock-in lines with respect to glial cell expression of lamin A.

Our studies provide new insights regarding the functional importance of the A-type lamins in the brain. First, we observed no neuropathology in *Lmna*$^{plao/plao}$ mice, which cannot make lamin C and produce little lamin A in brain parenchymal cells. Thus, it would appear that very low levels of A-type lamins in the brain are not associated with adverse consequences. This is very different from the situation with striated muscle, where an absence of lamins A and C causes myopathic changes and early death (16). Second, we observed no pathology or behavioral abnormalities in *Lmna*$^{plao-utr/plao-utr}$ mice, which produce

prelamin A (rather than lamin C) in brain parenchymal cells, demonstrating that lamin A production is not overtly toxic in the brain.

We previously reported that lamins B1 and B2 are expressed highly in the developing brain and that both proteins are crucial for neuronal migration (17–19). Neither lamin A nor lamin C is expressed in migrating neurons, but large amounts of lamin C are expressed after birth. From the current studies, we now understand why lamin A synthesis is low in brain parenchymal cells, but the physiologic 'rationale' for limiting lamin A expression in the brain is still elusive. The nuclear lamins are known to interact with a variety of inner nuclear membrane proteins as well as proteins in the chromatin (20,21). One possibility is that lamin C is better suited for interacting with the spectrum of nuclear envelope and chromatin proteins that are expressed in the brain. Another possibility is that lamin A expression in the brain, while well tolerated in laboratory mice, would be suboptimal in extenuating circumstances, e.g. in response to injury or metabolic stress.

Mice lacking miR-9 exhibit defective neuronal migration and impaired neuronal survival (22). Neither of these phenotypes were encountered in mice lacking the miR-9 binding site in prelamin A's 3′ UTR. Of course, this discrepancy is not surprising, given that miR-9 almost certainly has many dozens of targets, the majority of which await characterization. Once all of the miR-9 targets are defined and understood, it is possible that the rationale for miR-9 regulation of prelamin A expression will come into sharper focus.

MATERIALS AND METHODS

Generation of knock-in mice with mutations in prelamin A's 3′ UTR

The *Lmna*$^{PLAO-5NT}$ allele was created with a sequence-replacement vector identical to the one used to create the *Lmna*^{PLAO} allele (11), except that the miR-9 seed-binding sequence in prelamin A's 3′ UTR (CCAAAG) was changed to ACCCTG. The mutation was introduced into the 5′ arm of the *Lmna*^{PLAO} targeting vector by site-directed mutagenesis (QuikChange kit, Stratagene) with primer 5′-AGCAGGCCTGAAG ACCCTGAAAAATTTATC-3′ (and a complementary reverse primer). The vector used to create the *Lmna*$^{plao-utr}$ vector was also similar to the *Lmna*^{PLAO} vector, except that the sequences encoding prelamin A's 3′ UTR in the 5′ arm of the vector were replaced with lamin C's 3′ UTR (using the In-Fusion Advantage PCR cloning kit from Clontech). Lamin C's 3′ UTR was amplified with primers 5′-TGCAGCATCATGTAAGGCCCAGCC CACAAGGGTA-3′ and 5′-GACACCACAGCATCTGGCATT CCAAAACAT-3′ and then inserted into the 5′ arm of the *Lmna*^{PLAO} vector with primers 5′-AGATGCTGTGGTGTCT CTTTGTTG-3′ and 5′-TTACATGATGCTGCAGTTCTGG GAGCTCT-3′. The integrity of the vectors was verified by restriction endonuclease digestion and DNA sequencing.

After electroporating the vectors into 129/OlaHsd embryonic stem (ES) cells, targeted clones were identified by long-range PCR (TaKaRa LA Taq polymerase, Clontech) with primers A and NeoR on the 5′ end and primers NeoF and B on the 3′ end (see Supplementary Material, Table S3A for the primer sequences; Fig. 1A and B). The targeting events were confirmed by Southern blotting with *Eco*RI-cleaved genomic DNA and a 5′

47

flanking probe (11). The probe detected a 10.4-kb fragment in a wild-type *Lmna* allele; a 9.4-kb fragment in the *Lmna*[PLAO-5NT] allele and an 8.6-kb fragment in the *Lmna*[plao-utr] allele.

Targeted ES cell clones were injected into C57BL/6 blastocysts, and the resulting chimeras were bred with C57BL/6 females to generate heterozygous *Lmna* knock-in mice, which were then intercrossed to generate homozygotes. Genotyping was performed by PCR with primers C and D for the *Lmna*[PLAO-5NT] allele and primers E and F for the *Lmna*[plao-utr] allele (Fig. 1A and B).

All mice were fed a chow diet and housed in a virus-free barrier facility with a 12-h light/dark cycle. Animal protocols were approved by UCLA's Animal Research Committee.

Western blots

Protein extracts from mouse tissues were prepared as described (5,23). Briefly, snap-frozen mouse tissues were powdered with a chilled metal mortar and pestle, resuspended in ice-cold PBS containing 1 mM phenylmethylsulfonyl fluoride (PMSF), 1 mM NaF and protease inhibitors (Roche) and homogenized with a glass tissue grinder (Kontes). The cell pellets were resuspended in urea buffer [9 M urea, 10 mM Tris–HCl (pH 8.0), 1 mM NaF, 1 mM PMSF, 10 μM ethylenediaminetetraacetic acid 0.2% β-mercaptoethanol and a Roche Protease Inhibitors Cocktail Tablet], sonicated and centrifuged at 18,000*g* for 5 min to isolate the urea-soluble protein fraction. Protein extracts were size-fractionated on 4–12% gradient polyacrylamide Bis-Tris gels (Invitrogen) and transferred to a nitrocellulose membrane. Membranes were incubated with primary antibodies as indicated in Supplementary Material, Table S3B. Antibody binding was detected with infrared (IR)-dye-conjugated secondary antibodies (Rockland) and an Odyssey IR scanner (LI-COR).

Quantitative RT–PCR

Levels of lamin transcripts were assessed as described previously (19). Snap-frozen mouse tissues were homogenized in TRI reagent (Molecular Research Center), and total RNA was extracted according to the manufacturer's protocol. RNA was treated with DNase I (Ambion) and then reverse transcribed with oligo(dT), random primers and SuperScript III (Invitrogen). qPCRs were prepared with SYBR Green PCR Master Mix (Bioline) and performed on a 7900 Fast Real-Time PCR system (Applied Biosystems). Transcript levels were determined by the comparative cycle threshold method and normalized to levels of cyclophilin A.

Histology and immunofluorescence microscopy

Freshly harvested mouse tissues were fixed in 10% formalin (Evergreen) overnight at 4°C; tissues were then embedded in paraffin, sectioned (5 μm) and stained with hematoxylin and eosin. For immunohistochemical studies, mouse tissues were embedded in Optimum Cutting Temperature compound (Sakura Finetek), cryosectioned (10 μm) and fixed in ice-cold methanol. After rinsing with acetone, the sections were washed with 0.1% Tween-20 in tris-buffered saline and incubated with M.O.M. Mouse Ig Blocking Reagent (Vector Laboratories). Primary antibodies are listed in Supplementary Material,

Table S3B. Binding of primary antibodies was detected with Alexa Fluor-labeled donkey antibodies against goat, rabbit or rat IgG (Invitrogen); the binding of mouse monoclonal antibodies was detected with M.O.M. Biotinylated Anti-Mouse IgG Reagent (Vector Laboratories) and Alexa Fluor-conjugated streptavidin (Invitrogen). DNA was stained with 4′,6-diamidino-2-phenylindole.

Light microscopy images were captured with a Leica MZ6 dissecting microscope [a Plan 0.5× objective (air)] with a DFC290 digital camera (Leica) and a Nikon Eclipse E600 microscope [Plan Fluor 4×/0.13 NA or 10×/0.30 NA objectives (air)] with a DS-Fi2 camera (Nikon). The images were recorded with Leica Application Suite imaging software and NIS-Elements F (Nikon), respectively. Confocal microscopy was performed with a Zeiss LSM700 laser-scanning microscope [Plan Apochromat 10×/0.45 NA or 20×/0.80 NA objectives (air)]. Images along the *z*-axis were captured and merged images were generated with Zen 2010 software (Zeiss).

Behavioral analysis

The SHIRPA primary screen (13) was performed with adult *Lmna*[plao-utr/plao-utr] mice in the UCLA Behavioral Testing Core facility. The tests included observation of mice in a viewing jar and measurements of transfer arousal, muscle tone, autonomic behaviors and righting reflex. Rotarod testing (14) was also performed. All tests were performed in a blinded fashion.

Statistical analysis

Statistical analyses were performed with GraphPad QuickCalcs (http://www.graphpad.com/ last accessed on 29 October, 2013). Differences in levels of lamin transcripts, proteins and luciferase activities were analyzed by a two-tailed Student's *t*-test.

Conflict of Interest statement. None declared.

REFERENCES

1. Lin, F. and Worman, H.J. (1993) Structural organization of the human gene encoding nuclear lamin A and nuclear lamin C. *J. Biol. Chem.*, **268**, 16321–16326.
2. Worman, H.J., Fong, L.G., Muchir, A. and Young, S.G. (2009) Laminopathies and the long strange trip from basic cell biology to therapy. *J. Clin. Invest.*, **119**, 1825–1836.
3. De Sandre-Giovannoli, A., Bernard, R., Cau, P., Navarro, C., Amiel, J., Boccaccio, I., Lyonnet, S., Stewart, C.L., Munnich, A., Le Merrer, M. *et al.* (2003) Lamin a truncation in Hutchinson-Gilford progeria. *Science*, **300**, 2055.
4. Eriksson, M., Brown, W.T., Gordon, L.B., Glynn, M.W., Singer, J., Scott, L., Erdos, M.R., Robbins, C.M., Moses, T.Y., Berglund, P. *et al.* (2003) Recurrent de novo point mutations in lamin A cause Hutchinson-Gilford progeria syndrome. *Nature*, **423**, 293–298.
5. Jung, H.J., Coffinier, C., Choe, Y., Beigneux, A.P., Davies, B.S., Yang, S.H., Barnes, R.H. 2nd, Hong, J., Sun, T., Pleasure, S.J. *et al.* (2012) Regulation of

prelamin A but not lamin C by miR-9, a brain-specific microRNA. *Proc. Natl Acad. Sci. USA*, **109**, E423–E431.

6. Coffinier, C., Jung, H.J., Li, Z., Nobumori, C., Yun, U.J., Farber, E.A., Davies, B.S., Weinstein, M.M., Yang, S.H., Lammerding, J. *et al.* (2010) Direct synthesis of lamin A, bypassing prelamin a processing, causes misshapen nuclei in fibroblasts but no detectable pathology in mice. *J. Biol. Chem.*, **285**, 20818–20826.

7. Bartel, D.P. (2009) MicroRNAs: target recognition and regulatory functions. *Cell*, **136**, 215–233.

8. Bushati, N. and Cohen, S.M. (2007) microRNA functions. *Annu. Rev. Cell Dev. Biol.*, **23**, 175–205.

9. Gao, F.B. (2010) Context-dependent functions of specific microRNAs in neuronal development. *Neural Dev.*, **5**, 25.

10. Coolen, M. and Bally-Cuif, L. (2009) MicroRNAs in brain development and physiology. *Curr. Opin. Neurobiol.*, **19**, 461–470.

11. Davies, B.S., Barnes, R.H. 2nd, Tu, Y., Ren, S., Andres, D.A., Spielmann, H.P., Lammerding, J., Wang, Y., Young, S.G. and Fong, L.G. (2010) An accumulation of non-farnesylated prelamin A causes cardiomyopathy but not progeria. *Hum. Mol. Genet.*, **19**, 2682–2694.

12. Senyuk, V., Zhang, Y., Liu, Y., Ming, M., Premanand, K., Zhou, L., Chen, P., Chen, J., Rowley, J.D., Nucifora, G. *et al.* (2013) Critical role of miR-9 in myelopoiesis and EVI1-induced leukemogenesis. *Proc. Natl Acad. Sci. USA*, **110**, 5594–5599.

13. Rogers, D.C., Fisher, E.M., Brown, S.D., Peters, J., Hunter, A.J. and Martin, J.E. (1997) Behavioral and functional analysis of mouse phenotype: SHIRPA, a proposed protocol for comprehensive phenotype assessment. *Mamm. Genome*, **8**, 711–713.

14. Carter, R.J., Morton, J. and Dunnett, S.B. (2001) Motor coordination and balance in rodents. *Curr. Protoc. Neurosci.*, **Chapter 8**, Unit 8.12.

15. Nissan, X., Biondel, S., Navarro, C., Maury, Y., Denis, C., Girard, M., Martinat, C., De Sandre-Giovannoli, A., Levy, N. and Peschanski, M. (2012) Unique preservation of neural cells in Hutchinson-Gilford progeria syndrome Is due to the expression of the neural-specific miR-9 microRNA. *Cell Rep.*, **1**, 1–9.

16. van Engelen, B.G., Muchir, A., Hutchison, C.J., van der Kooi, A.J., Bonne, G. and Lammens, M. (2005) The lethal phenotype of a homozygous nonsense mutation in the lamin A/C gene. *Neurology*, **64**, 374–376.

17. Coffinier, C., Chang, S.Y., Nobumori, C., Tu, Y., Farber, E.A., Toth, J.I., Fong, L.G. and Young, S.G. (2010) Abnormal development of the cerebral cortex and cerebellum in the setting of lamin B2 deficiency. *Proc. Natl Acad. Sci. USA*, **107**, 5076–5081.

18. Coffinier, C., Jung, H.J., Nobumori, C., Chang, S., Tu, Y., Barnes, R.H. 2nd, Yoshinaga, Y., de Jong, P.J., Vergnes, L., Reue, K. *et al.* (2011) Deficiencies in lamin B1 and lamin B2 cause neurodevelopmental defects and distinct nuclear shape abnormalities in neurons. *Mol. Biol. Cell*, **22**, 4683–4693.

19. Jung, H.J., Nobumori, C., Goulbourne, C.N., Tu, Y., Lee, J.M., Tatar, A., Wu, D., Yoshinaga, Y., de Jong, P.J., Coffinier, C. *et al.* (2013) Farnesylation of lamin B1 is important for retention of nuclear chromatin during neuronal migration. *Proc. Natl Acad. Sci. USA*, **110**, E1923–E1932.

20. Schirmer, E.C. and Foisner, R. (2007) Proteins that associate with lamins: many faces, many functions. *Exp. Cell Res.*, **313**, 2167–2179.

21. Dauer, W.T. and Worman, H.J. (2009) The nuclear envelope as a signaling node in development and disease. Dev. Cell, **17**, 626–638.

22. Shibata, M., Nakao, H., Kiyonari, H., Abe, T. and Aizawa, S. (2011) MicroRNA-9 regulates neurogenesis in mouse telencephalon by targeting multiple transcription factors. J. Neurosci., **31**, 3407–3422.

23. Fong, L.G., Ng, J.K., Meta, M., Cote, N., Yang, S.H., Stewart, C.L., Sullivan, T., Burghardt, A., Majumdar, S., Reue, K. *et al.* (2004) Heterozygosity for Lmna deficiency eliminates the progeria-like phenotypes in Zmpste24-deficient mice. Proc. Natl Acad. Sci. USA, **101**, 18111–18116.

49

Supplemental material for:

New *Lmna* knock-in mice provide a molecular mechanism for the "segmental aging" in Hutchinson-Gilford progeria syndrome

Hea-Jin Jung *et al.*

SUPPLEMENTAL METHODS

Luciferase reporter assay

Luciferase reporter vectors (pmirGLO, Promega) with full-length prelamin A 3′ UTR, mutant versions of prelamin A's 3′ UTR with 3-nucleotide mutations (CAA>ACC, CAA>del) (Supplementary Material, Fig. S1A), or lamin C's 3′ UTR were reported previously (1). A luciferase reporter vector with the "ACCCT" mutation was generated by site-directed mutagenesis with primer 5′–AGCAGGCCTGAAGACCCTGAAAAATTTATC–3′ and a complementary reverse primer. HeLa and U-87 MG cells were cotransfected with the luciferase vectors along with either a miR-9 expression vector or an empty vector (2). After 24 h, the cells were lysed with Passive Lysis Buffer (Promega) and analyzed for firefly- and Renilla-luciferase activities with the Dual-Luciferase Reporter Assay System (Promega) and a Synergy 2 luminometer (Biotek).

Myeloid cell studies

Bone marrow cells were harvested from the femur and tibia by flushing with PBS. Red blood cells were removed by incubation in red blood cell lysis buffer (0.15 M NH_4Cl, 10

mM KHCO$_3$, 0.1 mM EDTA) at 37° C for 3 min. Peritoneal cells were collected by peritoneal lavage with PBS and resident macrophages were isolated by cell adherence in DMEM medium containing 10% FBS at 37ºC for 1 h. After washing with PBS twice, adherent cells were collected with cell scrapers.

For protein analysis, cells were lysed in urea buffer and processed as described in the *Materials and Methods.* microRNA levels were measured by qRT-PCR as described (1). Total RNA was isolated with an RNeasy kit (Qiagen) and reverse-transcribed with miRCURY LNA Universal cDNA synthesis kit II (Exiqon). qPCR reactions were performed on a 7900 Fast Real-Time PCR system (Applied Biosystems) with the ExiLENT SYBR Green PCR Master Mix and LNA PCR primers (Exiqon).

Fluorescence *in situ* hybridization

One-month-old mice were perfused with 4% paraformaldehyde (PFA) and tissues were cryoprotected in 20% sucrose overnight at 4° C. Tissues were then embedded in Optimum Cutting Temperature compound (Sakura Finetek) and sectioned (10 μm). *In situ* hybridization was performed with the miRCURY LNA microRNA ISH Optimization kit (Exiqon). Slides were treated with proteinase K (2 mg/ml) for 10 min at 37° C and then incubated in 3% hydrogen peroxidase in PBS to block endogenous peroxidase activity. After dehydration in 70%, 96%, and 99.9% ethanol, the slides were incubated with digoxigenin-labeled probes (40 nM) in 1× microRNA ISH buffer (Exiqon) for 1 h at 55° C and washed with 5×, 1×, and 0.2× SSC buffers (5 min each) at 55° C. Slides were then incubated with polymerized horseradish peroxidase (POD)–conjugated anti-digoxigenin sheep IgG (Roche). Antibody binding was detected with the TSA Plus Systems (PerkinElmer).

REFERENCES

1   Jung, H.J., Coffinier, C., Choe, Y., Beigneux, A.P., Davies, B.S., Yang, S.H., Barnes, R.H., 2nd, Hong, J., Sun, T., Pleasure, S.J. *et al.* (2012) Regulation of prelamin A but not lamin C by miR-9, a brain-specific microRNA. *Proc. Natl. Acad. Sci. U. S. A*., **109**, E423-431.

2   Delaloy, C., Liu, L., Lee, J.A., Su, H., Shen, F., Yang, G.Y., Young, W.L., Ivey, K.N. and Gao, F.B. (2010) MicroRNA-9 coordinates proliferation and migration of human embryonic stem cell-derived neural progenitors. *Cell Stem Cell*, **6**, 323-335.

3   Coffinier, C., Jung, H.J., Nobumori, C., Chang, S., Tu, Y., Barnes, R.H., 2nd, Yoshinaga, Y., de Jong, P.J., Vergnes, L., Reue, K. *et al.* (2011) Deficiencies in lamin B1 and lamin B2 cause neurodevelopmental defects and distinct nuclear shape abnormalities in neurons. *Mol. Biol. Cell*, **22**, 4683-4693.

4   Jung, H.J., Nobumori, C., Goulbourne, C.N., Tu, Y., Lee, J.M., Tatar, A., Wu, D., Yoshinaga, Y., de Jong, P.J., Coffinier, C. *et al.* (2013) Farnesylation of lamin B1 is important for retention of nuclear chromatin during neuronal migration. *Proc. Natl. Acad. Sci. U. S. A*, **110**, E1923-1932.

SUPPLEMENTAL FIGURES
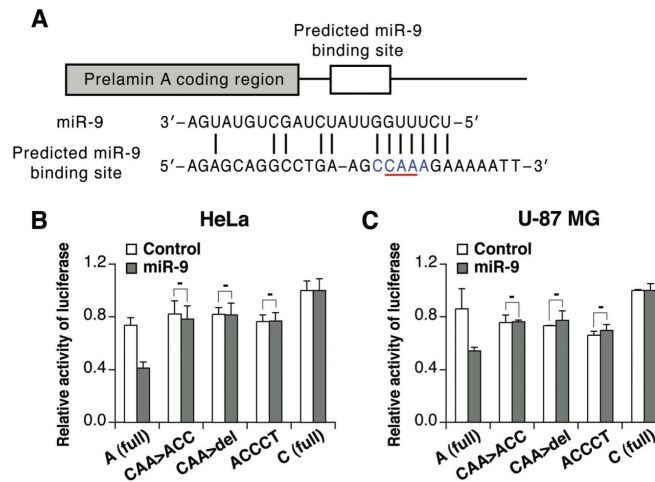
Figure S1. The "ACCCT mutation" in the seed-binding sequence of the miR-9 binding site in prelamin A's 3′ UTR abolishes the effects of miR-9 on prelamin A expression. (A) Mutation of the predicted miR-9 binding site in prelamin A's 3′ UTR. The location of the CCAAAG => ACCCTG mutation is indicated by blue font; the location of the three-nucleotide mutations (CAA>ACC and CAA>del), which were described previously (1), are underlined in red. (B and C) Luciferase assays in HeLa cells (B) and U-87 MG cells (C) that had been transfected with an empty vector (control) or a miR-9 expression vector (miR-9) along with luciferase reporter vectors in which the miR-9 seed-binding sequence (CCAAAG) in prelamin A's 3′ UTR was mutated. From left to right: A (full), wild-type 3′ UTR of prelamin A; CAA>ACC, substitution of nucleotides CAA in prelamin A's 3′ UTR with ACC; CAA>del, deletion of the CAA in prelamin A's 3′ UTR; ACCCT, substitution of the five nucleotides in prelamin A's 3′ UTR (CCAAA) with ACCCT; C (full), wild-type 3′ UTR of lamin C (1). Firefly luciferase activity levels were normalized to Renilla luciferase activity levels and compared to those in cells transfected with the luciferase vector containing the wild-type 3′ UTR of lamin C (set at 1.0). Values represent mean ± SD. The ACCCT mutation abolished the ability of miR-9 to reduce luciferase expression in both HeLa cells and U-87 MG cells. Consistent with earlier studies in HeLa cells (1), mutating (or deleting) three nucleotides (CAA) in the predicted miR-9 binding site also blocked the inhibition by miR-9. In these cell culture studies, the levels of miR-9 expression in the transfected cells were only ~10% of the levels normally observed in the cerebral cortex of wild-type mice (1). (–), $p > 0.05$.
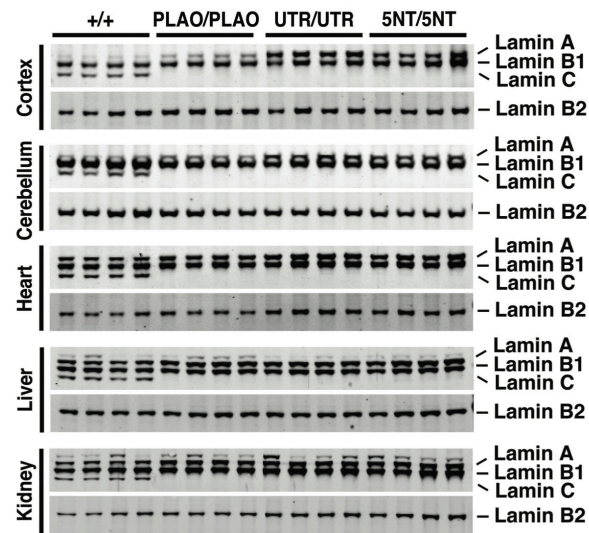
Figure S2. Western blot analysis of lamin B1 and lamin B2 expression in the cerebral cortex, cerebellum, heart, liver, and kidney from $Lmna^{+/+}$ (+/+), $Lmna^{PLAO/PLAO}$ (PLAO/PLAO), $Lmna^{PLAO-UTR/PLAO-UTR}$ (UTR/UTR), and $Lmna^{PLAO-5NT/PLAO-5NT}$ (5NT/5NT) mice. The same blots shown in Fig. 2A were re-probed with antibodies against lamin B1 and lamin B2. (See Fig. 2B–D for quantification of lamin B1 and lamin B2 signals.)

54
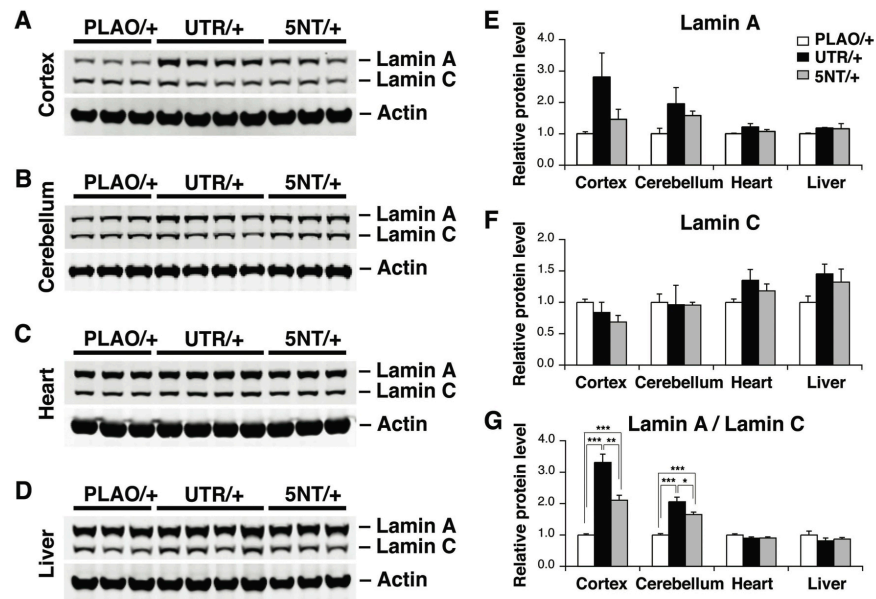
Figure S3. Western blot analysis of tissue extracts from *Lmna*^PLAO/+ (PLAO/+), *Lmna*^PLAO-UTR/+ (UTR/+), and *Lmna*^PLAO-5NT/+ (5NT/+) mice with antibodies against lamin A/C and actin. (A–D) Western blots of tissue extracts from 1-month-old mice. (E–G) Quantification of lamin A and lamin C levels relative to actin measured in panels A–D. Values represent mean ± SD. *$p < 0.05$; **$p < 0.005$; ***$p < 0.0005$.

55
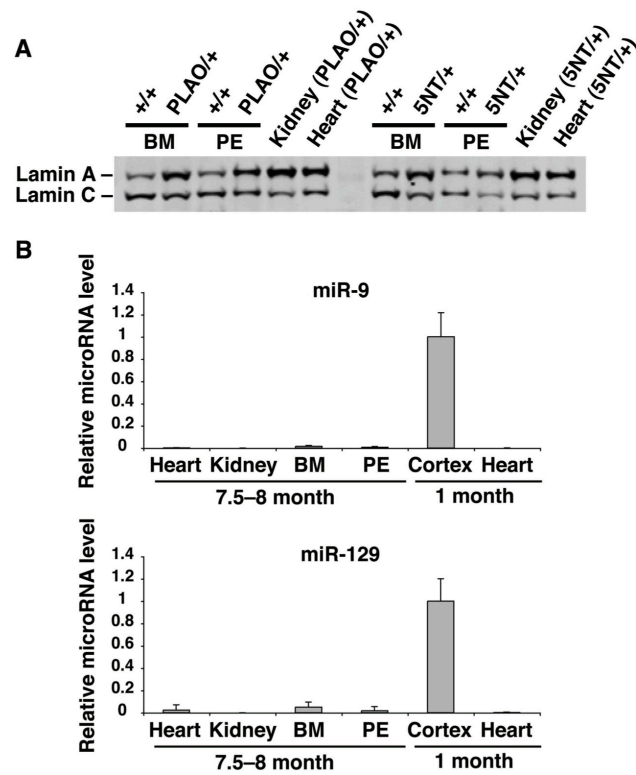
Figure S4. Lamin A and miR-9 expression in myeloid cells. (A) Western blot analysis of protein extracts of bone marrow myeloid cells (BM) and adherent peritoneal macrophages (PE) from *Lmna*^{PLAO/+} (PLAO/+), *Lmna*^{PLAO-5NT/+} (5NT/+), and wild-type (+/+) littermate mice. (B) qRT-PCR analysis of the levels of miR-9 or miR-129 in myeloid cells. Data was normalized to U6 snRNA. Values represent mean ± SD from four 1-month-old mice and four 7.5–8-month-old mice.
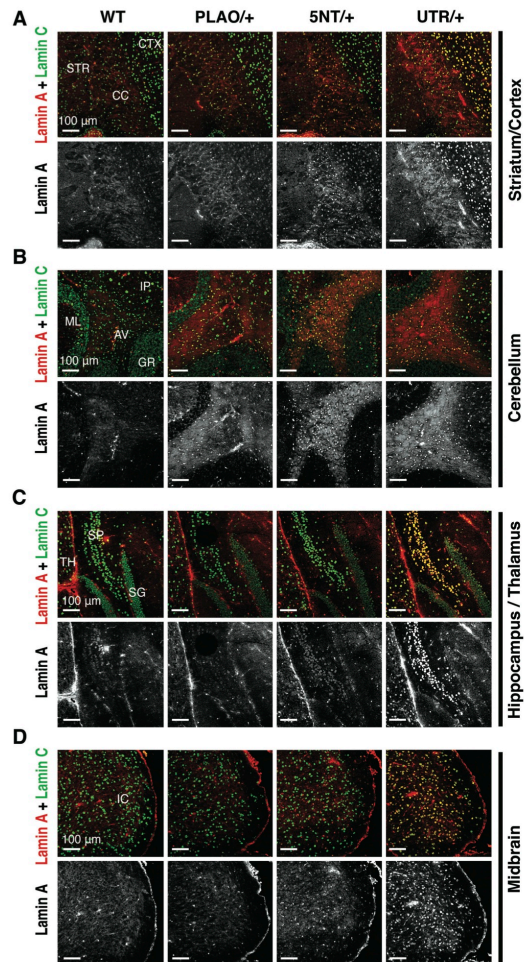
Figure S5. Immunofluorescence microscopy of the striatum/cortex, cerebellum, hippocampus/thalamus, and midbrain from wild-type (WT), *Lmna*[PLAO/+] (PLAO/+), *Lmna*[PLAO-5NT/+] (5NT/+), and *Lmna*[PLAO-UTR/+] (UTR/+) mice stained for lamin A (red or white) and lamin C (green). Scale bar, 100 μm. CTX, cerebral cortex; STR, striatum; CC, corpus callosum; ML, molecular layer; AV, arbor vitae; GR, granular layer; IP, interposed nucleus; SG, strata granulosum; SP, strata pyramidale; TH, thalamus; IC, inferior colliculus.

57
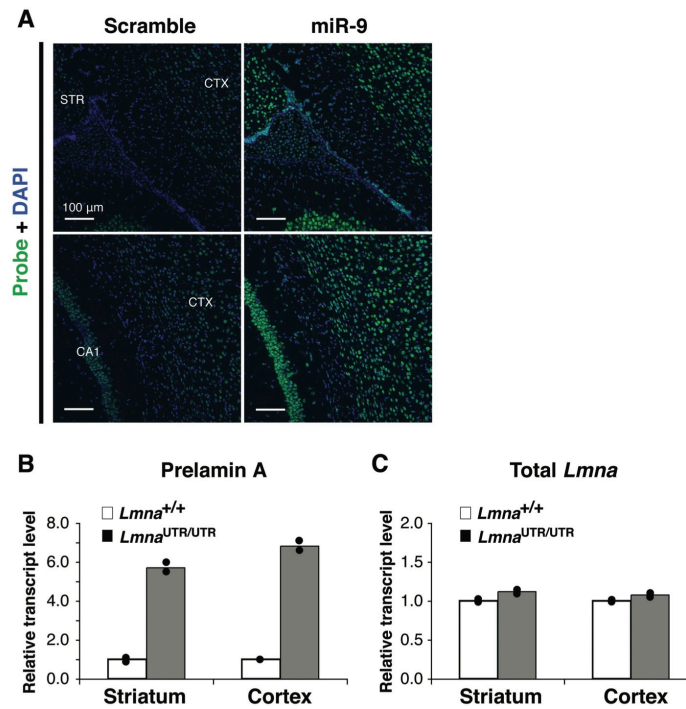
Figure S6. Expression of miR-9 and prelamin A transcripts in the striatum. (A) Fluorescence *in situ* hybridization on brain sections from 1-month-old *Lmna*[PLAO-UTR/+] mice with a miR-9 probe or a scrambled control probe. CTX, cerebral cortex; STR, striatum. Scale bar, 100 μm. (B) Quantitative RT-PCR analysis of prelamin A transcript levels and total *Lmna* transcript levels in the striatum and the cerebral cortex of *Lmna*^{+/+} (*n* = 2) and *Lmna*[PLAO-UTR/PLAO-UTR] mice (*n* = 2). Transcript levels were normalized to cyclophilin A and compared to levels in wild-type mice (set at 1.0).
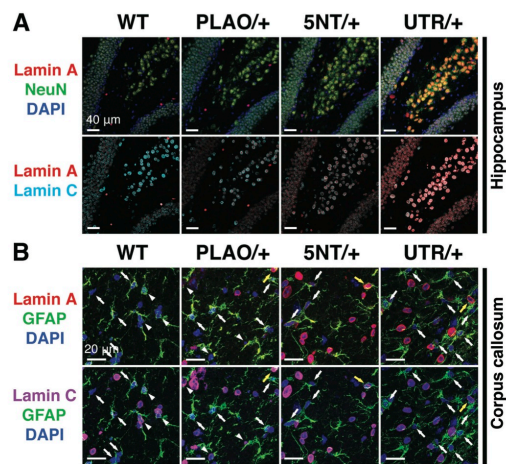
Figure S7. Immunofluorescence microscopy of the hippocampus or the corpus callosum from *Lmna*^PLAO/+^ (PLAO/+), *Lmna*^PLAO-5NT/+^ (5NT/+) and *Lmna*^PLAO-UTR/+^ (UTR/+) mice stained with antibodies against lamin A (red), lamin C (cyan in Panel A; magenta in Panel B), and either NeuN (green) in Panel A or GFAP (green) in Panel B. White arrowheads, lamin A–negative/lamin C–positive cells; white arrows, lamin A–negative/lamin C–negative cells; yellow arrows, lamin A–positive/lamin C–positive cells. Scale bars: (A) 40 µm; (B) 20 µm.

59
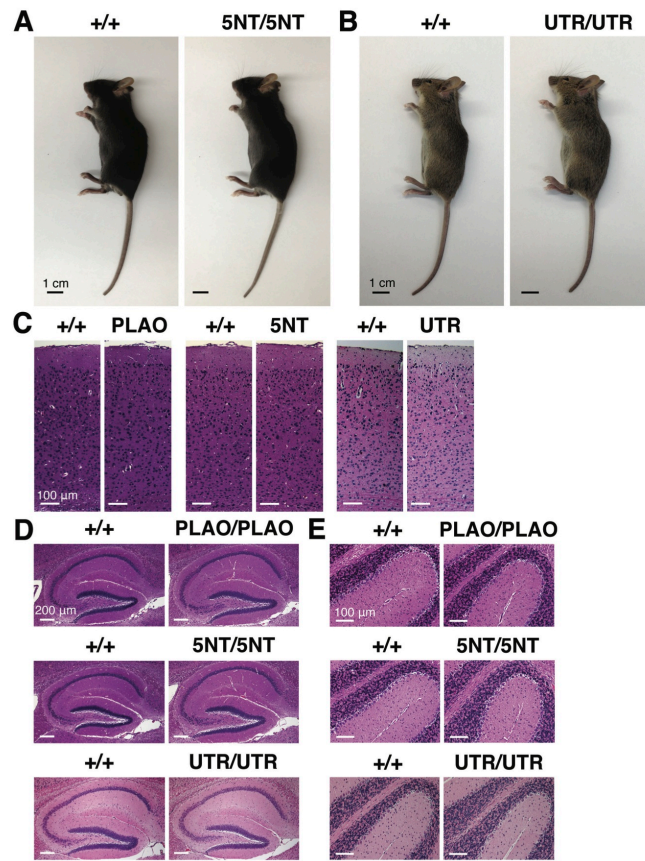
Figure S8. *Lmna*PLAO-5NT/PLAO-5NT and *Lmna*PLAO-UTR/PLAO-UTR mice are free of pathology. (A and B) Photographs of 1-month-old *Lmna*PLAO-5NT/PLAO-5NT (5NT/5NT), *Lmna*PLAO-UTR/PLAO-UTR (UTR/UTR), and wild-type (+/+) littermate mice. Scale bar, 1 cm. (C–E) Hematoxylin and eosin (H&E)–stained sections of the cerebral cortex (C), hippocampus (D), and cerebellum (E) from 1-month-old *Lmna*PLAO/PLAO (PLAO or PLAO/PLAO), *Lmna*PLAO-5NT/PLAO-5NT (5NT or 5NT/5NT) *Lmna*PLAO-UTR/PLAO-UTR (UTR or UTR/UTR), and wild-type (+/+) littermate mice. Scale bars: panel C, 100 μm; panel D, 200 μm; panel E, 100 μm.
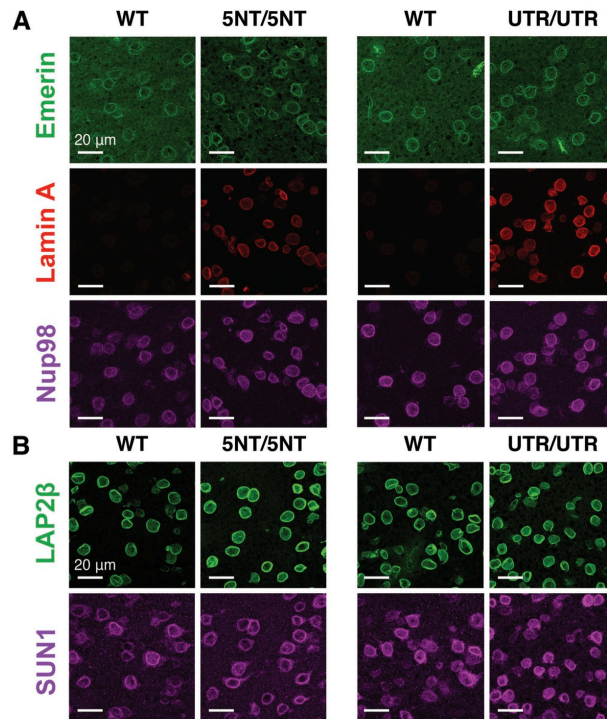
Figure S9. Increased lamin A expression in the brain does not affect localization of other nuclear membrane proteins. The cerebral cortex from $Lmna^{PLAO-5NT/PLAO-5NT}$ (5NT/5NT), $Lmna^{PLAO-UTR/PLAO-UTR}$ (UTR/UTR), and wild-type (WT) littermate mice was stained with antibodies against emerin (green), lamin A (red), and Nup98 (magenta) in (A) and LAP2β (green) and SUN1 (magenta) in (B). Scale bar, 20 µm.
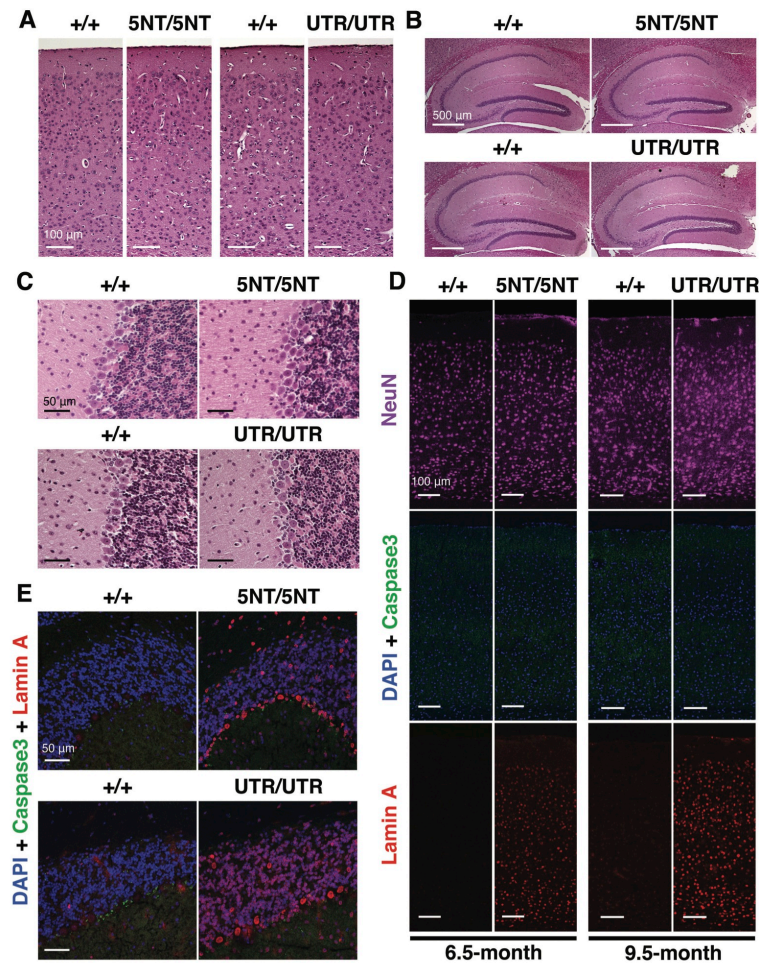
Figure S10. Absence of neuropathology in the brains of older *Lmna*[PLAO-5NT/PLAO-5NT] and *Lmna*[PLAO-UTR/PLAO-UTR] mice. (A–C) H&E–stained sections of the cerebral cortex (A), hippocampus (B), and cerebellum (C) from 6.5-month-old *Lmna*[PLAO-5NT/PLAO-5NT] (5NT/5NT) mice and 9.5-month-old *Lmna*[PLAO-UTR/PLAO-UTR] (UTR/UTR) mice along with wild-type (+/+) littermate mice. Scale bars: panel A, 100 µm; panel B, 500 µm; panel C, 50 µm. (D) Immunofluorescence microscopy of the cerebral cortex from 6.5-month-old *Lmna*[PLAO-5NT/PLAO-5NT] (5NT/5NT) and 9.5-month-old *Lmna*[PLAO-UTR/PLAO-UTR] (UTR/UTR) mice stained with antibodies against NeuN (magenta), active caspase 3 (green), and lamin A (red). Scale bar, 100 µm. (E) High-magnification images of the cerebellum from 6.5-month-old *Lmna*[PLAO-5NT/PLAO-5NT] (5NT/5NT) mice, 9.5-month-old *Lmna*[PLAO-UTR/PLAO-UTR] (UTR/UTR) mice, and wild-type (+/+) littermate mice stained with active caspase 3 (green) and lamin A (red). Scale bar, 50 µm.
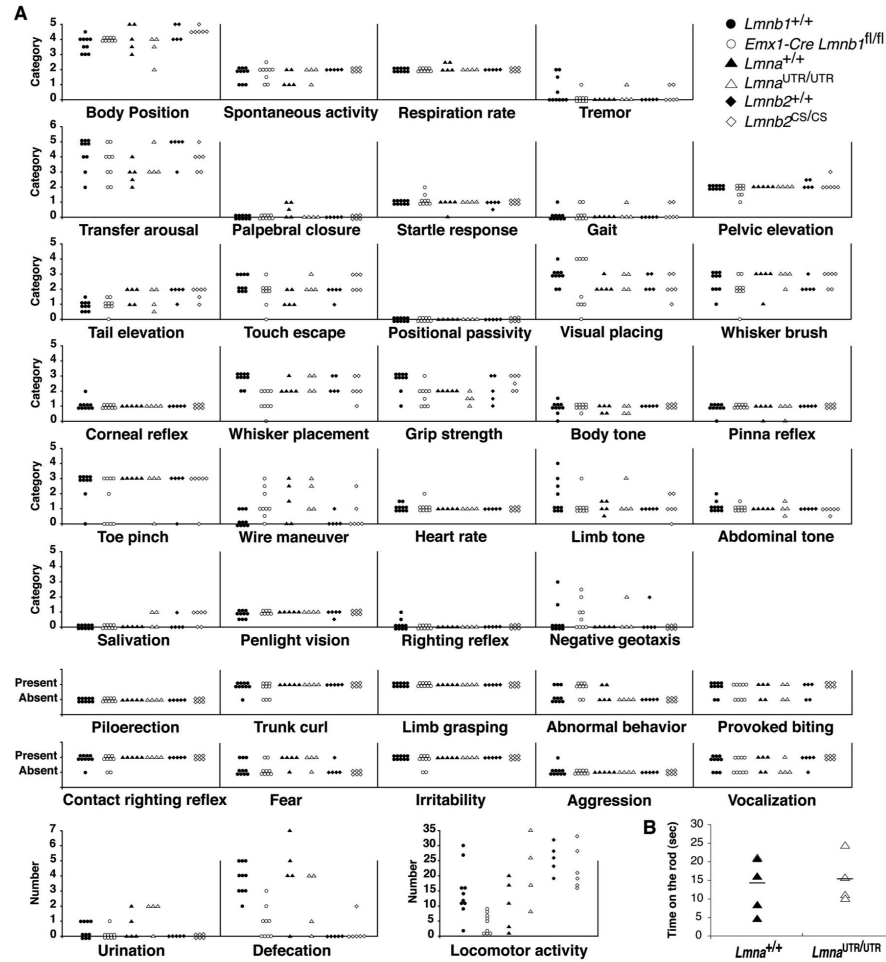
Figure S11. *Lmna*^PLAO-UTR/PLAO-UTR^ mice are indistinguishable from wild-type mice by SHIRPA behavioral screens (A) and by rotarod tests (B). Forebrain-specific *Lmnb1* knockout mice (*Emx1-Cre Lmnb1*^fl/fl^) (3), knock-in mice expressing nonfarnesylated lamin B2 (*Lmnb2*^CS/CS^) (4), and wild-type littermates were included as controls. No statistically significant differences were observed between wild-type mice and *Lmna*^PLAO-UTR/PLAO-UTR^ mice. See Supplementary Material, Table S2 for the description of each test.

		WT	PLAO	5NT	UTR	Lamin C
Cerebellum	Granule cells	–	–	–	–	+++
	Purkinje cells	–	–	–	++	++++
	Arbor vitae	–	++	++++	++++	+++
	Interposed nucleus	–	–	–	++	++++
	Molecular layer	–	–	–	–	++
Midbrain	Inferior colliculus	–	–	+	+++	++++
Cerebrum	Cerebral cortex	+	++	+++	++++	++++
	Corpus callosum	+	++	++++	++++	+++
	Striatum	–	–	–	+	++
Hippocampus	Strata granulosum	–	–	–	++	+++
	Strata pyramidale	+	+	++	++++	++++
	Thalamus	–	–	–	+++	++++
Olfactory bulb	Granule cells	–	–	–	++	+++
	Glomerular layer	–	–	–	++	+++
	Mitral cells	–	–	–	+	++++

Table S1. Lamin A expression in different regions of the brain from *Lmna*[PLAO-5NT/+] and *Lmna*[PLAO-UTR/+] mice, as judged by immunohistochemistry. +, ++, +++, and ++++ indicate the intensity of lamin A staining by immunohistochemistry [from + (very weak) to ++++ (very strong)]; – denotes undetectable lamin A expression (Fig. S4). Blue, regions of the brain in which lamin A expression was increased in *Lmna*[PLAO/+] mice compared with *Lmna*^{+/+} mice; yellow, regions of the brain in which lamin A expression was increased in *Lmna*[PLAO-5NT/+] mice compared with *Lmna*[PLAO/+] mice; green, regions of the brain in which lamin A expression was increased in *Lmna*[PLAO-UTR/+] mice compared with *Lmna*[PLAO-5NT/+] mice; grey, regions of the brain in which lamin A expression changed very little, even in *Lmna*[PLAO-UTR/+] mice.

64

Category	Test						
View Jar	**Body Position**	0-Completely flat	1-Lying on Side	2-Lying Prone	3-Sitting or standing	4-Rearing on hind legs	5-Repeated vertical leaping
	Spontaneous Activity	0-None, resting	1-Casual groom, slow movement	2-Vigorous groom, moderate movement	3-Vigorous, rapid/dart movement	4-Extremely vigorous, rapid/dart movement	
	Respiration Rate	0-Gasping, irregular	1-Slow, shallow	2-Normal	3-Hyperventilation		
	Tremor	0-None	1-Mild	2-Marked			
	Urination	Count					
	Defecation	Count					
Arena	**Transfer Arousal**	1-Prolonged freeze, slight movement	2-Extended freeze, moderate movement	3-Brief freeze, active movement	4-Barely freeze, immediate movement	5-No freeze, immediate movement	6-Extremely excited (manic)
	Locomotor Activity	Squares entered within 30s					
	Palpebral Closure	0-Eyes wide open	1-Eyes 1/2 closed	2-Eyes closed			
	Piloerection	0-None	1-Coat stood on end				
	Startle Response	0-None	1-Preyer reflex-flick of pinnae	2-Jump <1cm	3-Jump >1cm		
	Gait	0-Normal	1-Fluid but abnormal	2-Limited movement only	3-Incapacity		
	Pelvic Elevation	0-Markedly flattened	1-Barely touches	2-Normal (3mm)	3-Elevated (>3mm)		
	Tail Elevation	0-Dragging	1-Horizontally Extended	2-Elevated			
	Touch Escape	0-No response	1-Mild (escape to firm stroke)	2-Moderate (rapid response to light stroke)	3-Escape response to approach		
Held by Tail	**Positional Passivity**	0-Struggles when held by tail	1-Struggles when held by scruff	2-Struggles when laid supine	3-Struggles when held by hind legs	4-No struggle	
	Trunk Curl	0-present	1-absent				
	Limb grasping	0-present	1-absent				
	Abnormal Behavior	0-present	1-absent				
	Visual Placing	0-None	1-Upon nose contact	2-Upon vibrassa contact	3-Before contact-18mm	4-Early extension-25mm	
	Whisker Brush	0-No response	1-Response to vigorous brush	2-Response to mild brushing	3-Response to initial touch		
	Whisker placement	0-None	1-Upon head contact	2-Upon vibrassa contact	3-Before vibrassa contact		
Reflex	**Grip Strength**	0-None	1-Slight grip, semi-effective	2-Moderate grip, effective	3-Active grip, effective	4-Unusually effective	
	Body Tone	0-Flaccid, no return to normal	1-Slight resistance	2-Extreme resistence, boardlike			
	Pinna reflex	0-None	1-Active reaction, brisk flick	2-Hyperactive, repetitive flick			
	Corneal reflex	0-None	1-Active single eye blink	2-Multiple eye blink			
	Toe Pinch	0-None	1-Slight withdrawal	2-Moderate withdrawal, not brisk	3-Brisk, rapid withdrawal	4-Rapid extension/flexion	
	Wire Manoeuvre	0-Active grip with hindlegs	1-Difficulty grasp with hindlegs	2-Unable to grasp with hindlegs	3-Unable to lift hindlegs, falls	4-Fall immediately	
Supine Restraint	**Heart Rate**	0-Slow, bradycardia	1-Normal	2-Fast, tachycardia			
	Limb Tone	0-No resistence	1-Slight resistance	2-Moderate resistence	3-Marked resistence	4-Extreme resistence	
	Abdominal Tone	0-Flaccid, no return to normal	1-Slight resistence	2-Extreme resistence, boardlike			
	Salivation	0-None	1-Slight margin of submax	2-Wet zone entire sub-max			
	Provoked Biting	0-Absent	1-Present				
	Penlight Vision	0-No response	1-Pupil dilation	2-Rapid blinking			
Other	**Righting Reflex**	0-No impairment	1-Lands on side	2-Lands on back	3-Fails to right when on back		
	Contact Righting Reflex	0-Absent	1-Present				
	Negative Geotaxis	0-Turns and climbs on grid	1-Turns but then freezes	2-Moves, but fails to turn	3-Does not move w/in 30s	4-Falls off	
	Fear	0-None	1-Freeze with transfer arousal				
	Irritability	0-None	1-Struggle with supine restraint				
	Aggression	0-None	1-Provoked biting or attack				
	Vocalization	0-None	1-Provoked during handling				

Table S2. List of tests performed during the SHIRPA primary screen and the scoring criteria for each test.

65

A

A	5′–TCGAATCCGCATTGACAGCCTCT–3′
B	5′–AAAGTTCAGGCCCTTCTGGT–3′
C	5′–AGTACAACCTGCGCTCACGC–3′
D	5′–TGATGCTGCAGTTCTGGGAGC–3′
E	5′–ACAACCTAGTCACCCGCTCCTA–3′
F	5′–ATGTGTCTGCCCCTGAAAAC–3′
NeoF	5′–TGCTCCTGCCGAGAAAGTAT–3′
NeoR	5′–AAGCGAAGGAGCAAAGCTGCTA–3′

B

Antigen	Antibody	Species	Company	Western Blot	IHC
Actin	Polyclonal	Goat	Santa Cruz (sc-1616)	1:1000	
Caspase-3	Monoclonal	Rabbit	Cell Signaling (9664)		1:100
Ctip2	Monoclonal	Rat	Abcam (ab18465)		1:500
Cux1	Polyclonal	Rabbit	Santa Cruz (sc-13024)		1:100
GFAP	Monoclonal	Mouse	BD Pharmingen (556327)		1:800
Lamin A	Monoclonal	Mouse	Millipore (MAB3540)		1:400
Lamin A/C	Polyclonal	Goat	Santa Cruz (sc-6215)	1:400	
Lamin B1	Polyclonal	Goat	Santa Cruz (sc-6217)	1:400	1:400
Lamin B2	Monoclonal	Mouse	Invitrogen (33-2100)	1:400	
Lamin C	Polyclonal	Rabbit	Lifespan Biosciences (LS-B2972)		1:200
NeuN	Monoclonal	Mouse	Millipore (MAB377)		1:500
Olig2	Polyclonal	Rabbit	Millipore (AB9610)		1:500
LAP2β	Monoclonal	Mouse	BD Biosciences (611000)		1:400
Emerin	Monoclonal	Mouse	Novocastra (NCL-EMERIN)		1:200
SUN1	Polyclonal	Rabbit	Abcam (ab74758)		1:800
Nup98	Monoclonal	Rat	Abcam (ab50610)		1:250

Table S3. List of primers and primary antibodies. (A) Sequences of the primers used in 5′ and 3′ long-range PCR reactions and genotyping PCR reactions for the *Lmna*[PLAO-5NT] and *Lmna*[PLAO-UTR] alleles. (B) List of primary antibodies used in this study.

66

Chapter 4:

Farnesylation of Lamin B1 Is Important for Retention of Nuclear Chromatin During

Neuronal Migration

Farnesylation of lamin B1 is important for retention of nuclear chromatin during neuronal migration

Hea-Jin Jung[a], Chika Nobumori[b], Chris N. Goulbourne[b], Yiping Tu[b], John M. Lee[b], Angelica Tatar[b], Daniel Wu[b], Yuko Yoshinaga[c], Pieter J. de Jong[c], Catherine Coffinier[b], Loren G. Fong[b,1], and Stephen G. Young[a,b,d,1]

[a]Molecular Biology Institute, [b]Department of Medicine, and [d]Department of Human Genetics, University of California, Los Angeles, CA 90095; and [c]Children's Hospital Oakland Research Institute, Oakland, CA 94609

The role of protein farnesylation in lamin A biogenesis and the pathogenesis of progeria has been studied in considerable detail, but the importance of farnesylation for the B-type lamins, lamin B1 and lamin B2, has received little attention. Lamins B1 and B2 are expressed in nearly every cell type from the earliest stages of development, and they have been implicated in a variety of functions within the cell nucleus. To assess the importance of protein farnesylation for B-type lamins, we created knock-in mice expressing nonfarnesylated versions of lamin B1 and lamin B2. Mice expressing nonfarnesylated lamin B2 developed normally and were free of disease. In contrast, mice expressing nonfarnesylated lamin B1 died soon after birth, with severe neurodevelopmental defects and striking nuclear abnormalities in neurons. The nuclear lamina in migrating neurons was pulled away from the chromatin so that the chromatin was left "naked" (free from the nuclear lamina). Thus, farnesylation of lamin B1—but not lamin B2—is crucial for brain development and for retaining chromatin within the bounds of the nuclear lamina during neuronal migration.

nucleokinesis | CaaX motif | posttranslational modification | genetically modified mouse models

The nuclear lamina is an intermediate filament meshwork that lies beneath the inner nuclear membrane. This lamina provides structural support for the nucleus and also interacts with nuclear proteins and chromatin, thereby affecting many functions within the cell nucleus (1, 2). In mammals, the main protein components of the nuclear lamina are lamins A and C (A-type lamins) and lamins B1 and B2 (B-type lamins).

Both B-type lamins and prelamin A (the precursor of lamin A) terminate with a CaaX motif, which triggers three posttranslational modifications (3–5): farnesylation of the carboxyl-terminal cysteine (the "C" in the CaaX motif) (6), endoproteolytic cleavage of the last three amino acids (the -aaX) (7, 8), and carboxyl methylation of the newly exposed farnesylcysteine (9, 10). Prelamin A undergoes a second endoproteolytic cleavage event, mediated by zinc metalloproteinase STE24 (ZMPSTE24), which removes 15 additional amino acids from the carboxyl terminus, including the farnesylcysteine methyl ester (11–14). Lamins B1 and B2 do not undergo the second cleavage step and therefore retain their farnesyl lipid anchor.

The discovery that Hutchinson-Gilford progeria syndrome (HGPS) is caused by a LMNA mutation yielding an internally truncated farnesyl–prelamin A (15) has focused interest in the farnesylation of nuclear lamins. This interest has been fueled by the finding that disease phenotypes in mouse models of HGPS could be ameliorated by blocking protein farnesylation with a protein farnesyltransferase inhibitor (FTI) (16–19). Most recently, children with HGPS seemed to show a positive response to FTI treatment (20).

The prospect of using an FTI to treat children with HGPS naturally raises the issue of the importance of protein farnesylation for lamin B1 and lamin B2. The B-type lamins are expressed in all mammalian cells and have been highly conserved during vertebrate evolution. The B-type lamins have been reported to participate in many functions within the cell nucleus, including DNA replication (21) and the formation of the mitotic spindle (22). Recently, both lamin B1 and lamin B2 have been shown to be important for neuronal migration within the developing brain (23–26). A deficiency of either protein causes abnormal layering of cortical neurons (23, 24). Coffinier et al. (24) proposed that the neuronal migration defect might be the consequence of impaired integrity of the nuclear lamina. Whether the farnesylation of lamin B1 or lamin B2 is important for neuronal migration is not known.

Over the past few years, it has become increasingly clear that mouse models are important for elucidating the in vivo relevance of lamin posttranslational processing. In the case of prelamin A, cell culture studies suggested that protein farnesylation plays a vital role in the targeting of prelamin A to the nuclear rim (27–29), but recent studies with gene-targeted mice have raised questions about the in vivo relevance of those findings. For example, knock-in mice that produce mature lamin A directly (bypassing prelamin A synthesis and protein farnesylation) are free of disease, and the nuclear rim positioning of lamin A in the tissues of mice is quite normal (30).

To assess the importance of protein farnesylation for B-type lamins, we reasoned that mouse models would be even more important because these lamins are important for neuronal migration in the developing brain, a complex process that requires the use of animal models. In the present study, we investigated the in vivo functional relevance of protein farnesylation in B-type lamins by creating knock-in mice expressing nonfarnesylated versions of lamin B1 and lamin B2.

Significance

Both lamin B1 and lamin B2 have farnesyl lipid anchors, but the importance of this lipid modification has been unclear. We addressed that issue with knock-in mouse models. Mice expressing nonfarnesylated lamin B2 developed normally and were healthy. In contrast, mice expressing nonfarnesylated lamin B1 exhibited a severe neurodevelopmental abnormality accompanied by a striking defect in the cell nucleus. During the migration of neurons, the nuclear lamina was pulled free of the chromatin. Thus, farnesylation of lamin B1—but not lamin B2—is crucial for neuronal migration in the brain and for the retention of chromatin within the nuclear lamina.
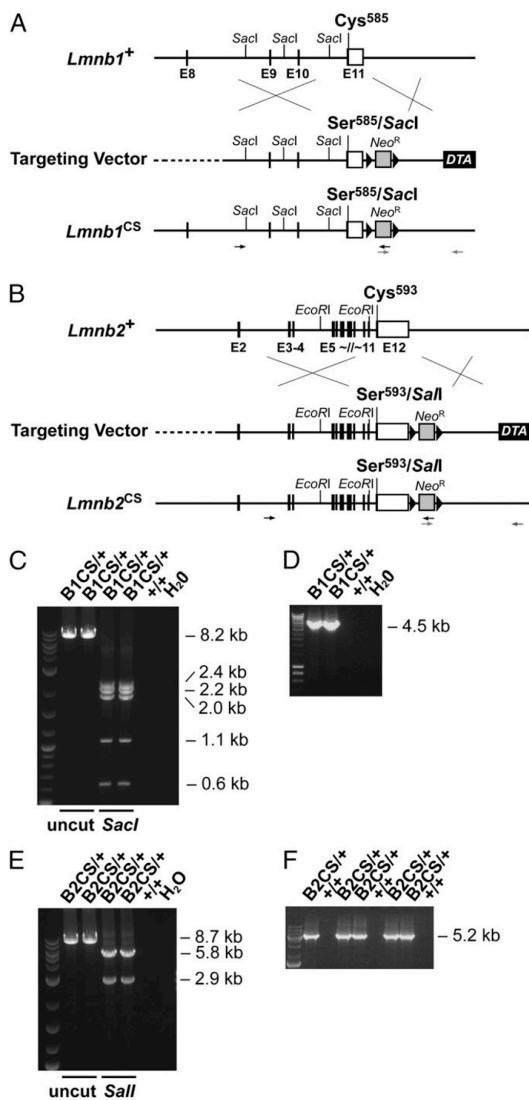
Results

Knock-In Mice Expressing Nonfarnesylated Versions of Lamin B1 and Lamin B2. We generated knock-in mice expressing nonfarnesylated versions of lamin B1 and lamin B2 by changing the cysteine (C) of the *CaaX* motif to a serine (S) (Fig. 1). The "Cys-to-Ser" alleles were designated *Lmnb1*[CS] and *Lmnb2*[CS]. New restriction sites were introduced in adjacent sequences (without changing any other amino acids) to facilitate genotyping. Targeted embryonic stem cell clones were initially identified by long-range PCR; the identity of the PCR products was confirmed by restriction endonuclease mapping (Fig. 1 *C–F*).

To determine if the targeted mutations abolished the farnesylation of lamins B1 and B2, we prepared primary mouse embryonic fibroblasts (MEFs) from embryonic day (E) 13.5 *Lmnb1*[CS/CS] and *Lmnb2*[CS/CS] embryos and performed metabolic labeling with a farnesol analog, 8-anilinogeraniol (AG) (31). AG is taken up by cells and incorporated into anilinogeranyl diphosphate, which is then used as a substrate by protein farnesyltransferase. Proteins modified by AG can be detected by Western blotting with an AG-specific monoclonal antibody (31). The *Lmnb1*[CS] and *Lmnb2*[CS] alleles worked as planned, eliminating farnesylation of lamin B1 and lamin B2, respectively. In *Lmnb1*[CS/CS] MEFs, AG was incorporated into lamin B2 but not lamin B1 (Fig. 2*A*); in *Lmnb2*[CS/CS] MEFs, AG was incorporated into lamin B1 but not lamin B2 (Fig. 2*B*). We also assessed the electrophoretic migration of nonfarnesylated lamins by SDS/PAGE because an absence of farnesylation retards the electrophoretic mobility of prenylated proteins (32). As expected, nonfarnesylated lamin B1 in *Lmnb1*[CS/CS] MEFs and nonfarnesylated lamin B2 in *Lmnb2*[CS/CS] MEFs migrated more slowly than the farnesylated lamins in wild-type MEFs (Fig. 2 *C* and *D*).

Next, we examined nuclear morphology in *Lmnb1*[CS/CS] and *Lmnb2*[CS/CS] MEFs by immunofluorescence microscopy. The absence of lamin B2 farnesylation did not perceptibly affect the localization of lamin B2, nor did it elicit nuclear shape abnormalities (Fig. 2*E*, *Right*). In contrast, nuclear morphology was abnormal in ∼30% of *Lmnb1*[CS/CS] MEFs (29.9 ± 13.6%) (Fig. 2*G*), with the nonfarnesylated lamin B1 and LAP2β (lamin-associated polypeptide 2) being distributed in a honeycomb fashion [Fig. 2 E (*Left*) and *F*]. The nonfarnesylated lamin B1 was concentrated at the nuclear rim, even in cells with a honeycomb distribution of lamin B1 (Fig. 2*F*, *Center*).

Lower Steady-State Levels of B-Type Lamins in the Absence of the Farnesyl Lipid Anchor. Previously, Yang et al. (32) found that abolishing the farnesylation of progerin (the mutant prelamin A in HGPS) accelerated the turnover of progerin resulting in reduced levels in cells. To determine if the absence of farnesylation affected steady-state levels of lamin B1 and lamin B2, we performed Western blots on protein extracts from wild-type, *Lmnb1*[CS/CS], and *Lmnb2*[CS/CS] MEFs. Levels of lamin B2 in *Lmnb2*[CS/CS] MEFs were similar to those in wild-type MEFs (Fig. S1*D*). In contrast, lamin B1 levels in *Lmnb1*[CS/CS] MEFs were ∼35% lower (35.1 ± 17.1%) than in wild-type MEFs (Fig. S1*B*). The lower lamin B1 levels in *Lmnb1*[CS/CS] MEFs raised a question about whether the honeycomb distribution of lamin B1 in those cells was because of the absence of the farnesyl lipid anchor or simply because of the lower levels of lamin B1 in cells. To address this issue, we used immunofluorescence microscopy to compare the frequency of the honeycomb nuclear phenotype in *Lmnb1*[CS/CS] and *Lmnb1*^{+/−}

Fig. 1. Knock-in mice expressing nonfarnesylated versions of lamin B1 and lamin B2. (*A*) Gene-targeting strategy to create the *Lmnb1*[CS] allele, in which the cysteine (Cys[585]) of the *CaaX* motif of *Lmnb1* is replaced with a serine (Ser[585]). A new restriction endonuclease site, SacI, was introduced into adjacent sequences to facilitate genotyping. Exons are depicted as black boxes; the 3′ UTR is white; *loxP* sites are represented by black arrowheads. Primer locations for 5′ (black) and 3′ (gray) long-range PCR reactions are indicated with arrows. (*B*) Gene-targeting strategy to create the *Lmnb2*[CS] allele, in which the cysteine (Cys[593]) of the *CaaX* motif of *Lmnb2* is replaced with a serine (Ser[593]). A SalI site was introduced in adjacent sequences. (*C*) The 5′ long-range PCR with the *Lmnb1*[CS] allele yields an 8.2-kb fragment (lanes 2 and 3). The identity of the PCR product was confirmed by SacI digestion; the SacI fragments (taking into account the newly introduced SacI site) were 2.4, 2.2, 2.0, 1.1, and 0.6 kb in length (lanes 4 and 5). No PCR product was amplified from wild-type DNA (lane 6). (*D*) The 3′ long-range PCR with the *Lmnb1*[CS] allele yields a 4.5-kb fragment (lanes 2 and 3). No PCR product was amplified from wild-type DNA (lane 4). (*E*) With the *Lmnb2*[CS] allele, the 5′

long-range PCR yields an 8.7-kb fragment. The identity of the PCR product was verified by digestion with SalI (with the newly introduced SalI site, the expected products were 5.8 and 2.9 kb) (lanes 4 and 5). No PCR product was obtained with wild-type DNA (lane 6). (*F*) The 3′ long-range PCR with the *Lmnb2*[CS] allele yields a 5.2-kb fragment (lanes 2, 4, 5, 7, and 8). No PCR product was obtained with wild-type DNA (lanes 3, 6, and 9).
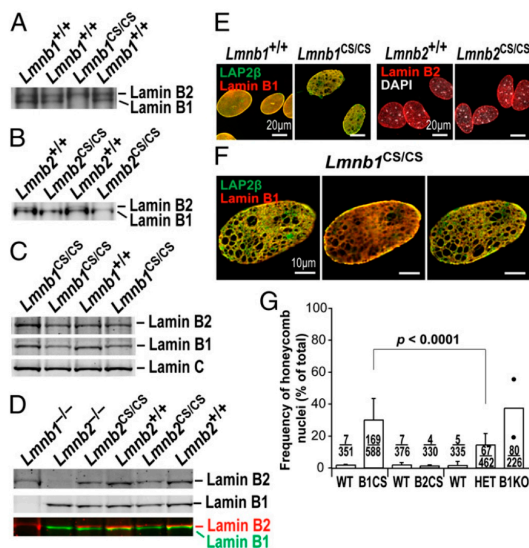
Fig. 2. Phenotypes of $Lmnb1^{CS/CS}$ and $Lmnb2^{CS/CS}$ MEFs. (*A* and *B*) Metabolic labeling studies showing an absence of lamin B1 and lamin B2 farnesylation in $Lmnb1^{CS/CS}$ and $Lmnb2^{CS/CS}$ MEFs, respectively. Wild-type ($Lmnb1^{+/+}$ and $Lmnb2^{+/+}$), $Lmnb1^{CS/CS}$, and $Lmnb2^{CS/CS}$ MEFs were incubated with the farnesol analog AG, and proteins labeled with AG were detected by Western blotting with an AG-specific monoclonal antibody (31). The lamin B1 in $Lmnb1^{CS/CS}$ MEFs and the lamin B2 in $Lmnb2^{CS/CS}$ MEFs were not labeled by AG. (*C* and *D*) Altered electrophoretic mobility of nonfarnesylated versions of lamin B1 and lamin B2. Protein extracts from $Lmnb1^{+/+}$, $Lmnb1^{CS/CS}$, $Lmnb2^{+/+}$, and $Lmnb2^{CS/CS}$ MEFs were size-fractionated on 7% (wt/vol) Tris-Acetate SDS/PAGE gels, and Western blots were performed with antibodies against lamin B1, lamin B2, or lamin C. The nonfarnesylated lamin B1 in $Lmnb1^{CS/CS}$ MEFs and the nonfarnesylated lamin B2 in $Lmnb2^{CS/CS}$ MEFs migrated more slowly than farnesyl–lamin B1 and farnesyl–lamin B2 in wild-type cells. (*E*) Immunofluorescence microscopy of $Lmnb1^{CS/CS}$ and $Lmnb2^{CS/CS}$ MEFs with antibodies against LAP2β (lamin-associated polypeptide 2; green) and lamin B1 (red) or lamin B2 (red). Images along the z axis were captured and merged (Zen 2010 software; Zeiss). In many $Lmnb1^{CS/CS}$ MEFs, LAP2β and lamin B1 were distributed in a honeycomb fashion. (Scale bar, 20 μm.) (*F*) Optical sections through a nucleus of a $Lmnb1^{CS/CS}$ MEF along the z axis (*Left*, top area; *Center*, middle area; *Right*, bottom area). Despite nuclear honeycombing, lamin B1 was concentrated at the nuclear rim (*Center*). (Scale bar, 10 μm.) (*G*) Frequency of honeycomb nuclear phenotype in primary MEFs. For each cell line, >100 cells were scored by two independent observers in a blinded fashion. From left to right, WT ($Lmnb1^{+/+}$), n = 3 cell lines; B1CS ($Lmnb1^{CS/CS}$), n = 5; WT ($Lmnb2^{+/+}$), n = 3; B2CS ($Lmnb2^{CS/CS}$), n = 3; WT ($Lmnb1^{+/+}$), n = 3; HET ($Lmnb1^{+/-}$), n = 4; and B1KO ($Lmnb1^{-/-}$), n = 2. The honeycomb nuclear phenotype was more frequent in $Lmnb1^{CS/CS}$ cells than in $Lmnb1^{+/-}$ cells ($P < 0.0001$). Values represent mean ± SD.

MEFs, where the levels of lamin B1 are very similar (64.9 ± 17.1% of wild-type levels in $Lmnb1^{CS/CS}$ cells vs.. 63.4 ± 8.0% in $Lmnb1^{+/-}$ cells; $P = 0.8819$) (Fig. S1 *B* and *F*). Interestingly, the honeycomb nuclear morphology was more frequent in $Lmnb1^{CS/CS}$ MEFs (29.9 ± 13.6%) than in $Lmnb1^{+/-}$ MEFs (14.3 ± 7.3%) ($P < 0.0001$) (Fig. 2*G*), implying that the absence of lamin B1 farnesylation contributes significantly to the honeycomb nuclear phenotype. Furthermore, in independently isolated lines of $Lmnb1^{CS/CS}$ MEFs, the levels of nonfarnesylated lamin B1 and the frequency of the honeycomb nuclei were positively correlated ($P = 0.0045$) (Fig. S1*H*), lending further support to the idea that nonfarnesylated lamin B1 causes nuclear honeycombing. The frequency of nuclear blebs in $Lmnb1^{CS/CS}$ and $Lmnb1^{+/-}$ cells was similar ($P = 0.87$) (Fig. S1*G*).

We also assessed levels of B-type lamins in the cerebral cortex of $Lmnb1^{CS/CS}$ and $Lmnb2^{CS/CS}$ mice. The levels of lamin B1 in the cortex were ~40% lower (40.5 ± 10.6%) in $Lmnb1^{CS/CS}$ embryos than in wild-type littermate control mice (Fig. S2 *A* and *B*), and lamin B2 levels were ~30% lower (29.6 ± 8.4%) in $Lmnb2^{CS/CS}$ embryos than in wild-type controls (Fig. S2 *C* and *D*). The reduced levels of nonfarnesylated lamins in the cerebral cortex were not because of reduced transcript levels; $Lmnb1$ and $Lmnb2$ transcript levels in $Lmnb1^{CS/CS}$ and $Lmnb2^{CS/CS}$ mice were normal, as judged by qRT-PCR (Fig. S2 *E* and *F*). We did not measure lamin A and lamin C levels because the expression of the $Lmna$ gene is negligible in newborn mice (33).

Interestingly, the levels of lamin B2 in the cortex of $Lmnb1^{CS/CS}$ embryos were ~37% lower (37.3 ± 14.4%) than in wild-type mice ($P = 0.048$) (Fig. S2 *A* and *B*), implying that the absence of lamin B1 farnesylation affects the turnover of lamin B2. $Lmnb2$ transcript levels in $Lmnb1^{CS/CS}$ mice were normal (Fig. S2*E*).

Farnesylation of Lamin B2, but Not Lamin B1, Is Dispensable. $Lmnb1^{CS/CS}$ mice died soon after birth, like $Lmnb1^{-/-}$ and $Lmnb2^{-/-}$ mice (23, 34). Newborn $Lmnb1^{CS/CS}$ mice and E19.5 embryos were nearly normal in size but had a flattened cranium (Fig. 3*A*). The brain in $Lmnb1^{CS/CS}$ mice was smaller than in wild-type mice, with the midbrain being most prominently affected [midbrain, 21.5 ± 7.6% smaller than in wild-type mice ($P < 0.0001$); cortex, 9.1 ± 4.6% smaller than in wild-type mice, ($P = 0.0072$)] (Fig. 3 *D*, *G*, and *J*). The developmental phenotypes in $Lmnb1^{CS/CS}$ embryos, however, were less severe than in $Lmnb1^{-/-}$ embryos, which were much smaller in size and had much smaller brains (Fig. 3 *C*, *F*, and *I*). Immunohistochemistry studies on the cerebral cortex of $Lmnb1^{CS/CS}$ embryos revealed abnormal layering of cortical neurons, but the defect was far milder than in $Lmnb1^{-/-}$ embryos (Fig. 3*K*) (24, 25). $Lmnb1^{+/-}$ mice were entirely normal and exhibited no detectable abnormalities in the brain (Fig. 3 *C*, *F*, and *I*).

In contrast to the $Lmnb1^{CS/CS}$ mice, $Lmnb2^{CS/CS}$ mice were normal at birth (Fig. 3 *B*, *E*, and *H*), grew normally, were fertile, and had a normal lifespan. Immunohistochemistry studies on the cerebral cortex of $Lmnb2^{CS/CS}$ embryos revealed no abnormalities (Fig. 3*K*).

We also examined the histology of heart, liver, kidney, skin, and intestine of $Lmnb1^{CS/CS}$ and $Lmnb2^{CS/CS}$ mice and found no abnormalities (Fig. S3 *A* and *B*). The lungs of newborn $Lmnb1^{CS/CS}$ mice appeared less mature and had fewer alveoli, a phenotype that was observed previously in lamin B1-deficient mice (34). Immunohistochemistry studies revealed a honeycomb distribution of lamin B1 in the lung and intestine of $Lmnb1^{CS/CS}$ mice, but not in the other tissues (Fig. S3 *C* and *D*).

Nuclear Lamina Is Pulled Away from the Chromatin in Migrating $Lmnb1^{CS/CS}$ Neurons. To assess nuclear integrity of $Lmnb1^{CS/CS}$ neurons, we isolated cortical neuronal progenitor cells (NPCs) from E13.5 embryos, generated neurospheres, cultured them in differentiation medium, and then studied the nuclear morphology of neurons as they migrated out of the neurospheres. Most of the neurons from wild-type mice ($Lmnb1^{+/+}$) had round or oval-shaped nuclei, with LAP2β and lamin B1 located mainly at the nuclear rim (Fig. 4*A*). In contrast, many $Lmnb1^{CS/CS}$ neurons had dumbbell-shaped nuclei (9.3 ± 4.5%) (Fig. 4*A*; but see also Fig. 6*D*). In those cells, most of the lamin B1 was located at one end of the "dumbbell," but the other end contained "naked chromatin" (by this we mean chromatin free of the nuclear lamina) (Fig. 4*A*, outlined in white). Both ends of the dumbbell-shaped nuclei contained DNA and were connected by a thin strand of DNA of varying length. Both ends of the nucleus—and the thin strand connecting them—were surrounded by LAP2β, a protein of the inner nuclear membrane (Figs. 4*A* and 5*A*). The lamin B1-containing end of the dumbbell-shaped nucleus was always in the leading edge of the cell, as judged by pericentrin staining (Fig. 4*B*,

70
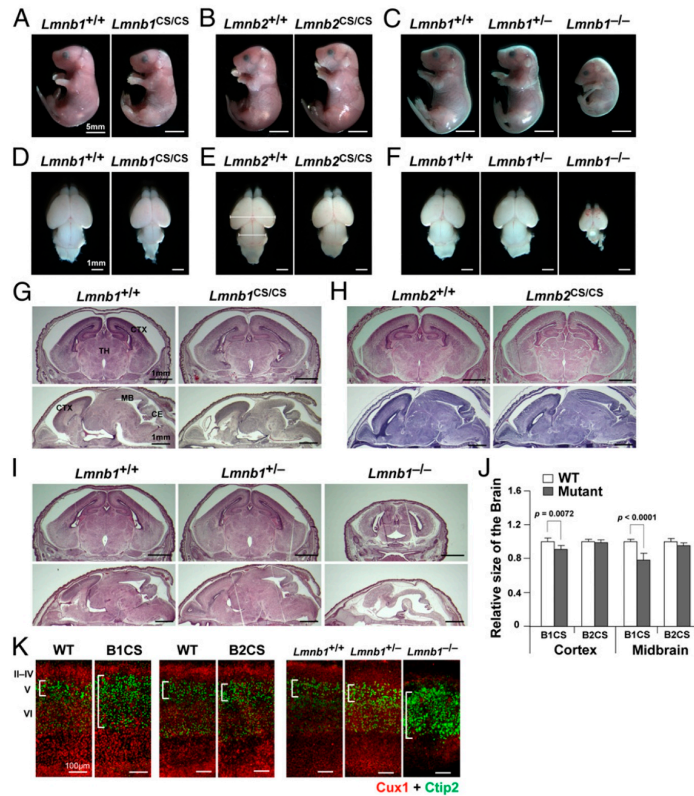
Fig. 3. $Lmnb1^{CS/CS}$ embryos have smaller brains and exhibit a defect in layering of neurons in the cerebral cortex. (*A–C*) Photographs of wild-type, $Lmnb1^{CS/CS}$, $Lmnb2^{CS/CS}$, $Lmnb1^{+/-}$, and $Lmnb1^{-/-}$ mice at E19– postnatal day (P)1. (Scale bars, 5 mm.) (*D–F*) Mouse brains viewed from the top at E19–P1. (Scale bars, 1 mm.) (*G–I*) H&E staining of coronal and sagittal brain sections at E19–P1. (Scale bars, 1 mm.) (*J*) Sizes of the cortex and midbrain in wild-type, $Lmnb1^{CS/CS}$ (B1CS), and $Lmnb2^{CS/CS}$ (B2CS) embryos (measured from the top of brains, see *E*). $Lmnb1^{+/+}$, $n = 6$; $Lmnb1^{CS/CS}$, $n = 5$; $Lmnb2^{+/+}$, $n = 4$; $Lmnb2^{CS/CS}$, $n = 5$. The midbrain was $21.5 \pm 7.6\%$ smaller in $Lmnb1^{CS/CS}$ mice than in wild-type mice, $P < 0.0001$; the cortex was $9.1 \pm 4.6\%$ smaller in $Lmnb1^{CS/CS}$ mice than in wild-type mice, $P = 0.0072$. Values represent mean $\pm$ SD (*K*) Immunofluorescence microscopy of the cerebral cortex of E19–P1 wild-type (WT, $Lmnb1^{+/+}$), $Lmnb1^{CS/CS}$ (B1CS), $Lmnb2^{CS/CS}$ (B2CS), $Lmnb1^{+/-}$, and $Lmnb1^{-/-}$ embryos with antibodies against Cux1 (red) and Ctip2 (green). The layering of cortical neurons in $Lmnb1^{-/-}$ embryos was abnormal, as reported previously (24). $Lmnb1^{CS/CS}$ mice also exhibited a cortical layering defect, but it was milder than in $Lmnb1^{-/-}$ mice. No abnormalities were detected in $Lmnb1^{+/-}$ mice. (Scale bars, 100 μm.)

arrows), but the naked chromatin was in the other end of the cell nucleus in the trailing edge of the cell (Fig. 4*B*, arrowheads). In a single field, it was common to observe neurons at different stages of DNA–lamin B1 separation (Fig. 4*B*, *Left* and *Center*).

The asymmetric distribution of nuclear envelope proteins in dumbbell-shaped nuclei of $Lmnb1^{CS/CS}$ neurons was not unique to lamin B1; lamin B2 was found along with lamin B1 in the leading end of dumbbell-shaped nuclei (Fig. 5 *A* and *C*). In addition, most of the signal for SUN1 [Sad1 and UNC84 domain containing 1, a component of the linker of nucleoskeleton and cytoskeleton complex (LINC)] and Nup98 (Nucleoporin 98, a nuclear pore protein) was located in the leading edge along with the B-type lamins (Fig. 5*E*). Dumbbell-shaped nuclei with the grossly asymmetric distribution of nuclear antigens and naked chromatin were rare in wild-type or $Lmnb2^{CS/CS}$ neurons (less than 2.4% of cells) (Figs. 5 *B*, *D*, and *F*, and 6*D*).

To assess whether the dumbbell-shaped nuclei are common among all types of migrating $Lmnb1^{CS/CS}$ cells, we performed wound healing studies in MEFs from wild-type and $Lmnb1^{CS/CS}$ mice. In

contrast to $Lmnb1^{CS/CS}$ neurons, the nuclear shapes of migrating $Lmnb1^{CS/CS}$ MEFs were normal (Fig. S4).

We also found similar dumbbell-shaped nuclei in $Lmnb1^{-/-}$ neurons. In those cells, lamin B2 and the nuclear pore proteins Nup98 and Nup153 were largely located in the leading edge of the nucleus, but naked chromatin was at the other end (Fig. 6 *A–C*). Quantitative analyses confirmed the high frequency of dumbbell-shaped nuclei in $Lmnb1^{-/-}$ and $Lmnb1^{CS/CS}$ neurons ($Lmnb1^{-/-}$, $42.2 \pm 7.6\%$; $Lmnb1^{CS/CS}$, $9.3 \pm 4.5\%$), (Fig. 6*D*). Of note, dumbbell-shaped nuclei were rare in $Lmnb1^{+/-}$ neurons ($1.4 \pm 3.9\%$; $Lmnb1^{+/-}$ vs.. $Lmnb1^{CS/CS}$, $P < 0.0001$), implying that the dumbbell-shaped nuclei in $Lmnb1^{CS/CS}$ neurons are a result of the absence of lamin B1 farnesylation and not because of lower levels of lamin B1 (Fig. 6*D*).

To determine if the dumbbell-shaped nuclei were simply a peculiarity of cultured neurospheres, we examined nuclear morphology in brains of $Lmnb1^{CS/CS}$ embryos. Remarkably, many neurons in the midbrain of $Lmnb1^{CS/CS}$ mice were markedly elongated and had naked chromatin devoid of a surrounding lamina (Fig. 7 *A*, *B*, and *D*). Once again, LAP2β was visible
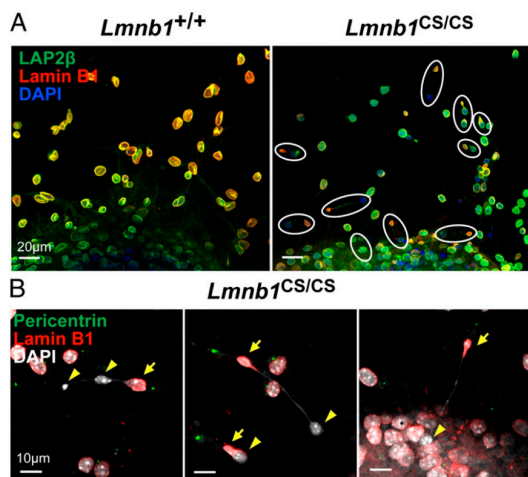
Fig. 4. Immunofluorescence microscopy images of dumbbell-shaped nuclei in *Lmnb1*$^{CS/CS}$ neurons (where the nuclear lamina is separated from the bulk of the chromatin). Cortical NPCs were isolated from E13.5 *Lmnb1*$^{+/+}$ and *Lmnb1*$^{CS/CS}$ embryos and cultured in serum-containing medium to generate neurospheres. The neurospheres were then cultured in differentiation medium to promote neuronal differentiation and migration. (*A*) Low-magnification images of cells stained with antibodies against LAP2β (green) and lamin B1 (red). DNA was stained with DAPI (blue). Images of neurons migrating near the edge of the neurospheres (at the bottom of the images) are shown. The nuclei of *Lmnb1*$^{+/+}$ neurons were mostly round, and LAP2β and lamin B1 were located mainly at the nuclear rim. In contrast, many migrating *Lmnb1*$^{CS/CS}$ neurons had dumbbell-shaped nuclei (outlined in white) surrounded by LAP2β. [The localization of LAP2β around both ends of the nucleus was clear in higher-magnification images (Fig. 5*A*).] In those cells, the nonfarnesylated lamin B1 was found at one end of the dumbbell, but the bulk of the chromatin was located in the other end of the dumbbell and lacked a coat of lamin B1 (naked chromatin). (Scale bars, 20 μm.) (*B*) Higher-magnification images of migrating *Lmnb1*$^{CS/CS}$ neurons stained with antibodies against pericentrin (green) and lamin B1 (red). DNA was visualized with DAPI (white). In the dumbbell-shaped *Lmnb1*$^{CS/CS}$ nuclei, lamin B1 was always found closer to the leading edge of the cells, as judged by pericentrin staining (arrows); naked chromatin was found in the trailing edge (arrowheads). The length of the thin strand of DNA connecting the two ends of dumbbell-shaped nuclei was variable but was occasionally longer than 70 μm. (Scale bars, 10 μm.)

around the naked chromatin, and it often exhibited a honeycomb pattern (Fig. 7*B*, arrowheads). Dumbbell-shaped nuclei connected by long thin DNA strands were occasionally observed in midbrain sections, but were less common than in the cultured cells because of the tight packing of cells and the vagaries of sectioning (Fig. 7*D*). No such abnormalities were found in the midbrain of wild-type or *Lmnb2*$^{CS/CS}$ mice (Fig. 7*C* and Fig. S5).

Dumbbell-shaped nuclei with naked DNA were also observed in the cortex of *Lmnb1*$^{CS/CS}$ embryos, but they were less frequent and were confined to the intermediate zone (Fig. S6*A*). Interestingly, honeycomb nuclei were found throughout the ventricular zone in *Lmnb1*$^{CS/CS}$ embryos (Fig. S6*B*). In wild-type and *Lmnb2*$^{CS/CS}$ embryos, honeycomb nuclei were very rare, and virtually all of the lamin B1 and lamin B2 were located at the nuclear rim (Fig. S6).

To determine if the absence of lamin B1 or lamin B2 farnesylation led to morphological abnormalities in the inner or outer nuclear membranes, we looked at the nuclear envelope of cortical neurons from E17.5 *Lmnb1*$^{CS/CS}$ mice by electron microscopy (Fig. 8). Many neurons in the cortex of *Lmnb1*$^{CS/CS}$

embryos (but not wild-type or *Lmnb2*$^{CS/CS}$ embryos) had nuclear blebs surrounded by an inner and outer nuclear membrane (Fig. 8 *A* and *B*, arrowheads). The blebs contained small amounts of chromatin, but far less than in the remainder of the nucleus (Fig. 8*C*, arrow). In some images, we observed separation of the inner and outer membranes but for the most part they were contiguous (Fig. 8*D* and Movie S1).

Discussion

Prelamin A prenylation has attracted considerable attention, whereas the importance of farnesylation for B-type lamins has been neglected. In the present study, we investigated the in vivo functional relevance of lamin B1 and lamin B2 farnesylation by creating knock-in mice expressing nonfarnesylated versions of lamins B1 and B2 (*Lmnb1*$^{CS/CS}$ and *Lmnb2*$^{CS/CS}$ mice). The targeted mutations worked as planned, abolishing the farnesylation of the lamin proteins, as judged by metabolic labeling studies and by altered migration of the mutant lamin proteins by SDS/PAGE. Our studies revealed that lamin B1's farnesyl lipid
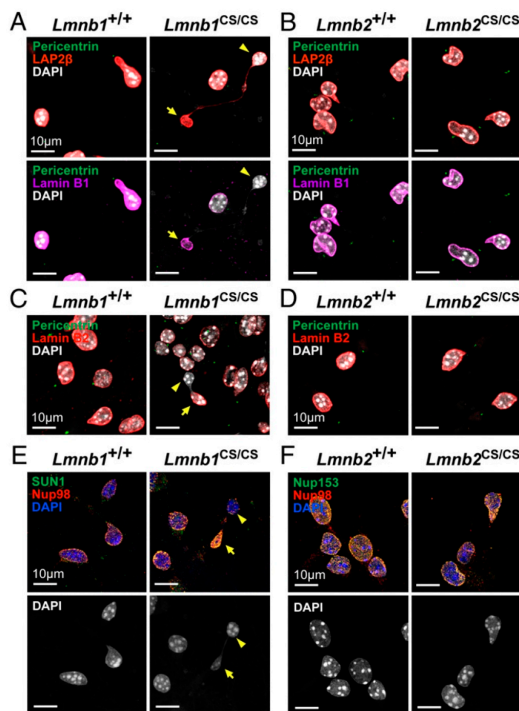
Fig. 5. Immunofluorescence microscopy images of neurons migrating out of neurospheres, illustrating the asymmetric distribution of nuclear envelope proteins. (*A* and *B*) Neurons stained for pericentrin (green), LAP2β (red), and lamin B1 (magenta); (*C* and *D*) pericentrin (green) and lamin B2 (red); (*E*) SUN1 (green) and Nup98 (red); and (*F*) Nup153 (green) and Nup98 (red). DNA was stained with DAPI (white except *Upper* area of *E* and *F*, where it is blue). In *Lmnb1*$^{CS/CS}$ neurons, lamin B2, SUN1, and Nup98 were located largely in the leading end of dumbbell-shaped nuclei (*A*, *C*, and *E*; arrows), but the other end contained nuclear lamina-free chromatin (arrowheads). Small amounts of SUN1 and Nup98 remnants were observed in the trailing end of the dumbbell-shaped nuclei (*E*). In *Lmnb2*$^{CS/CS}$ neurons, nuclear envelope proteins were normally located at the nuclear rim (*B*, *D*, *F*). (Scale bars, 10 μm.)

72
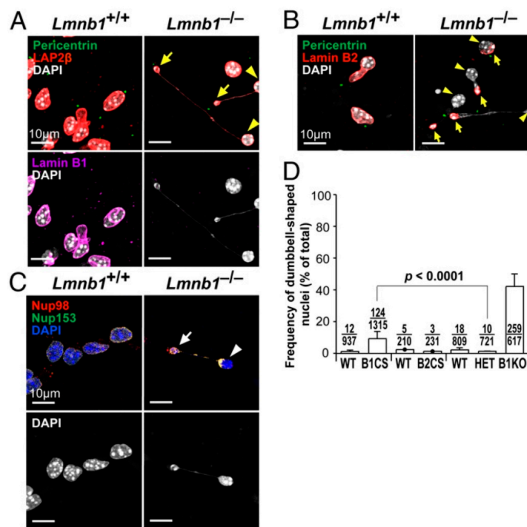
Fig. 6. Dumbbell-shaped nuclei in $Lmnb1^{-/-}$ neurons. (A–C) Immunofluorescence microscopy images of $Lmnb1^{+/+}$ and $Lmnb1^{-/-}$ neurons migrating from neurospheres, showing the asymmetric distribution of lamin B2 and nuclear pore proteins Nup98 and Nup153 in $Lmnb1^{-/-}$ neurons. (A) $Lmnb1^{+/+}$ and $Lmnb1^{-/-}$ neurons stained with antibodies against pericentrin (green), LAP2β (red), and lamin B1 (magenta); (B) pericentrin (green) and lamin B2 (red); (C) Nup98 (red) and Nup153 (green). DNA was visualized with DAPI (white except *Upper* area of C, where it is blue). (D) Frequency of dumbbell-shaped nuclei in WT and mutant neurons. From left to right, $Lmnb1^{+/+}$ (wild-type), $n = 4$; $Lmnb1^{CS/CS}$ (B1CS), $n = 5$; $Lmnb2^{+/+}$ (WT), $n = 1$; $Lmnb2^{CS/CS}$ (B2CS), $n = 1$; $Lmnb1^{+/+}$ (WT), $n = 4$; $Lmnb1^{+/-}$ (HET), $n = 3$; $Lmnb1^{-/-}$ (B1KO), $n = 3$. For each cell line, >180 cells were counted by two independent observers in a blinded fashion. Values represent mean ± SD.

anchor is essential for brain development and postnatal survival, but lamin B2 farnesylation is dispensable. Another major finding of our studies is that lamin B1 is required for the retention of chromatin within the bounds of the nuclear lamina during neuronal migration. In $Lmnb1^{CS/CS}$ mice, we observed many neurons in which the chromatin was detached from the nuclear lamina and left behind in the trailing edge of the cell. This nuclear abnormality has not been identified previously in neurons or any other cell types. Finally, our studies showed that the absence of the farnesyl lipid anchor leads to lower steady-state levels of the B-type lamins, particularly in the developing brain.

The phenotypes of $Lmnb2^{CS/CS}$ mice were distinct from those of $Lmnb2^{-/-}$ mice (23). $Lmnb2^{-/-}$ mice manifested striking neurodevelopmental abnormalities and died soon after birth. In contrast, $Lmnb2^{CS/CS}$ mice were normal with no detectable pathology. In particular, nonfarnesylated lamin B2 did not result in the neurodevelopmental abnormalities that accompany a complete deficiency of lamin B2. The phenotypes of $Lmnb1^{CS/CS}$ and $Lmnb1^{-/-}$ mice were also different. Both mice exhibited neuronal migration defects and perinatal lethality, but the overall size of newborn $Lmnb1^{CS/CS}$ mice was normal (except for the brain); in contrast, $Lmnb1^{-/-}$ embryos were extremely small (24, 34). It would appear that nonfarnesylated lamin B1 is adequate for the growth and development of most organ systems but not for development of the brain. Even in the brain, nonfarnesylated lamin B1 probably retains partial function because the neurodevelopmental defects in $Lmnb1^{CS/CS}$ mice were considerably milder than in $Lmnb1^{-/-}$ mice.

Earlier site-directed mutagenesis studies suggested that farnesylation is important for the targeting of both lamin B1 and lamin B2 to the nuclear envelope (35, 36). Thus, before embarking on the mouse studies, it would have been impossible to predict that abolishing the farnesylation of lamin B1 and lamin B2 would result in different phenotypes. Indeed, we believe that a key lesson of the current studies is that genetically modified mouse models are important for understanding the posttranslational modifications of nuclear lamins. This lesson has been underscored by studies on prelamin A processing. Earlier in vitro studies had suggested that prelamin A prenylation is important for lamin A function and its delivery to the nuclear rim (27–29), but recent studies with knock-in mouse models have suggested otherwise. Coffinier et al. (30) created knock-in mice that produce mature lamin A directly, bypassing prelamin A synthesis and farnesylation. The "mature lamin A" mice were healthy and fertile, and the lamin A in their tissues was positioned normally along the rim of the cell nucleus, indistinguishable from lamin A in the tissues of wild-type mice. Davies et al. (37) found that mice expressing nonfarnesylated prelamin A developed cardiomyopathy late in life, but the nonfarnesylated prelamin A was positioned normally at the nuclear rim. Neither the distinctive phenotypes of mature lamin A and nonfarnesylated prelamin A mice nor the nuclear rim localization of the lamin A proteins in these mice could have been predicted from cell culture studies alone.

Another intriguing finding of the current studies is that lamin B1's farnesyl lipid anchor is important for the retention of nuclear chromatin within the confines of the nuclear lamina during neuronal migration. The neurons that migrated away from cultured $Lmnb1^{CS/CS}$ neurospheres as well as neurons in the cortex and midbrain of $Lmnb1^{CS/CS}$ embryos exhibited a distinctive nuclear abnormality: dumbbell-shaped nuclei in which the nuclear
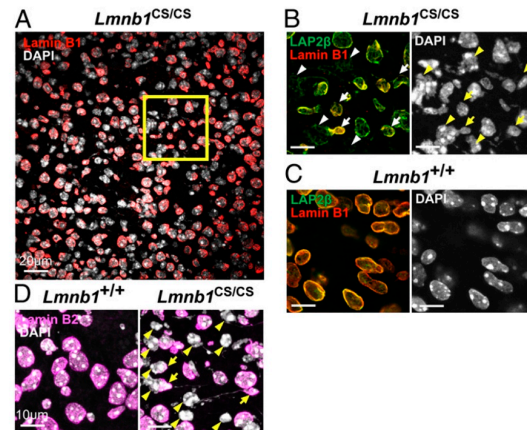
Fig. 7. Immunofluorescence microscopy of the midbrain (superior colliculus) from E19–P1 $Lmnb1^{+/+}$ and $Lmnb1^{CS/CS}$ embryos. (A) Low-magnification image of the $Lmnb1^{CS/CS}$ midbrain showing that nuclei with naked chromatin are widespread. The region outlined in yellow is shown in B. (Scale bars, 20 μm.) (B and C) Higher-magnification images of $Lmnb1^{CS/CS}$ and $Lmnb1^{+/+}$ midbrains. Sections were stained with antibodies against LAP2β (green) and lamin B1 (red); DNA was visualized with DAPI (white). Many neurons in $Lmnb1^{CS/CS}$ mice were elongated with an asymmetric distribution of lamin B1 (arrows) and chromatin lacking a coat of lamin B1 (arrowheads). The LAP2β surrounding the naked chromatin was often distributed irregularly and sometimes had a honeycomb distribution. (Scale bars, 10 μm.) (D) Sections of the midbrain stained for lamin B2 (magenta). Lamin B2 was also distributed asymmetrically at one end of the nucleus (arrows). Arrowheads indicate naked chromatin. (Scale bars, 10 μm.)
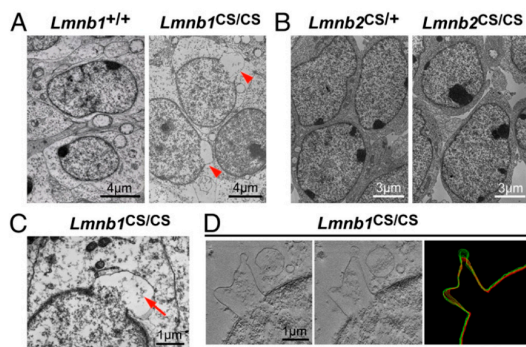
Fig. 8. Electron micrographs of cell nuclei in the cerebral cortex of E17.5 *Lmnb1*^{+/+}, *Lmnb1*[CS/CS], *Lmnb2*[CS/+], and *Lmnb2*[CS/CS] embryos. (*A* and *B*) Low-magnification electron micrographs. Many cortical cells in *Lmnb1*[CS/CS] embryos, but not wild-type or *Lmnb2*[CS/CS] embryos, exhibited nuclear blebs (arrowheads). (Scale bars: 4 μm in *A*; 3 μm in *B*.) (*C*) A higher-magnification image of a nuclear bleb in the cortex of an *Lmnb1*[CS/CS] embryo. Only a small amount of chromatin was present in the bleb (arrow). (Scale bar, 1 μm.) (*D*) EM tomography of the cerebral cortex of an *Lmnb1*[CS/CS] embryo. (*Left* and *Center*) Two sections from a total of 135 sections spanning 200 nm of the cell nucleus. (*Right*) 3D modeling of the inner (red) and outer (green) nuclear membranes, generated by tracing the membranes in every fifth section (14 total sections) of the tomogram. In many sections, the outer and inner nuclear membranes overlapped because of the plane of sectioning. The inner and outer nuclear membranes were generally closely associated in nuclear blebs but were occasionally separated. (Scale bar, 1 μm.)

lamina was separated from the bulk of the chromatin within the cell. The nuclear lamina was located in one end of the dumbbell closest to the leading edge of the cell, but most of the chromatin in the cell nucleus was naked, separated from the nuclear lamina and located at the opposite end of the nucleus. An inner nuclear membrane protein, LAP2β, was found around both ends of the dumbbell-shaped nuclei. The same naked chromatin abnormality was also identified in *Lmnb1*^{−/−} neurons.

The nuclear shape abnormalities in the neurons of *Lmnb1*^{−/−} and *Lmnb1*[CS/CS] mice are likely caused by deformational stresses that accompany neuronal migration. During neuronal migration, the nucleus is repeatedly pulled by microtubule-associated cytoplasmic motors toward the centrosome near the leading edge of the cell (nucleokinesis) (38, 39). The microtubule network almost certainly binds to the cell nucleus through interactions with LINC complex (involving SUN1/2 and Nesprin-1/2) (40, 41), and this same complex likely binds to the nuclear lamina (40, 42). We suspect that the dumbbell-shaped nuclei and naked chromatin in migrating *Lmnb1*[CS/CS] neurons are a consequence of weakened interactions between the nuclear lamina and the inner nuclear membrane (Fig. 9). Lamin B1's hydrophobic farnesyl lipid anchor is almost certainly embedded in the inner nuclear membrane (43) and functions to affix the nuclear lamina to the nuclear membranes (35, 36). In *Lmnb1*[CS/CS] mice, the cytoplasmic motors likely remain quite effective in pulling the LINC complex/nuclear lamina toward the centrosome in the leading edge of the cell. However, the elimination of lamin B1's farnesyl lipid anchors would reduce hydrophobic interactions that normally affix the lamina to the inner nuclear membrane. Thus, as the nuclear lamina is pulled forward, we suspect that much of the chromatin lags behind at the opposite end of the nucleus and escapes into the potential space between the nuclear lamina and the inner nuclear membrane (through honeycomb-like pores) (Fig. 9). This model would explain why the bulk of the nuclear chromatin near the trailing edge of the cell remains covered by nuclear membranes (as judged by

LAP2β staining). Wild-type neurons would be protected from a similar pathologic event because lamin B1's farnesyl lipid anchors firmly affix the lamina to the inner nuclear membrane, eliminating the potential space between the nuclear lamina and the inner nuclear membrane. In addition, wild-type cells have a more even distribution of the nuclear lamina (a tighter "weave" of the meshwork with little honeycombing), perhaps limiting any tendency for the chromatin to escape from the nuclear lamina (Fig. 9).

Our findings indicate that the farnesyl lipid anchor on lamin B1 is functionally more important than that on lamin B2. Neither naked chromatin nor dumbbell-shaped nuclei were present in *Lmnb2*[CS/CS] neurons, and *Lmnb2*[CS/CS] mice had no neuro-developmental defects. Thus, the ability of *Lmnb2*[CS/CS] neurons to make farnesyl–lamin B1 appeared to be sufficient to prevent neuronal migration defects. The reverse was not the case; the production of farnesyl–lamin B2 in *Lmnb1*[CS/CS] mice was inadequate to prevent neurodevelopmental abnormalities.

Another explanation for the different phenotypes of *Lmnb1*[CS/CS] and *Lmnb2*[CS/CS] mice would be distinct interactions of lamin B1 and lamin B2 with binding partners in the nuclear envelope (1). Lamin B1 and lamin B2 proteins are ∼60% identical at the amino acid level, but the sequences are more divergent at the carboxyl terminus (including the sequence of the *CaaX* motif) (Fig. S7). These differences could lead to functional differences and different affinities for potential binding partners. Also, the extent to which the Cys-to-Ser substitution affects binding interactions could be significantly different for lamin B1 and lamin B2.

Finally, our studies showed that the absence of the farnesyl lipid anchor influences steady-state levels of the B-type lamins in cells and tissues. In *Lmnb1*[CS/CS] MEFs, lamin B1 levels were reduced to the levels observed in *Lmnb1*^{+/−} cells. Low levels of lamin B1 were also observed in brain extracts of *Lmnb1*[CS/CS] mice, and low levels
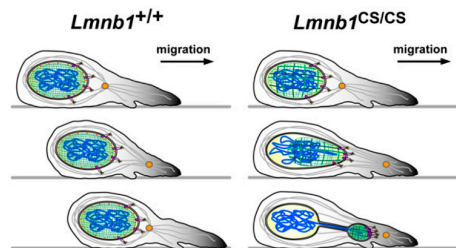
Fig. 9. A model to explain dumbbell-shaped nuclei and naked chromatin in migrating neurons of *Lmnb1*[CS/CS] mice. (*Left*) The nuclear lamina (green) in neurons of wild-type mice (*Lmnb1*^{+/+}) is tightly woven and is affixed to the inner nuclear membrane by the farnesyl lipid anchors on B-type lamins (red). During neuronal migration, the nucleus is pulled by microtubule-associated dynein motors (yellow) toward the centrosome (orange) in the leading edge of the cell. Pulling the nucleus forward depends on connections between the microtubule network (gray strands) and the LINC complex of the nuclear envelope (SUN1/2, purple; Nesprin-1/2 pink) as well as connections between the LINC complex and the nuclear lamina. (*Right*) In *Lmnb1*[CS/CS] neurons, the nuclear lamina is no longer tightly affixed to the inner nuclear membrane because of the absence of the farnesyl lipid anchor on lamin B1 (creating a potential space between the nuclear lamina and the inner nuclear membrane). In addition, the B-type lamins exhibit a honeycomb distribution (i.e., the "nuclear lamina meshwork" is not tightly woven). During neuronal migration, the nuclear lamina is pulled forward, exactly as in wild-type mice, but the chromatin (blue) escapes from the confines of the nuclear lamina (through honeycomb-like pores) into the space between the nuclear lamina and inner nuclear membrane. This process creates dumbbell-shaped nuclei in which the nuclear lamina is in one end of the dumbbell (closest to the leading edge of the cell); the bulk of the chromatin is located in the other end of the dumbbell (surrounded by nuclear membranes).

of lamin B2 were observed in brain extracts from $Lmnb2^{CS/CS}$ mice. The targeted mutations had no effect on $Lmnb1$ or $Lmnb2$ transcript levels, so the low levels of lamin B1 in $Lmnb1^{CS/CS}$ brains and lamin B2 in $Lmnb2^{CS/CS}$ brains were likely because of increased turnover of the nonfarnesylated lamins. In support of this idea, Yang et al. (32) showed that a Cys-to-Ser mutation in progerin accelerates the turnover of progerin and leads to lower progerin levels in cells and tissues. The effect of the $Lmnb1^{CS}$ and $Lmnb2^{CS}$ mutations on the levels of B-type lamins was more pronounced in the developing brain (where the expression of A-type lamins is negligible) than in MEFs (where the A-type lamin expression is high). It seems possible, therefore, that the expression of A-type lamins in MEFs limits the accelerated turnover of nonfarnesylated lamin B proteins. Finally, it is noteworthy that the levels of lamin B2 were significantly reduced in brain extracts from $Lmnb1^{CS/CS}$ mice. One possibility is that some of the lamin B2 in $Lmnb1^{CS/CS}$ neurons cells exists as heterodimers with non-farnesylated lamin B1 and that the increased turnover of non-farnesylated lamin B1 causes a secondary increase in the turnover of lamin B2.

In summary, the present studies illuminate the in vivo functional relevance of protein farnesylation for lamin B1 and lamin B2. In the case of lamin B2, farnesylation appeared to be of minimal importance, given that $Lmnb2^{CS/CS}$ mice had no detectable pathology in the brain (or in any other tissues) and had a normal lifespan. In contrast, the farnesylation of lamin B1 is clearly important, given that $Lmnb1^{CS/CS}$ mice displayed defective neuronal migration in the developing brain. We also observed distinctive dumbbell-shaped nuclei in $Lmnb1^{CS/CS}$ neurons, with the nuclear lamina being separated from the majority of the chromatin within cells. These abnormalities likely result from defective interactions between the nuclear lamina and the inner nuclear membrane (Fig. 9). Finally, our studies demonstrate that the farnesylation of the B-type lamins is important for maintaining normal levels of those proteins in cells, particularly in the brain.

Materials and Methods

Generation of Knock-In Mice Expressing Nonfarnesylated Versions of Lamin B1 and Lamin B2. The targeting vectors for the $Lmnb1^{CS}$ and $Lmnb2^{CS}$ alleles were generated by site-directed mutagenesis of the BAC clones CH38-24P17 and CH38-14G10 (containing wild-type $Lmnb1$ and $Lmnb2$, respectively). In both alleles, the codon encoding the cysteine in the *CaaX* motif was replaced with a codon encoding a serine: TGT > TCT in the $Lmnb1^{CS}$ allele and TGC > AGT in the $Lmnb2^{CS}$ allele. A new SacI site was introduced into the $Lmnb1^{CS}$ allele adjacent to the Cys > Ser mutation (AAGCTG > GAGCTC), and a new SalI site was introduced into the $Lmnb2^{CS}$ allele (GCCGAC > GTCGAC); these changes did not alter the amino acid sequence of the proteins.

The gene-targeting vectors were generated by BAC recombineering in DY380 cells (44). The point mutations were introduced using primers 5′-TGA-CTTTCCTTCTGTTTC CCCTCTCAGGGAGCCCCAAGAGCATCCAATAAGAGCTCTG-CCATTATGTGAA-3′ (the mutated nucleotides are underlined) and 5′-TTCTAGC-TTGAGGAAGATCGAC CATGTCTTGACAAGTTCACATAATGGCAGAGCTCTTATT-GGATGCTCT-3′ for the $Lmnb1^{CS}$ allele; and 5′-TGCATCCTCCCTCATTCCTTG-CAGGGGGACCCAAGG ACTACCTCAAGGGGCAGTCGACTGATGTGAAACC-3′ and 5′-TTTAGGGGCTCT GGGGACCATGGTGACCGTGGGGCAGGTTTCACATCAGTC-GACTGCCCCTTGAGGTAGT-3′ for the $Lmnb2^{CS}$ allele. A *lox*P-Neo^R-*lox*P selection cassette was introduced 1.5-kb downstream of the point mutations using primers with 50-bp homology sequences at both ends. Gaps were repaired with primers 5′-CAGGTTCGATGCTCAGAACCTCT ATCAGGTTGCTTCCTGACCA-CACCTGATCCTGTGTGAAATTGTTATCCGC-3′ and 5′-CGCCAAAGTTGCCCTGT-GACCTGTATATACTTGTCCTGGTGTGTGAGG CCCCACTGGCCGTCGTTTTACA-3′ for the $Lmnb1^{CS}$ allele; and 5′-AGGCTCCGTC AAATGCATGGGCCTATCCTGAG-AAGGGCAAGGTGTTAGGA-3′ and 5′-AGTCC AGTGTGTAGATGTTGTAGAACG-GGTGGCGATAGATGCGTGCCACG-3′ for the $Lmnb2^{CS}$ allele. The sequences of the targeting vectors were confirmed by DNA sequencing.

The vectors were linearized with AsiSI and electroporated into E14Tg2A ES cells. After selection with G418 (125 mg/mL; Gibco, Invitrogen), ES cell colonies were screened for recombination on the 5′-end by long-range PCR (2× Extensor Long Range PCR Master Mix; Thermo Scientific) with primers 5′—GATCTGGCCTTCCTGTCC AGAACTA-3′ and 5′-AATATCACGGGTAGCCAACG-CTATG-3′ for the $Lmnb1^{CS}$ allele and 5′-AGGATGGCCTTGACGAGTAAGACTG-3′

and 5′-AATATCACGGGT AGCCAACGCTATG-3′ for the $Lmnb2^{CS}$ allele. Recombination on the 3′-end was detected with primers 5′-GTGGAGAGGCT-ATTCGGCTATGACT-3′ and 5′-GAGGCA GGAAATAAATTCCCAGAGG-3′ for the $Lmnb1^{CS}$ allele, and 5′-GTGGAGAGGCTATTCGGCTATGACT-3′ and 5′-AAGA-GGCACCAGTTGGGTGTTACAT-3′ for the $Lmnb2^{CS}$ allele. The products of the 5′ long-range PCR were confirmed by restriction endonuclease digestion, taking advantage of the new restriction endonuclease sites in the targeted alleles. The fidelity of the mutant alleles was also confirmed by sequencing cDNA from the targeted ES cell clones.

After verifying that the targeted clones were euploid, two independently targeted ES cell lines were injected into C57BL/6 blastocysts. Male chimeras from both clones were mated with C57BL/6 females to create heterozygous mice ($Lmnb1^{CS/+}$ and $Lmnb2^{CS/+}$). Mice heterozygous for each targeted allele were intercrossed to generate homozygous mice ($Lmnb1^{CS/CS}$ and $Lmnb2^{CS/CS}$). Genotyping was performed by PCR with primers 5′-CCATGTACGCACTCTG-GATG-3′ (B1CSgF), 5′-ACTGTCATGAGTCATACTGCAAA-3′ (B1CSgR) and 5′-CGAAGTTATCATTAATTGCGTTG-3′ (B1CSgRMut) for the $Lmnb1^{CS}$ allele; and 5′-AGGTCCTCAGGGGTCTGTTT-3′ (B2CSgF), 5′-CACCATGTGGTTGCTGGTAT-3′ (B2CSgR) and 5′-TAATTGCGTTGCGCCATCT-3′ (B2CSgR Mut) for the $Lmnb2^{CS}$ allele. B1CSgF and B1CSgR primers yield a 350-bp PCR product from the wild-type allele; B1CSgF and B1CSgRMut primers yield a 250-bp PCR product from the $Lmnb1^{CS}$ allele; B2CSgF and B2CSgR primers yield a 352-bp PCR product from the wild-type allele; B1CSgF and B1CSgRMut primers yield a 272-bp PCR product from the $Lmnb2^{CS}$ allele.

All mice were fed a chow diet and housed in a virus-free barrier facility with a 12-h light/dark cycle. All animal protocols were approved by the University of California at Los Angeles's Animal Research Committee.

Knockout Mice. $Lmnb2^{-/-}$ mice have been described previously (23). $Lmnb1$ knockout mice ($Lmnb1^{-/-}$) were generated by breeding mice homozygous for a $Lmnb1$ conditional knockout allele ($Lmnb1^{fl/fl}$) (45) with mice harboring an Ella-*Cre* transgene (11).

Western Blots. Protein extracts from MEFs and mouse tissues were prepared as described previously (46–48). MEFs were resuspended in urea buffer (9 M urea, 10 mM Tris·HCl pH 8.0, 1 mM NaF, 1 mM PMSF, 10 μM EDTA, 0.2% β-mercaptoethanol, and a Roche Protease Inhibitors Mixture Tablet), sonicated, and centrifuged to isolate the urea-soluble protein fraction. Snap-frozen mouse tissues were pulverized using a chilled metal mortar and pestle, resuspended in ice-cold PBS with 1 mM NaF, 1 mM PMSF, and a Roche Protease Inhibitors Mixture Tablet, and then homogenized with a glass tissue grinder (Kontes). The cell pellets were resuspended in urea buffer, sonicated, and centrifuged to remove insoluble cell debris. Protein extracts were size-fractionated on 4–12% (wt/vol) gradient polyacrylamide Bis·Tris gels or 7% (wt/vol) Tris-Acetate gels (Invitrogen) and then transferred to nitrocellulose membranes. The membranes were incubated with the following antibodies: a goat polyclonal antibody against lamin A/C (1:400) (sc-6215; Santa Cruz); a goat polyclonal antibody against lamin B1 (1:400) (sc-6217; Santa Cruz); a mouse monoclonal antibody against lamin B2 (1:400) (33-2100; Invitrogen); and a goat polyclonal antibody against actin (1:1,000) (sc-1616; Santa Cruz). Antibody binding was assessed with infrared dye-conjugated secondary antibodies (Rockland) and quantified with an Odyssey infrared scanner (LI-COR).

Metabolic Labeling Studies to Detect Protein Farnesylation. Primary MEF cells were plated in six-well plates at ~70% confluency. After 3 h, the cells were treated with AG at 25 μM (31, 49) and incubated for another 48 h. Protein extracts were prepared in urea buffer, size-fractionated on 7% (wt/vol) Tris-Acetate gels (Invitrogen), and transferred to nitrocellulose membranes. A mouse monoclonal antibody against AG (1:4,000) (31) was used to detect the incorporation of AG into proteins (including lamin B1 and lamin B2). Antibody binding was detected with HRP-conjugated anti-mouse IgG (1:4,000) (GE Healthcare), ECL Plus Western Blotting Detection Reagents (GE Healthcare), and Hyperfilm ECL (GE Healthcare).

Histology and Immunofluorescence Microscopy. Mouse tissues were fixed in 10% (vol/vol) formalin (Evergreen) overnight at 4 °C, embedded in paraffin, sectioned (5-μm-thick), and stained with H&E. For immunohistochemical staining, mouse tissues were embedded in Optimum Cutting Temperature compound (Sakura Finetek) and tissue sections (10-μm-thick) were prepared with a cryostat. The sections were fixed in ice-cold methanol, rinsed with acetone, washed with 0.1% Tween-20 in TBS, and incubated with MOM Mouse Ig Blocking Reagent (Vector Laboratories). For cultured cells (MEFs and NPCs), the cells were grown on coverslips, washed with PBS containing 1 mM CaCl$_2$ and 1 mM MgCl$_2$, fixed in ice-cold methanol, rinsed with acetone, permeabilized with 0.1% Triton X-100 in PBS containing 1 mM CaCl$_2$ and 1 mM

75

MgCl$_2$, and then incubated with PBS containing 1 mM CaCl$_2$, 1 mM MgCl$_2$, 10% (vol/vol) FBS, and 0.2% BSA. The following primary antibodies were used: a goat polyclonal antibody against lamin B1 (1:400) (sc-6217; Santa Cruz); a mouse monoclonal antibody against lamin B2 (1:100) (33-2100; Invitrogen); a mouse monoclonal antibody against LAP2β (1:400) (611000; BD Biosciences); a rabbit polyclonal antibody against Cux1 (1:100) (sc-13024; Santa Cruz); a rat monoclonal antibody against Ctip2 (1:500) (ab18465; Abcam); a rabbit polyclonal antibody against pericentrin (1:1,000) (ab4448; Abcam); a mouse polyclonal antibody against SUN1 (1:400) (H00023353-B01P, Abnova); a rat monoclonal antibody against Nup98 (1:250) (ab50610; Abcam); and a mouse monoclonal antibody against Nup153 (1:250) (ab24700; Abcam). Antibody binding was detected with a variety of Alexa Fluor–labeled donkey antibodies against goat, rabbit, rat, or mouse IgG (Invitrogen). DNA was stained with DAPI.

Light microscopy images were captured with a Leica MZ6 dissecting microscope (Plan 0.5× or 1.0× objectives, air) with a DFC290 digital camera (Leica) and a Nikon Eclipse E600 microscope (Plan Fluor 20×/0.50 NA or 40×/0.75 NA objectives, air) with a SPOT RT slider camera (Diagnostic Instruments). The images were recorded with Leica Application Suite imaging software and SPOT 4.7 software (Diagnostic Instruments), respectively. Confocal fluorescence microscopy was performed with a Zeiss LSM700 laser-scanning microscope with a Plan Apochromat 20×/0.80 NA objective (air) or a Plan Apochromat 63×/1.4 NA oil-immersion objective. Images along the z axis were captured and merged with Zen 2010 software (Zeiss).

To analyze the frequency of nuclear abnormalities in MEFs and NPCs, z-stack images were obtained with a Plan Apochromat 63×/1.4 NA oil-immersion objective, and all of the images were scored by two independent observers in a blinded fashion.

Quantitative RT-PCR. Snap-frozen mouse tissues were homogenized in TRI reagent (Molecular Research Center). Total RNA was extracted according to the manufacturer's protocol and treated with DNase I (Ambion). RNA was then reverse-transcribed with random primers, oligo(dT), and SuperScript III (Invitrogen). Quantitative RT-PCR (qPCR) reactions were performed on a 7900 Fast Real-Time PCR system (Applied Biosystems) with SYBR Green PCR Master Mix (Bioline). Transcript levels were determined by the comparative cycle threshold method and normalized to levels of cyclophilin A.

Neuronal Migration Studies. Cortical neuronal progenitors were isolated as previously described (24). Briefly, the telencephalon of E13.5 mouse embryos was dissected and digested with 0.25% trypsin-EDTA (Gibco) at room temperature for 20 min. To generate neurospheres, dissociated cells were cultured in conical bottom microplates with DMEM containing 10% (vol/vol) FBS

for 5 d. Neurospheres were suspended by gentle pipetting, plated on poly-L-lysine–coated coverslips, and then cultured for an additional 4 d in neuronal differentiation medium (1:1 mixture of DMEM/F12 and Neurobasal medium, supplemented with B-27 and N2 supplements; all from Gibco) before analysis.

Electron Microscopy. Fresh mouse tissues were fixed in a 100 mM sodium cacodylate solution containing 2.5% (vol/vol) glutaraldehyde and 2% (wt/vol) paraformaldehyde overnight at 4 °C. The fixed tissues were incubated with 1% (wt/vol) osmium tetroxide for 1 h at room temperature, washed with distilled water, and then incubated with 2% (wt/vol) uranyl acetate overnight at 4 °C in the dark. The next day, the tissues were rinsed with distilled water, dehydrated by serial incubations with 20%, 30%, 50%, 70%, and 100% (vol/vol) acetone for 30 min each, and infiltrated with Spurr's resin. To polymerize the resin, the tissues were incubated in fresh Spurr's resin overnight at 70 °C. Tissue sections (50-nm-thick) were prepared with a Diatome diamond knife and a Leica UCT Ultramicrotome, placed on 200 mesh copper grids, and stained with Reynolds lead citrate for 5 min. Images were captured using a 100CX JEOL electron microscope at 80 kV.

For EM tomography, 200-nm-thick sections were collected on formvar-coated copper slot grids. Following staining, 10-nm colloidal gold particles were applied to both surfaces of the grid to serve as fiducial markers for subsequent image analysis. Dual-axis tilt series (–65° to +65° at 1° intervals) were obtained with a computerized tilt stage in a FEI Tecnai TF20 electron microscope operating at 200 kV. Tomographic reconstruction and modeling was performed with the IMOD software package (50).

Statistical Analysis. Statistical analyses were performed with Prism software version 4.0 (GraphPad) and GraphPad QuickCalcs (www.graphpad.com). Differences in nuclear abnormalities were analyzed with a Fisher's exact test. Interdependence between expression levels of lamin B1 and the frequency of nuclear abnormalities was assessed by a test of Pearson's correlation. Differences in brain size and in expression levels of lamin B1 in MEFs were analyzed by a two-tailed Student t test.

1. Schirmer EC, Foisner R (2007) Proteins that associate with lamins: Many faces, many functions. *Exp Cell Res* 313(10):2167–2179.
2. Dittmer TA, Misteli T (2011) The lamin protein family. *Genome Biol* 12(5):222.
3. Worman HJ, Fong LG, Muchir A, Young SG (2009) Laminopathies and the long strange trip from basic cell biology to therapy. *J Clin Invest* 119(7):1825–1836.
4. Davies BS, Fong LG, Yang SH, Coffinier C, Young SG (2009) The posttranslational processing of prelamin A and disease. *Annu Rev Genomics Hum Genet* 10:153–174.
5. Schafer WR, Rine J (1992) Protein prenylation: Genes, enzymes, targets, and functions. *Annu Rev Genet* 26:209–237.
6. Wolda SL, Glomset JA (1988) Evidence for modification of lamin B by a product of mevalonic acid. *J Biol Chem* 263(13):5997–6000.
7. Vorburger K, Kitten GT, Nigg EA (1989) Modification of nuclear lamin proteins by a mevalonic acid derivative occurs in reticulocyte lysates and requires the cysteine residue of the C-terminal CXXM motif. *EMBO J* 8(13):4007–4013.
8. Otto JC, Kim E, Young SG, Casey PJ (1999) Cloning and characterization of a mammalian prenyl protein-specific protease. *J Biol Chem* 274(13):8379–8382.
9. Clarke S, Vogel JP, Deschenes RJ, Stock J (1988) Posttranslational modification of the Ha-ras oncogene protein: evidence for a third class of protein carboxyl methyltransferases. *Proc Natl Acad Sci USA* 85(13):4643–4647.
10. Dai Q, et al. (1998) Mammalian prenylcysteine carboxyl methyltransferase is in the endoplasmic reticulum. *J Biol Chem* 273(24):15030–15034.
11. Bergo MO, et al. (2002) Zmpste24 deficiency in mice causes spontaneous bone fractures, muscle weakness, and a prelamin A processing defect. *Proc Natl Acad Sci USA* 99(20):13049–13054.
12. Corrigan DP, et al. (2005) Prelamin A endoproteolytic processing in vitro by recombinant Zmpste24. *Biochem J* 387(Pt 1):129–138.
13. Pendás AM, et al. (2002) Defective prelamin A processing and muscular and adipocyte alterations in Zmpste24 metalloproteinase-deficient mice. *Nat Genet* 31(1):94–99.
14. Barrowman J, Hamblet C, George CM, Michaelis S (2008) Analysis of prelamin A biogenesis reveals the nucleus to be a CaaX processing compartment. *Mol Biol Cell* 19(12):5398–5408.
15. Eriksson M, et al. (2003) Recurrent de novo point mutations in lamin A cause Hutchinson-Gilford progeria syndrome. *Nature* 423(6937):293–298.
16. Fong LG, et al. (2006) A protein farnesyltransferase inhibitor ameliorates disease in a mouse model of progeria. *Science* 311(5767):1621–1623.

17. Yang SH, Qiao X, Fong LG, Young SG (2008) Treatment with a farnesyltransferase inhibitor improves survival in mice with a Hutchinson-Gilford progeria syndrome mutation. *Biochim Biophys Acta* 1781(1-2):36–39.
18. Yang SH, et al. (2006) A farnesyltransferase inhibitor improves disease phenotypes in mice with a Hutchinson-Gilford progeria syndrome mutation. *J Clin Invest* 116(8): 2115–2121.
19. Young SG, Fong LG, Michaelis S (2005) Prelamin A, Zmpste24, misshapen cell nuclei, and progeria—New evidence suggesting that protein farnesylation could be important for disease pathogenesis. *J Lipid Res* 46(12):2531–2558.
20. Gordon LB, et al. (2012) Clinical trial of a farnesyltransferase inhibitor in children with Hutchinson-Gilford progeria syndrome. *Proc Natl Acad Sci USA* 109(41):16666–16671.
21. Moir RD, Montag-Lowy M, Goldman RD (1994) Dynamic properties of nuclear lamins: Lamin B is associated with sites of DNA replication. *J Cell Biol* 125(6):1201–1212.
22. Tsai MY, et al. (2006) A mitotic lamin B matrix induced by RanGTP required for spindle assembly. *Science* 311(5769):1887–1893.
23. Coffinier C, et al. (2010) Abnormal development of the cerebral cortex and cerebellum in the setting of lamin B2 deficiency. *Proc Natl Acad Sci USA* 107(11):5076–5081.
24. Coffinier C, et al. (2011) Deficiencies in lamin B1 and lamin B2 cause neurodevelopmental defects and distinct nuclear shape abnormalities in neurons. *Mol Biol Cell* 22(23): 4683–4693.
25. Kim Y, et al. (2011) Mouse B-type lamins are required for proper organogenesis but not by embryonic stem cells. *Science* 334(6063):1706–1710.
26. Young SG, Jung HJ, Coffinier C, Fong LG (2012) Understanding the roles of nuclear A- and B-type lamins in brain development. *J Biol Chem* 287(20):16103–16110.
27. Krohne G, Waizenegger I, Höger TH (1989) The conserved carboxy-terminal cysteine of nuclear lamins is essential for lamin association with the nuclear envelope. *J Cell Biol* 109(5):2003–2011.
28. Holtz D, Tanaka RA, Hartwig J, McKeon F (1989) The CaaX motif of lamin A functions in conjunction with the nuclear localization signal to target assembly to the nuclear envelope. *Cell* 59(6):969–977.
29. Hennekes H, Nigg EA (1994) The role of isoprenylation in membrane attachment of nuclear lamins. A single point mutation prevents proteolytic cleavage of the lamin A precursor and confers membrane binding properties. *J Cell Sci* 107(Pt 4):1019–1029.

MEDICAL SCIENCES

76

30. Coffinier C, et al. (2010) Direct synthesis of lamin A, bypassing prelamin a processing, causes misshapen nuclei in fibroblasts but no detectable pathology in mice. *J Biol Chem* 285(27):20818–20826.

31. Troutman JM, Roberts MJ, Andres DA, Spielmann HP (2005) Tools to analyze protein farnesylation in cells. *Bioconjug Chem* 16(5):1209–1217.

32. Yang SH, Andres DA, Spielmann HP, Young SG, Fong LG (2008) Progerin elicits disease phenotypes of progeria in mice whether or not it is farnesylated. *J Clin Invest* 118(10): 3291–3300.

33. Röber RA, Weber K, Osborn M (1989) Differential timing of nuclear lamin A/C expression in the various organs of the mouse embryo and the young animal: a developmental study. *Development* 105(2):365–378.

34. Vergnes L, Péterfy M, Bergo MO, Young SG, Reue K (2004) Lamin B1 is required for mouse development and nuclear integrity. *Proc Natl Acad Sci USA* 101(28):10428–10433.

35. Kitten GT, Nigg EA (1991) The CaaX motif is required for isoprenylation, carboxyl methylation, and nuclear membrane association of lamin B2. *J Cell Biol* 113(1):13–23.

36. Izumi M, Vaughan OA, Hutchison CJ, Gilbert DM (2000) Head and/or CaaX domain deletions of lamin proteins disrupt preformed lamin A and C but not lamin B structure in mammalian cells. *Mol Biol Cell* 11(12):4323–4337.

37. Davies BS, et al. (2010) An accumulation of non-farnesylated prelamin A causes cardiomyopathy but not progeria. *Hum Mol Genet* 19(13):2682–2694.

38. Solecki DJ, Govek EE, Tomoda T, Hatten ME (2006) Neuronal polarity in CNS development. *Genes Dev* 20(19):2639–2647.

39. Wynshaw-Boris A, Gambello MJ (2001) LIS1 and dynein motor function in neuronal migration and development. *Genes Dev* 15(6):639–651.

40. Zhang X, et al. (2009) SUN1/2 and Syne/Nesprin-1/2 complexes connect centrosome to the nucleus during neurogenesis and neuronal migration in mice. *Neuron* 64(2):173–187.

41. Lombardi ML, et al. (2011) The interaction between nesprins and sun proteins at the nuclear envelope is critical for force transmission between the nucleus and cytoskeleton. *J Biol Chem* 286(30):26743–26753.

42. Coffinier C, Fong LG, Young SG (2010) LINCing lamin B2 to neuronal migration: Growing evidence for cell-specific roles of B-type lamins. *Nucleus* 1(5):407–411.

43. Zhang FL, Casey PJ (1996) Protein prenylation: Molecular mechanisms and functional consequences. *Annu Rev Biochem* 65:241–269.

44. Liu P, Jenkins NA, Copeland NG (2003) A highly efficient recombineering-based method for generating conditional knockout mutations. *Genome Res* 13(3):476–484.

45. Yang SH, et al. (2011) An absence of both lamin B1 and lamin B2 in keratinocytes has no effect on cell proliferation or the development of skin and hair. *Hum Mol Genet* 20(18):3537–3544.

46. Steinert P, Zackroff R, Aynardi-Whitman M, Goldman RD (1982) Isolation and characterization of intermediate filaments. *Methods Cell Biol* 24:399–419.

47. Fong LG, et al. (2004) Heterozygosity for Lmna deficiency eliminates the progeria-like phenotypes in Zmpste24-deficient mice. *Proc Natl Acad Sci USA* 101(52):18111–18116.

48. Jung HJ, et al. (2012) Regulation of prelamin A but not lamin C by miR-9, a brain-specific microRNA. *Proc Natl Acad Sci USA* 109(7):E423–E431.

49. Dechat T, et al. (2007) Alterations in mitosis and cell cycle progression caused by a mutant lamin A known to accelerate human aging. *Proc Natl Acad Sci USA* 104(12): 4955–4960.

50. Mastronarde DN (1997) Dual-axis tomography: An approach with alignment methods that preserve resolution. *J Struct Biol* 120(3):343–352.

77

Supporting Information

SI Materials and Methods

Wound-Healing Assay. Primary mouse embryonic fibroblast (MEF) cells were plated in 24-well plates with glass coverslips and grown to confluency. Cells were then scraped with a sterile p1000 pipette tip, washed with PBS, and incubated with fresh culture medium at 37 °C for 4 h. Cells were then fixed and stained for immunofluorescence microscopy.

Protein Sequence Alignment. Protein sequences of mouse lamin B1 (ENSMUSP00000025486) and mouse lamin B2 (ENSMUSP00000136524) were aligned using Clustal Omega (v1.1.0) with the default setting (www.ebi.ac.uk/Tools/msa/clustalo/).
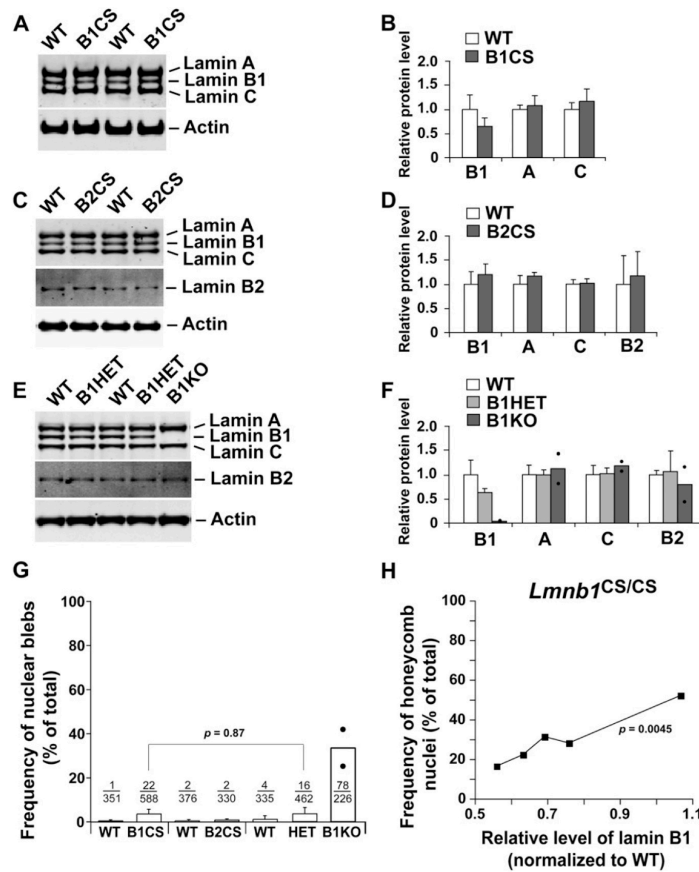
Fig. S1. Levels of nuclear lamin proteins and nuclear shape abnormalities in $Lmnb1^{CS/CS}$ and $Lmnb2^{CS/CS}$ MEFs. (*A–F*) Western blots (*A, C, E*) and quantification of lamin protein levels relative to actin (*B, D, F*) in WT, $Lmnb1^{CS/CS}$ (B1CS), $Lmnb2^{CS/CS}$ (B2CS), $Lmnb1^{+/-}$ (B1HET), and $Lmnb1^{-/-}$ (B1KO) MEFs (mean ± SD). The levels of lamin B1 in $Lmnb1^{CS/CS}$ MEFs were ~35% lower than in wild-type cells (*B*) (*P* = 0.06) and similar to levels of lamin B1 in $Lmnb1^{+/-}$ cells (*F*) (where the levels were ~37% lower than in wild-type cells; *P* = 0.06). (*G*) Frequency of nuclear blebs in the MEFs that were analyzed in Fig. 2 *A–F*. The frequency of nuclear blebs in $Lmnb1^{-/-}$ MEFs was higher than in wild-type MEFs (*P* < 0.0001). Frequencies of blebs in $Lmnb1^{CS/CS}$ and $Lmnb1^{+/-}$ cells were similar (*P* = 0.87); both were higher than in wild-type cells (*P* < 0.0001). Values represent mean ± SD. (*H*) Correlation between levels of nonfarnesylated lamin B1 and the frequency of honeycomb nuclei. Each point represents five individual $Lmnb1^{CS/CS}$ MEF cell lines (used in *G* and Fig. 2*G*). The frequency of honeycomb nuclei in $Lmnb1^{CS/CS}$ MEFs was positively correlated with lamin B1 levels (*P* = 0.0045).

Fig. S2. Absence of the farnesyl lipid anchor lowers steady-state levels of lamin B1 and lamin B2 in the cortex. (*A* and *B*) Western blot analysis and quantification of lamin B1 and B2 levels in the cerebral cortex of embryonic day (E) 19 to postnatal day (P) 1 *Lmnb1*$^{+/+}$ (WT), *Lmnb1*$^{CS/CS}$ (B1CS), and *Lmnb1*$^{+/-}$ (B1HET) mice. Lamin B1 and lamin B2 levels were normalized to actin levels. Lamin B1 levels were ~40% lower in *Lmnb1*$^{CS/CS}$ mice than in wild-type mice; this was the case in knock-in mice derived from two different ES cell lines (clones 22 and 9). *Lmnb1*$^{+/+}$, $n = 5$; *Lmnb1*$^{CS/CS}$, $n = 7$; *Lmnb1*$^{+/-}$, $n = 2$. Values represent mean ± SD. *$P < 0.05$; **$P < 0.005$. (*C* and *D*) Western blot analysis and quantification of lamin B1 and lamin B2 levels in the cerebral cortex of E19–P1 *Lmnb2*$^{+/+}$ (WT) and *Lmnb2*$^{CS/CS}$ (B2CS) mice. Values represent mean ± SD *Lmnb2*$^{+/+}$, $n = 5$; *Lmnb2*$^{CS/CS}$, $n = 5$. Lamin B1 and lamin B2 levels were normalized to actin. Lamin B2 levels were ~30% lower in *Lmnb2*$^{CS/CS}$ mice than in wild-type mice; this was the case in mice generated from two ES cell lines (clones 116 and 121). *$P < 0.005$. (*E* and *F*) Quantitative RT-PCR analysis of *Lmnb1* and *Lmnb2* transcript levels in the cerebral cortex of E19–P1 *Lmnb1*$^{+/+}$ (WT), *Lmnb1*$^{CS/CS}$ (B1CS), *Lmnb1*$^{+/-}$ (B1HET), *Lmnb2*$^{+/+}$ (WT), and *Lmnb2*$^{CS/CS}$ (B2CS) mice. Transcript levels were normalized to cyclophilin A and compared with levels in wild-type mice (set at 1.0). Values represent mean ± SD. *Lmnb1*$^{+/+}$, $n = 5$; *Lmnb1*$^{CS/CS}$, $n = 7$; *Lmnb1*$^{+/-}$, $n = 2$; *Lmnb2*$^{+/+}$, $n = 5$; *Lmnb2*$^{CS/CS}$, $n = 5$.

Fig. S3. Histological and immunohistochemical examination of tissues from *Lmnb1*^CS/CS and *Lmnb2*^CS/CS embryos. (*A* and *B*) H&E staining of the heart, liver, kidney, lung, skin, and intestine from *Lmnb1*^CS/+, *Lmnb1*^CS/CS, *Lmnb2*^+/+, and *Lmnb2*^CS/CS mice at E19–P1. The lungs of *Lmnb1*^CS/CS mice appeared immature with fewer alveoli and thicker interstitial spaces as described earlier in *Lmnb1* knockout mice (1). No pathology was detected in the other tissues. (Scale bars, 0.5 mm.) (*C*) Immunofluorescence microscopy of the lung, intestine, and skin from *Lmnb1*^+/+ and *Lmnb1*^CS/CS embryos (E19–P1). Frozen tissue sections were stained with antibodies against lamin B1 (red) and lamin B2 (green). DNA was stained with DAPI (blue). Images along the *z* axis were captured and merged with Zen 2010 software (Zeiss). Both lamin B1 and lamin B2 were located mainly at the nuclear rim in the skin of *Lmnb1*^CS/CS embryos. The cell nuclei in the lung and intestine of *Lmnb1*^CS/CS mice exhibited a honeycomb distribution of B-type lamins (similar to the finding in MEFs) (Fig. 2*E*). (Scale bars, 20 μm.) (*D*) Higher-magnification images of individual optical sections of the lung from *Lmnb1*^CS/CS mice illustrating the nuclear honeycomb phenotype. The distribution of lamin B1 (white) within cells is shown. (Scale bar, 5 μm.)

1. Vergnes L, Péterfy M, Bergo MO, Young SG, Reue K (2004) Lamin B1 is required for mouse development and nuclear integrity. *Proc Natl Acad Sci USA* 101(28):10428–10433.

80

LAP2 + Lamin B1 + DAPI
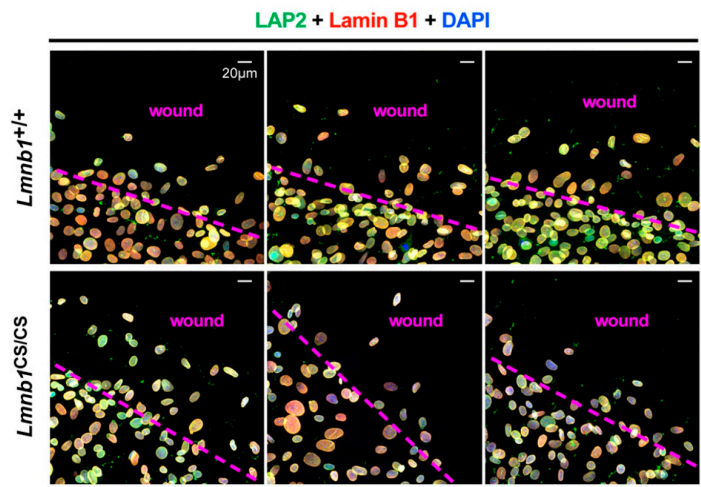
Fig. S4. Wound-healing assay with *Lmnb1*^{+/+} and *Lmnb1*[CS/CS] MEFs. Confluent monolayers were scraped, with the goal of visualizing cells that migrate in and close the "wound." Cells were stained with antibodies against LAP2β (lamin-associated polypeptide 2; green) and lamin B1 (red); DNA was stained with DAPI (blue). The edge of the initial wound is indicated with a dashed line (magenta). The shapes of cell nuclei in migrating *Lmnb1*[CS/CS] MEFs were essentially normal, and no dumbbell-shaped nuclei were observed. (Scale bars, 20 μm.)

Lamin B1 + DAPI   Lamin B2 + DAPI   DAPI
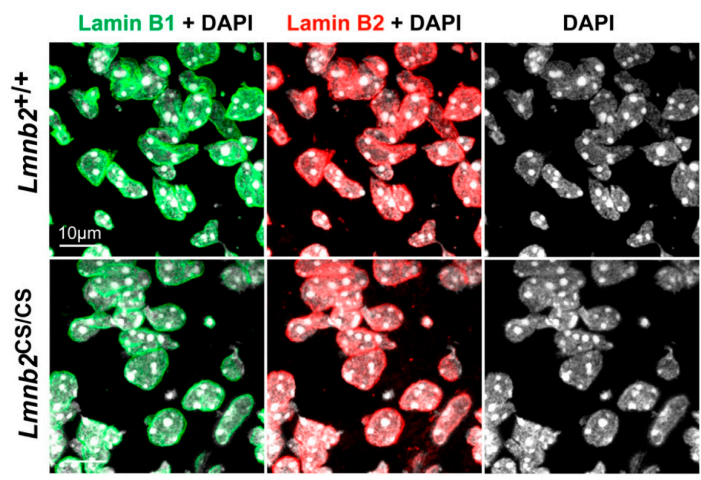
Fig. S5. Immunofluorescence microscopy of the midbrain (superior colliculus) from E19–P1 *Lmnb2*^{+/+} and *Lmnb2*[CS/CS] embryos. Sections were stained with antibodies against lamin B1 (green) and lamin B2 (red); DNA was stained with DAPI (white). No dumbbell-shaped nuclei and naked chromatin were observed in *Lmnb2*[CS/CS] midbrains. (Scale bar, 10 μm.)

81
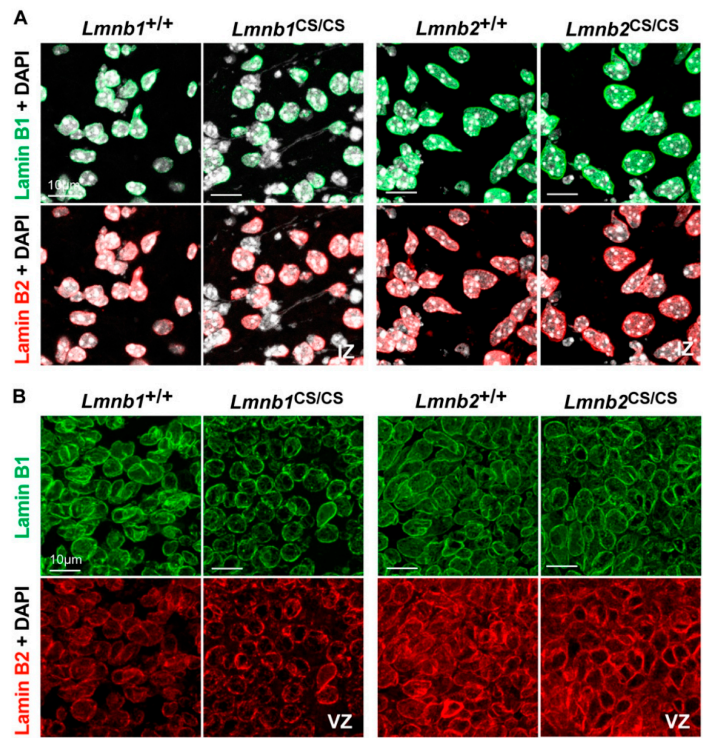
Fig. S6. Immunofluorescence microscopy of the cerebral cortex from E19–P1 *Lmnb1*^{+/+}, *Lmnb1*[CS/CS], *Lmnb2*^{+/+}, and *Lmnb2*[CS/CS] embryos. Frozen sections were stained with antibodies against lamin B1 (green) and lamin B2 (red); DNA was stained with DAPI (white). (*A*) Intermediate zone (IZ) of the cerebral cortex, showing dumbbell-shaped nuclei and "naked chromatin" in *Lmnb1*[CS/CS] embryos. (*B*) Ventricular zone (VZ), showing honeycomb distribution of lamin B1 in *Lmnb1*[CS/CS] embryos. No nuclear abnormalities were found in *Lmnb2*[CS/CS] embryos. (Scale bars, 10 μm.)

```
Lamin B1    MATATPVQQQRAGSRASAPATPLSPTRLSRLQEKEELRELNDRLAVYIDKVRSLETENSA
Lamin B2    ---------MASLPPHAGPATPLSPTRLSRLQEKEELRELNDRLAHYIDRVRALELENDR
            :       :.**************************** ***:**:** **.

Lamin B1    LQLQVTEREEVRGRELTGLKALYETELADARRALDDTARERAKLQIELGKFKAEHDQLLL
Lamin B2    LLLLRISEKEEVTTREVSGIKTLYESELADARRVLDETARERARLQIEIGKVQAELEEARK
            * *::*:*** **::*:*:***:*******.**:******:****:**.:** ::

Lamin B1    NYAKKESDLSGAQIKLREYEAALNSKDAALATALGDKKSLEGDLEDLKDQIAQLEASLSA
Lamin B2    SAKKREGELTVAQGRVKDLESLFHRSEAELATALSDKQGLETEVAELRAQLAKAEDGHAV
            . *:*.:*: ** :::: *: :. ..:* *****.**:.** :: :*: *:*: * . :.

Lamin B1    AKKQLADETLLKVDLENRCQSLTEDLEFRKNMYEEEINETRRKHETRLVEVDSGRQIEYE
Lamin B2    AKKQLEKETLMRVDLENRCQSLQEELAFSKSVFEEEVRETRRRHERRLVEVDSSRQQEYD
            ***** .***::********** *:* * *.::***:.****:** *******.** **:

Lamin B1    YKLAQALHEMREQHDAQVRLYKEELEQTYHAKLENARLSSEMNTSTVNSAREELMESRMR
Lamin B2    FKMAQALEDLRSQHDEQVRLYRVELEQTYQAKLDNAKLLSDQNDKAAHAAREELKEARMR
            :*:****.::*.*** *****: ******:***:**:* *: * .:..:***** *:***

Lamin B1    IESLSSQLSNLQKESRACLERIQELEDMLAKERDNSRRMLSDREREMAEIRDQMQQQLSD
Lamin B2    VESLSYQLLGLQKQASAAENHIHELEEEALAGERDKFRKMLDAKEQEMTEVRDAMQQQLAE
            :**** ** ***:: *. ::*:***: ** ***: *:**. :*:**:*:** *****::

Lamin B1    YEQLLDVKLALDMEISAYRKLLEGEEERLKLSPSPSSRVTVSRASSSRSV--------RT
Lamin B2    YQELLDIKLALDMEISAYRKLLEGEEERLKLSPSPSSRITISRATSSSSSSGVGMSVGQ
            *:.:***:***********************************:*:***:** *

Lamin B1    TRGKRKRVDVEESEAS--------SSVSISHSASATGNVCIEEIDVDGKFIRLKNTSEQD
Lamin B2    GRGKRRRLETEDTSGSPSRASRVSSGSRLAQQTVATGVVNIDEVDPEGRFVRLKNSSDKD
            ****:*::.*::..*      *.  :::.: *** * *:*:* :*:*:****:*::*

Lamin B1    QPMGGWEMIRKI-GDTSVSYKYTSRYVLKAGQTVTVWAANAGVTASPPTDLIWKNQNSWG
Lamin B2    QSLGNWRIKRQVLEGEDIAYKFTPKYVLRAGQTVTVWAAGAGATHSPPSTLVWKSQTNWG
            * :* *.: *::   .::**:* :***:********** **.* ***: *:**.*..**

Lamin B1    TGEDVKVILKNSQGEEVAQRSTVFKTTIPEEEEEEEEEPIGVAVEEERFHQQGAPRASNK
Lamin B2    PGESFRTALVSADGEEVAVKAAKHSSVQGRENGEEEEEEEAEFGEEDLFHQQGDPRTTSR
            **..:. * .::***** ::: ..:.  .*: ***** .  **: ***** **::.:

Lamin B1    SCAIM
Lamin B2    GCRLM
            .:* :*
```

Fig. S7. Amino acid sequence alignment of mouse lamin B1 and lamin B2. An asterisk (*) represents a fully conserved residue; a colon (:) represents a residue with strongly similar properties; a period (.) represents a residue with weakly similar properties. The position of the "Cys-to-Ser" mutation in lamin B1 and lamin B2 are indicated with a red box.

83
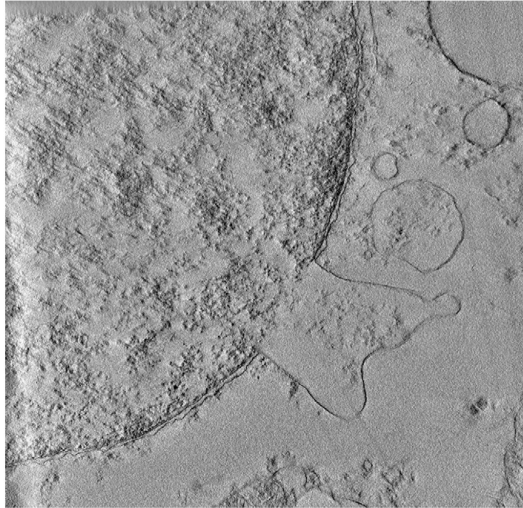
Movie S1. EM tomography of the cerebral cortex of an *Lmnb1*[CS/CS] embryo illustrating a nuclear bleb surrounded by an inner and outer nuclear membrane. (See Fig. 8*D* for the scale bar.)

Movie S1

84

Chapter 5:

An Absence of All Nuclear Lamins in Keratinocytes Leads to Defective Skin Barrier

Development and Interspersion of Nuclear Membrane Proteins with Chromatin

ABSTRACT

Until recently, dogma held that the B-type lamins were essential proteins in eukaryotic cells with vital functions in DNA replication, gene transcription, heterochromatin organization, and mitotic spindle assembly. However, recent studies have challenged this notion. Mice lacking both lamin B1 and lamin B2 in keratinocytes had no skin pathology and the keratinocytes showed normal growth rate and heterochromatin distribution in the nucleus. Also, an absence of both B-type lamins in hepatocytes did not lead to liver pathology. More surprisingly, mouse embryonic stem cells without any of the nuclear lamins were reported to proliferate and differentiate normally and to form teratomas upon subcutaneous injection into immune-deficient mice. In the current study, we generated keratinocyte-specific *Lmna/Lmnb1/Lmnb2* triple-knockout mice to investigate whether nuclear lamins are required for proliferation and differentiation of cells *in vivo*. Mice lacking all nuclear lamins in skin keratinocytes manifested skin barrier defects and died soon after birth due to lethal dehydration. Also, neutral lipids were abnormally accumulated in the stratum corneum of the triple-knockout skin. Nuclear membrane proteins were often mislocalized in nucleoplasm and interspersed with the chromatin. These studies suggest that nuclear lamins are essential for the vitality of keratinocytes *in vivo* and the normal skin barrier development.

INTRODUCTION

The B-type lamins have been considered to play crucial roles in eukaryotic cells. Many previous *in vitro* studies have contributed to this view. For example, lamin B was shown to localize to sites of DNA replication during S-phase in cultured cells (1). Disruption of nuclear lamin organization by dominant-negative lamin B mutants in *Xenopus* eggs extracts blocked DNA

replication (2, 3), mitotic spindle assembly (4), and nuclear envelope assembly in interphase (5). In addition, RNAi-mediated knockdown of lamin B1 and lamin B2 led to mitotic arrest (6). The importance of B-type lamins in chromatin organization and gene expression at the nuclear periphery was also suggested (7, 8).

However, until recently, the *in vivo* relevance of those cell culture studies to the roles of B-type lamins had never been tested. To address this issue, Yang *et al*. (9) generated mice lacking both lamin B1 and lamin B2 in skin keratinocyte using *Lmnb1* and *Lmnb2* conditional knockout alleles. Surprisingly, a complete absence of both lamin B1 and lamin B2 in skin keratinocytes had no discernible effect on keratinocyte growth or on the complex developmental programs of the skin and hair. Even though misshapen nuclei were observed in *Lmnb1/Lmnb2*– deficient keratinocytes in culture, nuclear abnormalities were never found within the skin of the keratinocyte-specific *Lmnb1/Lmnb2* double knockout mice (9). Similarly, a loss of B-type lamins in hepatocytes had no adverse impacts on the liver (10). More recently, Kim *et al*. (11) reported that mouse embryonic stem (ES) cells grew and differentiated normally *in vitro* without any of the nuclear lamins. They also showed that *Lmna/Lmnb1/Lmnb2* triple-knockout mouse ES cells were capable of forming teratomas when injected subcutaneously into immune-deficient mice. All these discoveries were unexpected and raised doubts about whether the B-type lamins truly have unique roles in mitosis, DNA replication, etc.

Of note, the expression levels of A-type lamins are quite low in mouse ES cells raising a possibility that loss of A-type lamins in addition to B-type lamins might have a minimal impact on those cells. In addition, effects of a complete lamin deficiency on cell differentiation are unclear. In the current study, we explored whether nuclear lamins are dispensable for the vitality of cells *in vivo* using mice lacking all nuclear lamins in skin keratinocytes. Keratinocytes express

87

high levels of A-type lamins and undergo complex developmental program repeatedly. For these reasons, we chose skin-specific knockout mice as a model system to address the question.

RESULTS

Generation of mice lacking both A-type and B-type lamins in keratinocytes

We generated keratinocyte-specific *Lmna*/*Lmnb1*/*Lmnb2* triple-knockout mice (*Lmna*$^{-/-}$*Lmnb1*$^{fl/fl}$*Lmnb2*$^{fl/fl}$*K14Cre* or *Lmna*$^{-/-}$*Lmnb1*$^{\Delta/\Delta}$*Lmnb2*$^{\Delta/\Delta}$) by crossing conventional *Lmna* knockout mice (12) with conditional *Lmnb1*/*Lmnb2* double-knockout mice carrying keratin 14– *Cre* transgene (9).

Both A-type and B-type lamins were undetectable in skin keratinocytes of newborn *Lmna*$^{-/-}$*Lmnb1*$^{\Delta/\Delta}$*Lmnb2*$^{\Delta/\Delta}$ mice by immunohistochemistry (Fig. 5.1). Expression of lamin A, lamin C, lamin B1, and lamin B2 proteins in primary keratinocytes isolated from newborn *Lmna*$^{-/-}$*Lmnb1*$^{\Delta/\Delta}$*Lmnb2*$^{\Delta/\Delta}$ mice were also minimal (Fig. 5.S1).

Defective skin barrier development in *Lmna*$^{-/-}$*Lmnb1*$^{\Delta/\Delta}$*Lmnb2*$^{\Delta/\Delta}$ mice

Lmna$^{-/-}$*Lmnb1*$^{\Delta/\Delta}$*Lmnb2*$^{\Delta/\Delta}$ mice were born at the expected Mendelian frequency (Fig. 5.2A) and were similar in size to control littermates (either *Lmna*$^{+/+}$*Lmnb1*$^{\Delta/\Delta}$*Lmnb2*$^{\Delta/\Delta}$ or *Lmna*$^{+/-}$*Lmnb1*$^{\Delta/\Delta}$*Lmnb2*$^{\Delta/\Delta}$) (Fig. 5.2B). However, the triple-knockout mice often exhibited ichthyosis phenotype (Fig. 5.2, B and C) and none of them survived over weaning age (Fig. 5.2A). They also showed defective and retarded skin barrier development, as judged by toluidine blue staining (Fig. 5.2D). In *Lmna*$^{+/+}$*Lmnb1*$^{\Delta/\Delta}$*Lmnb2*$^{\Delta/\Delta}$ mice, the dye could not penetrate into the skin, but in the triple-knockout mice, the overall skin was darkly stained with the dye and the staining was more intense in the forelimb paws.

We suspected that the early death of $Lmna^{-/-}Lmnb1^{\Delta/\Delta}Lmnb2^{\Delta/\Delta}$ mice related to the defective skin barrier. To assess this idea, we compared epidermal water loss by measuring body weight changes after separating newborn pups from the mother to prevent milk intake (Fig. 5.2E). Either $Lmna^{+/+}Lmnb1^{\Delta/\Delta}Lmnb2^{\Delta/\Delta}$ or $Lmna^{+/-}Lmnb1^{\Delta/\Delta}Lmnb2^{\Delta/\Delta}$ mice lost less than 3% of their body weight over 7 h of observation. In contrast, $Lmna^{-/-}Lmnb1^{\Delta/\Delta}Lmnb2^{\Delta/\Delta}$ mice lost more than 10% of their body weight and were lethally dehydrated.

Abnormal accumulation of neutral lipids in the stratum corneum of *Lmna^{-/-}Lmnb1^{\Delta/\Delta}Lmnb2^{\Delta/\Delta}* mice

Previously, neutral lipid metabolism, particularly triacylglycerol (TAG) hydrolysis, has been associated with skin barrier defects (13). Epidermal permeability barrier is formed in the stratum corneum (the cornified layer of the skin) and the lipids in the extracellular matrix of the stratum corneum are crucial for the barrier function. Even while TAG is a minor lipid species secreted by lamellar bodies from keratinocytes, mice lacking CGI-58 (comparative gene identification-58), an essential protein for TAG hydrolysis, manifest ichthyosiform skin defect (14). Also, all known NLSD (neutral lipid storage disease) patients with mutations in the CGI-58 gene suffer from ichthyosis (15). To examine whether the ichthyosis phenotype of $Lmna^{-/-}Lmnb1^{\Delta/\Delta}Lmnb2^{\Delta/\Delta}$ mice relates to abnormal deposition of neutral lipids in the stratum corneum, we stained skin sections from newborn $Lmna^{-/-}Lmnb1^{\Delta/\Delta}Lmnb2^{\Delta/\Delta}$ mice with BODIPY, a dye staining neutral lipids (16) (Fig. 5.3). In the skin of $Lmna^{+/+}Lmnb1^{\Delta/\Delta}Lmnb2^{\Delta/\Delta}$ mice, lipid droplets were found around hair follicles, but not in the stratum corneum. However, in the skin of $Lmna^{-/-}Lmnb1^{\Delta/\Delta}Lmnb2^{\Delta/\Delta}$ mice, large amounts of lipid droplets were stained in the stratum corneum.

Interspersion of nuclear membrane proteins with chromatin in *Lmna⁻ᐟ⁻Lmnb1^{Δ/Δ}Lmnb2^{Δ/Δ}* keratinocytes

Next, we assessed whether an absence of all nuclear lamins affects localization of nuclear membrane proteins that are known to interact with lamins. LAP2β, the largest isoform of LAP2 (lamina-associated polypeptide 2), is an integral protein of the inner nuclear membrane (INM). *In vitro* binding assays showed that LAP2β bound to lamin B1 (17) and lamins were proposed to affect targeting of LAP2β proteins to the INM (18). Interestingly, in *Lmna^{+/+}Lmnb1^{Δ/Δ}Lmnb2^{Δ/Δ}* keratinocytes lacking both lamin B1 and lamin B2, LAP2β was normally located at the nuclear rim (Fig. 5.4). In contrast, in *Lmna⁻ᐟ⁻Lmnb1^{Δ/Δ}Lmnb2^{Δ/Δ}* keratinocyte lacking all nuclear lamins, LAP2β was often found within the nucleoplasm in a patchy distribution and interspersed with the chromatin. The localization of LAP2β was normal in the dermis of *Lmna⁻ᐟ⁻Lmnb1^{Δ/Δ}Lmnb2^{Δ/Δ}* mice, which expresses B-type lamins (Fig. 5.4).

We also examined localization of emerin by immunohistochemistry (Fig. 5.S2). Emerin is an inner nuclear membrane protein associated with Emery-Dreifuss muscular dystrophy (EDMD) (19). In *Lmna⁻ᐟ⁻* cells, emerin was mislocalized to the endoplasmic reticulum (ER) (12) and A-type lamins, particularly Lamin A, have been suggested to assist targeting of emerin to the nuclear envelope (20). Similar to LAP2β, emerin was mainly found at the nuclear rim in *Lmna^{+/+}Lmnb1^{Δ/Δ}Lmnb2^{Δ/Δ}* keratinocytes. As expected, in dermal fibroblasts of *Lmna⁻ᐟ⁻Lmnb1^{Δ/Δ}Lmnb2^{Δ/Δ}* mice without A-type lamins, emerin was located in the ER. However, in the epidermal keratinocytes of the same mice (which do not express B-type lamins, as well as A-type lamins), emerin was often observed in the nucleoplasm (Fig. 5.S2).

DISCUSSION

Earlier cell biology studies suggested that B-type lamins have unique and essential roles in the nucleus including DNA replication, gene regulation, chromatin organization, and mitosis (1-8). However, recent genetic studies argue against this view. Yang *et al*. (9) generated keratinocyte-specific *Lmnb1*/*Lmnb2* double-knockout mice (*Lmnb1*$^{\Delta/\Delta}$*Lmnb2*$^{\Delta/\Delta}$) and showed that B-type lamins are dispensable in keratinocytes. The double-knockout mice were free of pathology in the skin and hair and proliferation of *Lmnb1*$^{\Delta/\Delta}$*Lmnb2*$^{\Delta/\Delta}$ keratinocytes was similar to that of wild-type keratinocytes. Heterochromatin distribution and nuclear envelope were also normal (9). In a subsequent study by Kim *et al*. (2), mouse ES cells lacking all nuclear lamins appeared to grow normally and differentiate into fibroblasts, neural and cardiac lineages. In the current study, we aimed to test *in vivo* relevance of nuclear lamins using keratinocyte-specific *Lmna*/*Lmnb1*/*Lmnb2* triple-knockout mice (*Lmna*$^{-/-}$*Lmnb1*$^{\Delta/\Delta}$*Lmnb2*$^{\Delta/\Delta}$). Intriguingly, *Lmna*$^{-/-}$*Lmnb1*$^{\Delta/\Delta}$*Lmnb2*$^{\Delta/\Delta}$ mice died within a couple of days after birth due to lethal desiccation. The mice showed defects in skin barrier development with ichthyosis phenotype and deposited abnormally large amounts of neutral lipids in the stratum corneum. Nuclear abnormality was also observed in *Lmna*$^{-/-}$*Lmnb1*$^{\Delta/\Delta}$*Lmnb2*$^{\Delta/\Delta}$ skin keratinocytes: nuclear membrane proteins were interspersed with the chromatin within nucleoplasm.

The skin pathology of *Lmna*$^{-/-}$*Lmnb1*$^{\Delta/\Delta}$*Lmnb2*$^{\Delta/\Delta}$ mice has never been observed in either *Lmna*$^{-/-}$ mice (12) or *Lmnb1*$^{\Delta/\Delta}$*Lmnb2*$^{\Delta/\Delta}$ mice (9); which implies that the skin phenotype is an accumulative result of loss of both A-type and B-type lamins. This finding seems contradictory to the previous study by Kim *et al*. (2)—the authors showed that mouse ES cells without any nuclear lamins were indistinguishable to wild-type ES cells in the growth and differentiation. However, it is conceivable that the discrepancy between two studies comes from different

expression levels of nuclear lamins in ES cells and keratinocytes. The expression of A-type lamins increases significantly upon differentiation even while its expression is easily detectable even in ES cells (21-23). Yang *et al*. (9) proposed that high levels of A-type lamins in keratinocytes might compensate the lack of B-type lamins in $Lmnb1^{\Delta/\Delta}Lmnb2^{\Delta/\Delta}$ mice saving the mice from skin pathology. Perhaps, loss of A-type lamins in addition to B-type lamins might have more detrimental impacts on the vitality of such kinds of cells. Another possibility is that keratinocytes might be more vulnerable to a complete absence of nuclear lamins than ES cells because keratinocytes undergo complicated differentiation process repeatedly.

Recently, Jahn *et al*. (24) reported that the $Lmna^{-/-}$ mice, which were initially generated by Sullivan *et al*. (12) and have been widely used in the lamin field, express truncated lamin A lacking exons 8–11. This finding raised concerns about possible impacts of the truncated lamin A on the mouse physiology and interpretation of studies using this mouse model. In the current study, we used the same $Lmna^{-/-}$ mouse model to generate $Lmna^{-/-}Lmnb1^{\Delta/\Delta}Lmnb2^{\Delta/\Delta}$ mice and we appreciate that we should be cautious in the interpretation of our findings. However, the $Lmna^{-/-}$ mice (12) do not manifest skin pathology implying that the truncated lamin A does not function as a dominant-negative mutant at least in the skin. How much the truncated lamin A retains the normal functions of wild-type lamin A is unknown, but it is clear that the partial function, if there is any, of the truncated lamin A is not enough to rescue the skin pathology of $Lmna^{-/-}Lmnb1^{\Delta/\Delta}Lmnb2^{\Delta/\Delta}$ mice.

In the stratum corneum of $Lmna^{-/-}Lmnb1^{\Delta/\Delta}Lmnb2^{\Delta/\Delta}$ mice, abnormal deposition of neutral lipids was observed. This finding in part explains ichthyosis phenotype of the mice. In normal skin, triacylglycerol is secreted by lamellar bodies from keratinocytes and hydrolyzed by a lipase producing fatty acids; that are required for the generation of acylceramide to form skin

barrier and also suggested functioning as a ligand for nuclear hormone receptor to activate epidermal differentiation program (13). It would be interesting to compare levels of different lipid species in the stratum corneum of $Lmna^{+/+}Lmnb1^{\Delta/\Delta}Lmnb2^{\Delta/\Delta}$ and $Lmna^{-/-}$ $Lmnb1^{\Delta/\Delta}Lmnb2^{\Delta/\Delta}$ mice. How the absence of all nuclear lamins leads to accumulation of neutral lipids is currently unclear. We suspect that the answer might relate to the observation that nuclear membrane proteins were mislocalized in nucleoplasm and interspersed with the chromatin—these nuclear abnormalities could alter signaling pathways across the nuclear envelope and gene expression profiles (25).

Mislocalization of LAP2β and emerin in the nucleoplasm in the absence of all nuclear lamins seems quite plausible because nuclear lamins are a structural scaffolding for the nucleus. The nuclear lamina might function as a physical barrier of the nucleus assisting segregation of nucleoplasmic and cytoplasmic compartments; which is particularly likely because emerin was found in the nucleoplasm in the absence of B-type lamins in addition to A-type lamins. If it was just a loss of assistance of lamins to target emerin to the nuclear envelope, emerin is more likely found in the ER like what happens in $Lmna^{-/-}$ cells. To test this idea, ultrastructural examination of $Lmna^{-/-}Lmnb1^{\Delta/\Delta}Lmnb2^{\Delta/\Delta}$ nucleus by electron microscopy will be required.

This study suggests that nuclear lamins are required for keratinocyte differentiation and normal skin barrier development. However, it is not clear whether a complete absence of nuclear lamins has adverse impacts on proliferation of keratinocytes *in vivo*. The number of keratinocytes in the newborn $Lmna^{-/-}Lmnb1^{\Delta/\Delta}Lmnb2^{\Delta/\Delta}$ mice seems comparable to that in $Lmna^{+/+}Lmnb1^{\Delta/\Delta}Lmnb2^{\Delta/\Delta}$ mice implying that there is no significant defect in the growth. *In vivo* bromodeoxyuridine (BrdU) labeling studies or skin transplantation would provide a clear-cut answer.

MATERIALS AND METHODS

Histology and Immunofluorescence Microscopy

Freshly harvested mouse abdominal and back skins were embedded in OCT (Optimum Cutting Temperature) compound (Sakura Finetek) and sectioned (10-µm) with a cryostat. The sections were fixed either in ice-cold methanol (followed by acetone rinse) or 4% PFA, washed with 0.1% Tween-20 in TBS, and incubated with M.O.M. Mouse Ig Blocking Reagent (Vector Laboratories). The following primary antibodies were used: a mouse monoclonal antibody against mature lamin A (1:400) (MAB3540; Millipore); a goat polyclonal antibody against lamin B1 (1:400) (sc-6217; Santa Cruz); a mouse monoclonal antibody against lamin B2 (1:100) (33-2100; Invitrogen); a mouse monoclonal antibody against LAP2β (1:400) (611000; BD Biosciences); a mouse monoclonal antibody against Emerin (1:200) (NCL-EMERIN; Novocastra); and a rabbit polyclonal antibody against keratin 14 (1:800) (PRB-155P; Covance). M.O.M. Biotinylated Anti–Mouse IgG Reagent (Vector Laboratories) and Alexa Fluor–conjugated streptavidin (Invitrogen) were used to detect binding of mouse monoclonal primary antibodies; Alexa Fluor–labeled donkey antibodies against goat or rabbit IgG (Invitrogen) were used to detect binding of other primary antibodies. Confocal microscopy images were recorded with a Zeiss LSM700 laser-scanning microscope [Plan Apochromat 20×/0.80 NA (air) or 63×/1.4 NA (oil) objectives]. Z-stacked images were generated with Zen 2010 software (Zeiss).

Light microscopy images were captured with a Leica MZ6 dissecting microscope [a Plan 0.5× objective (air)] with a DFC290 digital camera (Leica) and were recorded with Leica Application Suite imaging software.

Western Blots

Primary keratinocytes were isolated from the skin of newborn mouse as described previously (26). Briefly, the skin was floated on cold 0.25% trypsin (without EDTA) with dermal side facing down and was incubated overnight at 4°C. Next morning, the epidermis was gently separated from the dermis and was physically dissociated with a blade. Isolated keratinocytes were seeded on collagen I–coated plates and cultured in KGM-2 BulletKit medium (Lonza) at 37°C. After 4–6 days, cells were harvested and the cell pellets were lysed in urea buffer [9 M urea, 10 mM Tris-HCl (pH 8.0), 1 mM NaF, 1 mM PMSF, 10 μM EDTA, 0.2%-mercaptoethanol, and a Roche Protease Inhibitors Cocktail Tablet]. Protein extracts were separated on 4–12% gradient polyacrylamide Bis-Tris gels (Invitrogen) and transferred to a nitrocellulose membrane. The membranes were then incubated with the following primary antibodies: a goat polyclonal antibody against lamin A/C (1:400) (sc-6215; Santa Cruz); a goat polyclonal antibody against lamin B1 (1:400) (sc-6217; Santa Cruz); a mouse monoclonal antibody against lamin B2 (1:400) (33-2100; Invitrogen); a rabbit polyclonal antibody against keratin 14 (1:800) (PRB-155P; Covance); and a goat polyclonal antibody against actin (1:1000) (sc-1616; Santa Cruz). Binding of primary antibodies was detected with infrared (IR)-dye–conjugated secondary antibodies (Rockland) and an Odyssey infrared scanner (LI-COR).

Skin Permeability Assay

Toluidine blue staining to assess skin permeability was performed following the protocol described earlier (27). Briefly, newborn mice were euthanized; dehydrated in 25%, 50%, 75% and 100% methanol serially for 2 min each; and rehydrated in 75%, 50%, and 25%

methanol for 1 min each. After washing in PBS twice for 3 min each, mice were incubated in 0.1% toluidine blue solution (in PBS) for 3 h at room temperature followed by destaining in PBS for 20 min.
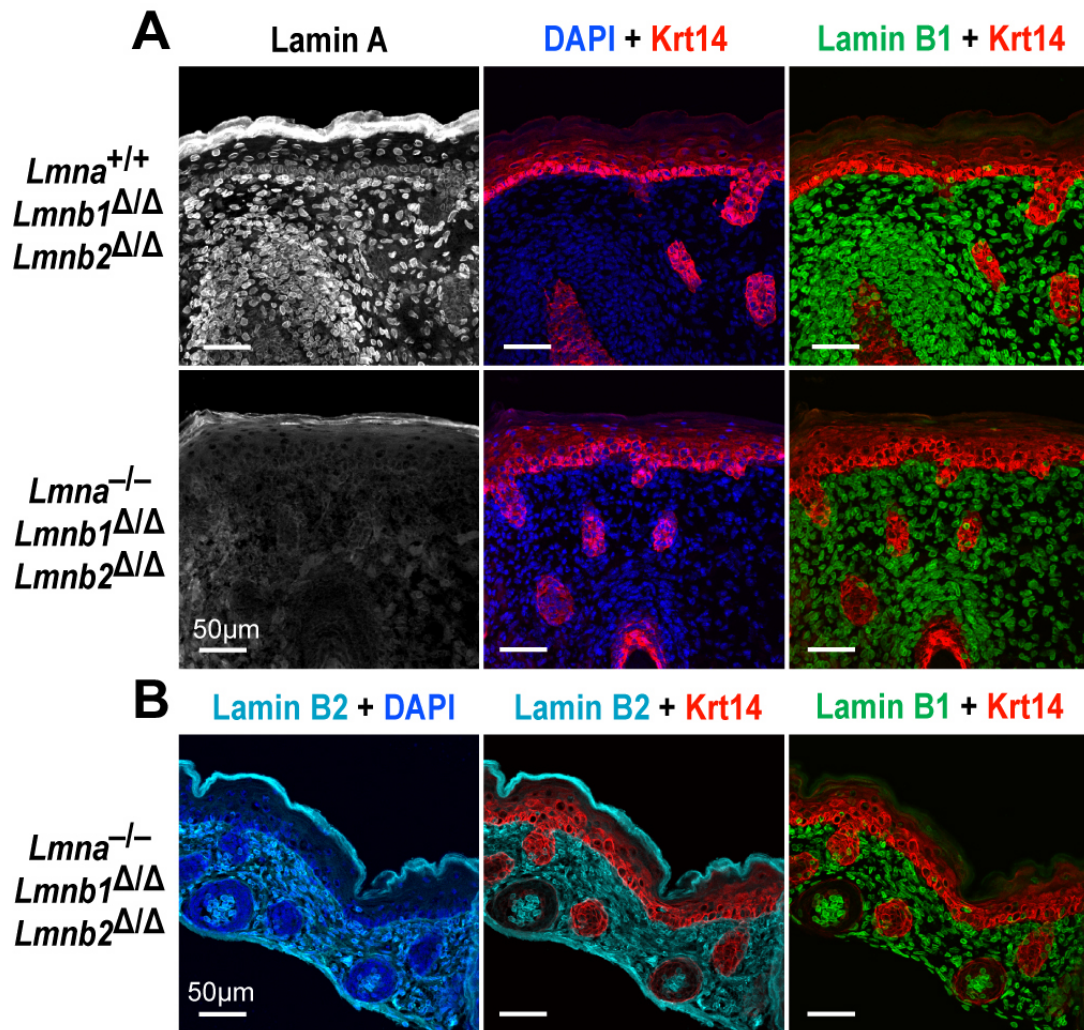
Figure 5.1 Generation of mice lacking both A-type and B-type lamins in skin keratinocytes. Skin sections from newborn *Lmna+/+Lmnb1Δ/ΔLmnb2Δ/Δ* and *Lmna−/−Lmnb1Δ/ΔLmnb2Δ/Δ* mice were stained with antibodies against keratin 14 (Krt14, red) and lamin B1 (green) along with an antibody against lamin A (white) (A) or lamin B2 (cyan) (B). DNA was visualized with DAPI (blue). As expected, both lamin B1 and lamin B2 were not detected in the keratin 14–positive keratinocytes in the epidermis of *Lmna−/−Lmnb1Δ/ΔLmnb2Δ/Δ* mice; lamin A expression was not detected in the whole skin tissue. Scale bar, 50 μm.
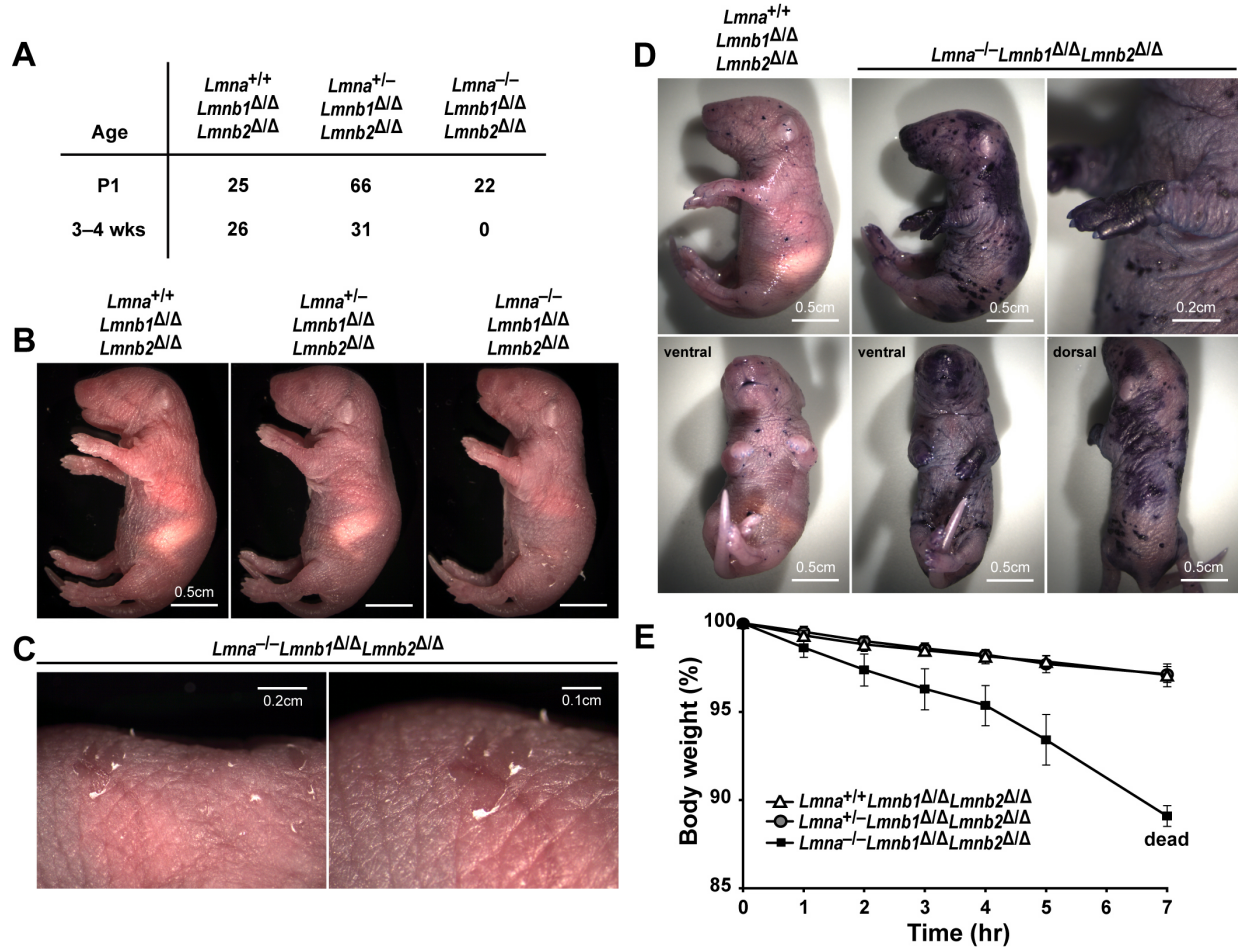
**Figure 5.2** *Lmna⁻/⁻Lmnb1^(Δ/Δ)Lmnb2^(Δ/Δ)* mice die soon after birth with skin barrier defects. (A) Numbers of mice per genotype at P1 and weaning age (3–4wks). (B and C) Images of newborn *Lmna⁺/⁺Lmnb1^(Δ/Δ)Lmnb2^(Δ/Δ)*, *Lmna⁺/⁻Lmnb1^(Δ/Δ)Lmnb2^(Δ/Δ)*, and *Lmna⁻/⁻Lmnb1^(Δ/Δ)Lmnb2^(Δ/Δ)* mice. *Lmna⁻/⁻Lmnb1^(Δ/Δ)Lmnb2^(Δ/Δ)* mice had ichthyosis phenotype. Scale bar, 0.5 cm. (D) Skin permeability barrier assay using toluidine blue solution. In contrast to *Lmna⁺/⁺Lmnb1^(Δ/Δ)Lmnb2^(Δ/Δ)* mice, the overall skin of *Lmna⁻/⁻Lmnb1^(Δ/Δ)Lmnb2^(Δ/Δ)* mice were stained with the dye and the staining was strongest in the forelimb paw. Scale bar, 0.5 cm. (E) Epidermal water loss test with *Lmna⁺/⁺Lmnb1^(Δ/Δ)Lmnb2^(Δ/Δ)* (*n*=3), *Lmna⁺/⁻Lmnb1^(Δ/Δ)Lmnb2^(Δ/Δ)* (*n*=5), and *Lmna⁻/⁻Lmnb1^(Δ/Δ)Lmnb2^(Δ/Δ)* mice (*n*=4). *Lmna⁻/⁻Lmnb1^(Δ/Δ)Lmnb2^(Δ/Δ)* mice were lethally dehydrated in 7 h of observation.
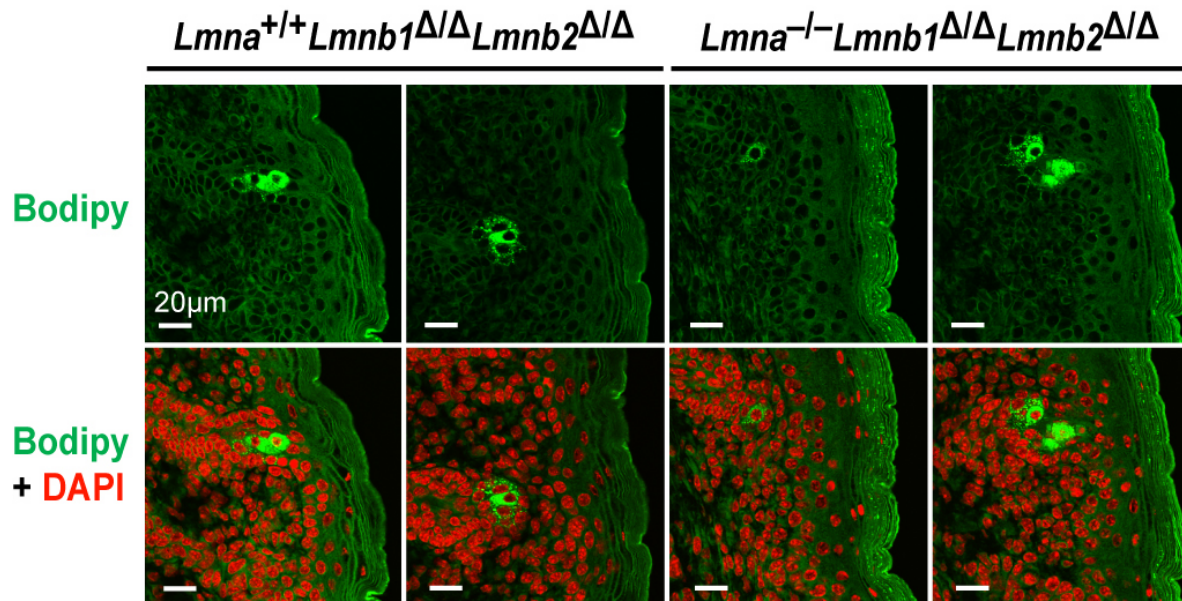
Figure 5.3 Abnormal accumulation of neutral lipids in the stratum corneum of $Lmna^{-/-}$ $Lmnb1^{\Delta/\Delta}Lmnb2^{\Delta/\Delta}$ mice. Skin sections from newborn $Lmna^{+/+}Lmnb1^{\Delta/\Delta}Lmnb2^{\Delta/\Delta}$ and $Lmna^{-/-}$ $Lmnb1^{\Delta/\Delta}Lmnb2^{\Delta/\Delta}$ mice were stained with BODITY (green); DNA was visualized with DAPI (red). Scale bar, 20 μm.
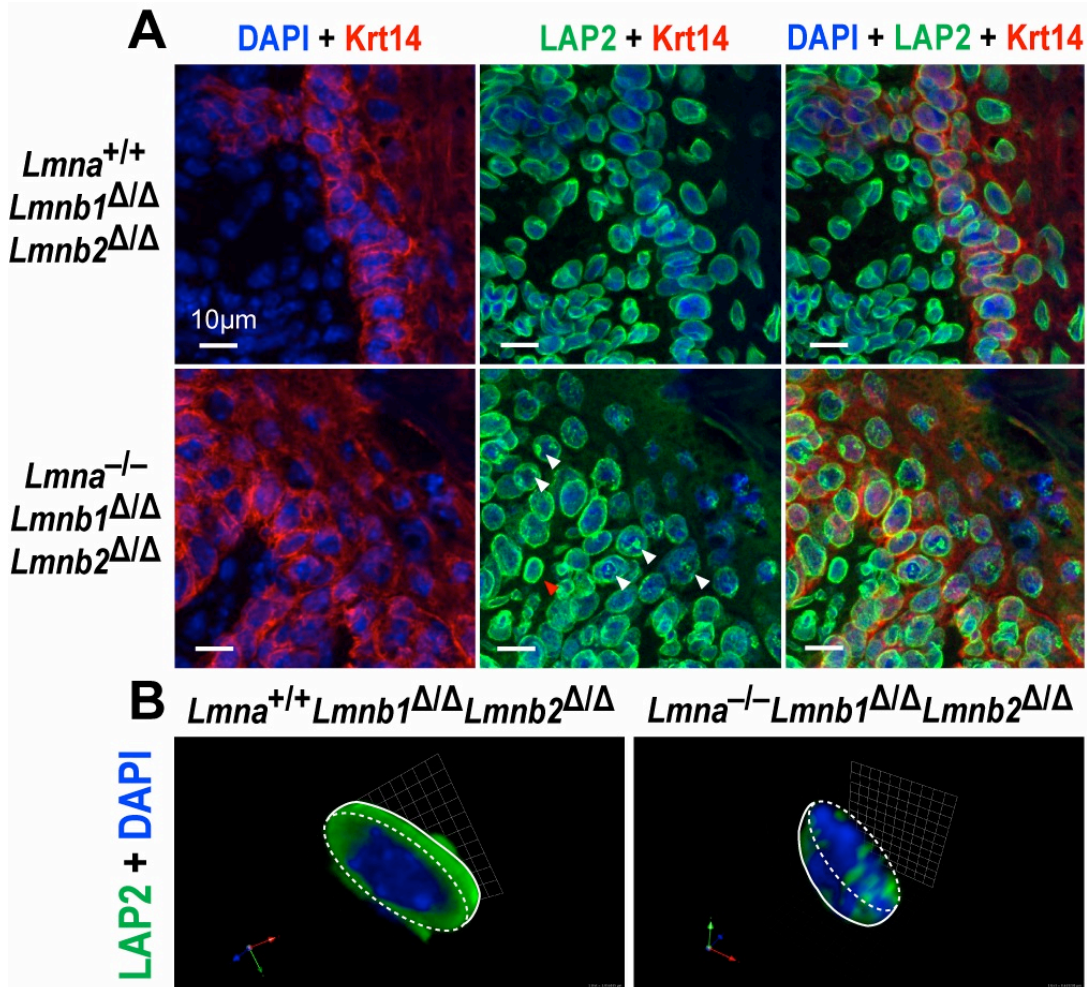
Figure 5.4 Interspersion of LAP2β with chromatin in the absence of all nuclear lamins. (A) Immunofluorescence microscopy of newborn skin sections stained for keratin 14 (Krt14, red) and LAP2β (green). DNA was stained with DAPI (blue). In the keratin 14–positive keratinocytes in the epidermis of *Lmna⁻/⁻Lmnb1^{Δ/Δ}Lmnb2^{Δ/Δ}* mice, LAP2β was abnormally located in the nucleoplasm in a patchy distribution (white arrowheads); in the keratin 14–negative dermal fibroblasts of the same mice where B-type lamins are expressed, LAP2β was normally located at the nuclear rim (red arrowhead). Scale bar, 10 μm. (B) 3D-images of "half-cut open" nuclei stained for LAP2β (green). Images along the z-axis were captured and 3D-images were constructed with Volocity 5.4. The boundary of nuclei is outlined with white dashed lines.
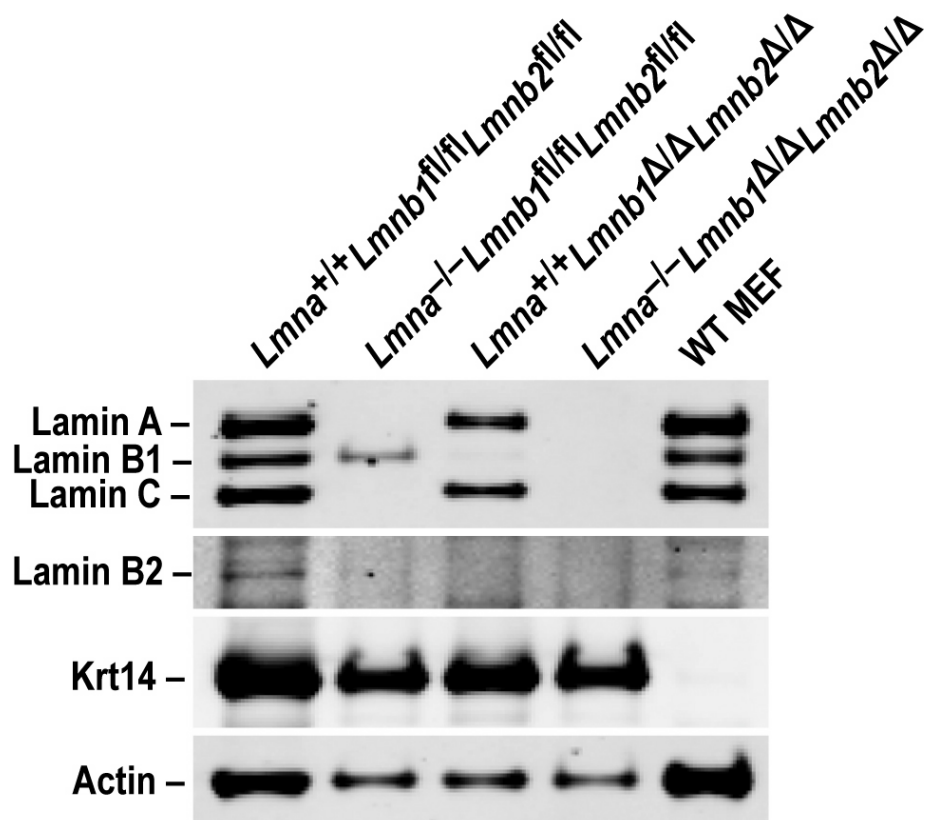
Figure 5.S1 Western blot analysis of lamin expression in primary keratinocytes in culture. All of the lamins (A, B1, B2, and C) were barely detected in the protein extracts of *Lmna*^−/−^*Lmnb1*^Δ/Δ^*Lmnb2*^Δ/Δ^ keratinocytes.
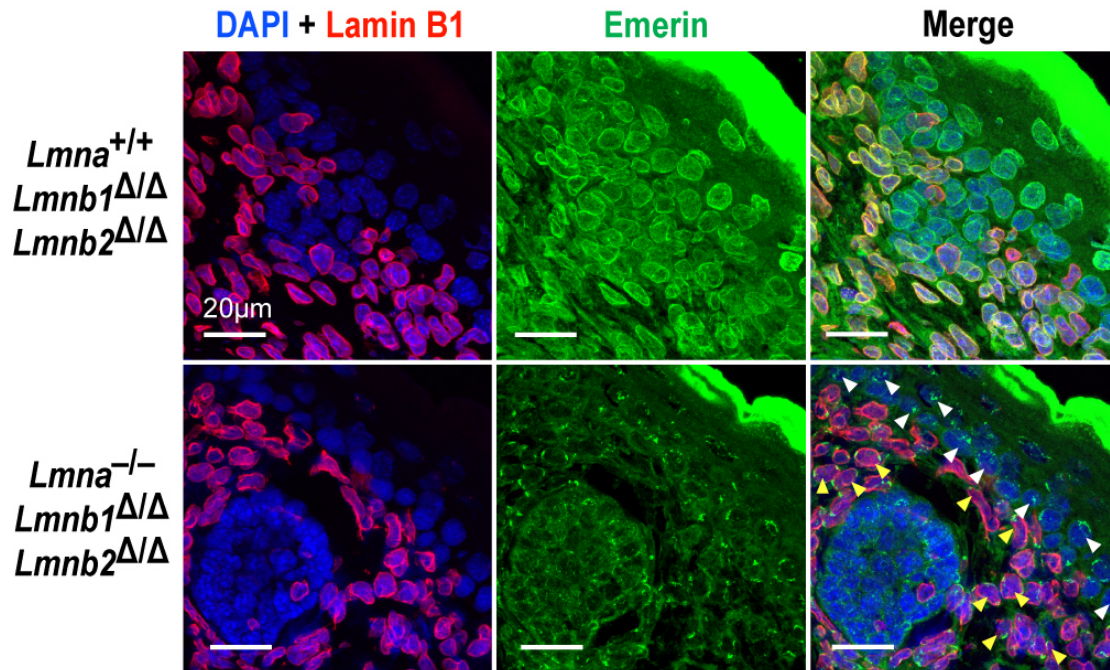
Figure 5.S2 Mislocalization of emerin in the nucleoplasm in the absence of all nuclear lamins. Skin sections from newborn *Lmna⁺/⁺Lmnb1^{Δ/Δ}Lmnb2^{Δ/Δ}* and *Lmna⁻/⁻Lmnb1^{Δ/Δ}Lmnb2^{Δ/Δ}* mice were stained with antibodies against lamin B1 (red) and emerin (green); DNA was visualized with DAPI (blue). In the epidermal keratinocytes of *Lmna⁻/⁻Lmnb1^{Δ/Δ}Lmnb2^{Δ/Δ}* mice, emerin was mainly found in the nucleoplasm (white arrowheads); in the dermal fibroblasts of the same mice in which B-type lamins are expressed (but A-type lamins are absent), emerin was located in the ER (12). Scale bar, 20 μm.

REFERENCES

1. Moir RD, Montag-Lowy M, and Goldman RD (1994) Dynamic properties of nuclear lamins: lamin B is associated with sites of DNA replication. *J Cell Biol* 125:1201-1212.

2. Moir RD, Spann TP, Herrmann H, and Goldman RD (2000) Disruption of nuclear lamin organization blocks the elongation phase of DNA replication. *J Cell Biol* 149:1179-1192.

3. Ellis DJ, Jenkins H, Whitfield WG, and Hutchison CJ (1997) GST-lamin fusion proteins act as dominant negative mutants in Xenopus egg extract and reveal the function of the lamina in DNA replication. *J Cell Sci* 110 (Pt 20):2507-2518.

4. Tsai MY, Wang S, Heidinger JM, Shumaker DK, Adam SA, Goldman RD, and Zheng Y (2006) A mitotic lamin B matrix induced by RanGTP required for spindle assembly. *Science* 311:1887-1893.

5. Lopez-Soler RI, Moir RD, Spann TP, Stick R, and Goldman RD (2001) A role for nuclear lamins in nuclear envelope assembly. *J Cell Biol* 154:61-70.

6. Harborth J, Elbashir SM, Bechert K, Tuschl T, and Weber K (2001) Identification of essential genes in cultured mammalian cells using small interfering RNAs. *J Cell Sci* 114:4557-4565.

7. Tang CW, Maya-Mendoza A, Martin C, Zeng K, Chen S, Feret D, Wilson SA, and Jackson DA (2008) The integrity of a lamin-B1-dependent nucleoskeleton is a fundamental determinant of RNA synthesis in human cells. *J Cell Sci* 121:1014-1024.

8. Belmont AS, Zhai Y, and Thilenius A (1993) Lamin B distribution and association with peripheral chromatin revealed by optical sectioning and electron microscopy tomography. *J Cell Biol* 123:1671-1685.

9. Yang SH, Chang SY, Yin L, Tu Y, Hu Y, Yoshinaga Y, de Jong PJ, Fong LG, and Young SG (2011) An absence of both lamin B1 and lamin B2 in keratinocytes has no effect on cell proliferation or the development of skin and hair. *Hum Mol Genet* 20:3537-3544.

10. Yang SH, Jung HJ, Coffinier C, Fong LG, and Young SG (2011) Are B-type lamins essential in all mammalian cells? *Nucleus* 2:562-569.

11. Kim Y, Zheng X, and Zheng Y (2013) Proliferation and differentiation of mouse embryonic stem cells lacking all lamins. *Cell Res* 23:1420-1423.

12. Sullivan T, Escalante-Alcalde D, Bhatt H, Anver M, Bhat N, Nagashima K, Stewart CL, and Burke B (1999) Loss of A-type lamin expression compromises nuclear envelope integrity leading to muscular dystrophy. *J Cell Biol* 147:913-920.

13. Radner FP, Grond S, Haemmerle G, Lass A, and Zechner R (2011) Fat in the skin: Triacylglycerol metabolism in keratinocytes and its role in the development of neutral lipid storage disease. *Dermatoendocrinol* 3:77-83.

14. Radner FP, Streith IE, Schoiswohl G, Schweiger M, Kumari M, Eichmann TO, Rechberger G, Koefeler HC, Eder S, Schauer S, Theussl HC, Preiss-Landl K, Lass A, Zimmermann R, Hoefler G, Zechner R, and Haemmerle G (2010) Growth retardation, impaired triacylglycerol catabolism, hepatic steatosis, and lethal skin barrier defect in mice lacking comparative gene identification-58 (CGI-58). *J Biol Chem* 285:7300-7311.

15. Lefevre C, Jobard F, Caux F, Bouadjar B, Karaduman A, Heilig R, Lakhdar H, Wollenberg A, Verret JL, Weissenbach J, Ozguc M, Lathrop M, Prud'homme JF, and Fischer J (2001) Mutations in CGI-58, the gene encoding a new protein of the esterase/lipase/thioesterase subfamily, in Chanarin-Dorfman syndrome. *Am J Hum Genet* 69:1002-1012.

16. Adeyo O, Allan BB, Barnes RH, 2nd, Goulbourne CN, Tatar A, Tu Y, Young LC, Weinstein MM, Tontonoz P, Fong LG, Beigneux AP, and Young SG (2014) Palmoplantar Keratoderma along with Neuromuscular and Metabolic Phenotypes in Slurp1-Deficient Mice. *J Invest Dermatol*.

17. Foisner R, and Gerace L (1993) Integral membrane proteins of the nuclear envelope interact with lamins and chromosomes, and binding is modulated by mitotic phosphorylation. *Cell* 73:1267-1279.

18. Furukawa K, Fritze CE, and Gerace L (1998) The major nuclear envelope targeting domain of LAP2 coincides with its lamin binding region but is distinct from its chromatin interaction domain. *J Biol Chem* 273:4213-4219.

19. Bione S, Maestrini E, Rivella S, Mancini M, Regis S, Romeo G, and Toniolo D (1994) Identification of a novel X-linked gene responsible for Emery-Dreifuss muscular dystrophy. *Nat Genet* 8:323-327.

20. Raharjo WH, Enarson P, Sullivan T, Stewart CL, and Burke B (2001) Nuclear envelope defects associated with LMNA mutations cause dilated cardiomyopathy and Emery-Dreifuss muscular dystrophy. *J Cell Sci* 114:4447-4457.

21. Eckersley-Maslin MA, Bergmann JH, Lazar Z, and Spector DL (2013) Lamin A/C is expressed in pluripotent mouse embryonic stem cells. *Nucleus* 4:53-60.

22. Lebel S, Lampron C, Royal A, and Raymond Y (1987) Lamins A and C appear during retinoic acid-induced differentiation of mouse embryonal carcinoma cells. *J Cell Biol* 105:1099-1104.

23. Rober RA, Weber K, and Osborn M (1989) Differential timing of nuclear lamin A/C expression in the various organs of the mouse embryo and the young animal: a developmental study. *Development* 105:365-378.

24. Jahn D, Schramm S, Schnolzer M, Heilmann CJ, de Koster CG, Schutz W, Benavente R, and Alsheimer M (2012) A truncated lamin A in the Lmna -/- mouse line: implications for the understanding of laminopathies. *Nucleus* 3:463-474.

25. Dauer WT, and Worman HJ (2009) The nuclear envelope as a signaling node in development and disease. *Dev Cell* 17:626-638.

26. Lichti U, Anders J, and Yuspa SH (2008) Isolation and short-term culture of primary keratinocytes, hair follicle populations and dermal cells from newborn mice and keratinocytes from adult mice for in vitro analysis and for grafting to immunodeficient mice. *Nat Protoc* 3:799-810.

27. Koch PJ, de Viragh PA, Scharer E, Bundman D, Longley MA, Bickenbach J, Kawachi Y, Suga Y, Zhou Z, Huber M, Hohl D, Kartasova T, Jarnik M, Steven AC, and Roop DR (2000) Lessons from loricrin-deficient mice: compensatory mechanisms maintaining skin barrier function in the absence of a major cornified envelope protein. *J Cell Biol* 151:389-400.